Doctoral Dissertation

Effect of Degraded Characteristics of Corroded PC Steel Strands on Prestressed Concrete Beams under Static and Fatigue Loads
（腐食した PC 鋼ストランドの特性の低下が静的荷重と疲労荷重を受けるプレストレストコンクリートはりに与える影響）

(January, 2024)

Graduate school of Engineering

Kobe University

李 静遠

Li Jingyuan

Supervisor: Associate Professor Tomohiro Miki

Abstract

Vehicle overloading and environmental corrosion are two of the main causes of reduced service life of bridge structures. Vehicle overloading can easily cause fatigue damage within the concrete and environmental corrosion can lead to a reduction in the durability of the bridge structure, which can further aggravate the degree of damage within the concrete. In this paper, corrosion tests were first carried out on PC strands under working state to study the effect of corrosion on prestress force, and tensile tests were carried out after corrosion to study their mechanical properties after corrosion. Static and fatigue tests were then carried out on some of the prestressed concrete beams after corrosion of the strands, with the following main findings:

1. In this study, the relaxation machine was innovatively combined with a traditional electrochemical accelerated corrosion device to test the effect of corrosion on PC strands in working state. The specimens were divided into two groups according to the prestressing levels and the corrosion degree was controlled by controlling the corrosion time. After the corrosion test, the strands that didn't rupture during the corrosion test were subjected to tensile tests to test their residual properties. The test results show that the prestressing force of prestressing strands decreases with the increase of corrosion degree, excluding the effect of relaxation properties, and the whole process can be divided into two stages: linear decrease and rapid decrease. Corrosion leads to a reduction in the ultimate load carrying capacity of the strand. After that, in order to further investigate the prestressing force deterioration process of PC strands due to corrosion, the strain gauges were attached to every steel wires in the outer ring of the PC strands and the wire's fracture characteristics were observed after wires rupture. Test result show that the prestress degradation is divided into two stages; the beginning and development of the second stage are related to the maximum cross-sectional area loss and the type of fracture of the wire, respectively. The prestress loss is the result of the internal force balance after the deterioration of tensile properties. The tensile test results show that corrosion leads to degradation of the tensile properties of PC strands, the ultimate tensile capacity of corroded PC strands is related to the fracture state, and the shape and cross-sectional area loss of the corroded PC wire affect the fracture mode of the PC wire.

2. By conducting strand corrosion tests on the same batch of 17 prestressed concrete beams, the test beams were divided into two groups according to two corrosion locations, in the middle of the beam and at the edge of the beam, and the strain change in the outer ring of the strand was measured during the corrosion process and compared with that of PC strands corrosion test. The results show that the strain loss in the outer ring of the wire increases linearly with the degree of corrosion and is independent of the corrosion location, the bonding reduces the strain loss of the outer ring wires. The prestress loss of the strand was calculated based on the strain loss, and it was found that the prestress force of the bonded PC strand in the beam had the same deterioration pattern as that of the unbonded PC strand.

3. Eleven beams from the corroded specimen and the uncorroded beam were subjected to static load tests to investigate the effect of strand corrosion on the static performance of the test beam. The results show that the corrosion of the strand not only causes the damage form of some of the prestressed concrete beams to change from ductile to brittle damage, the cracking load decreases linearly with increasing corrosion and is independent of the corrosion location, and the effect of corrosion on ductility is much more significant than that on ultimate load carrying capacity. The fracture of the strand is the main cause of the change in damage form. Combined with the results of Chapter 2, the forces on the strand during loading of the specimen are analyzed and the mid-span deflection of the strand when fracture occurs is predicted.

4. Fatigue tests were conducted on six corroded beams and one uncorroded beam, and the fatigue-damaged specimens were subjected to static tests to test their residual load capacity. The results show that when the corrosion degree is low, the fatigue damage of the corroded beam is caused by the fatigue fracture of the longitudinal reinforcement. The fatigue damage increases with the corrosion degree, the higher the corrosion degree the greater the strain accumulation in the longitudinal reinforcement, and the specimen with the corrosion location in the span has a greater deterioration in performance when the corrosion degree is the same. The results of static loading show that the load capacity of the beams with fatigue damage is significantly reduced. The load carrying capacity decreases with the increase of corrosion, and the effect of corrosion in the span is greater. The crack width during loading was also greater.

Acknowledgments

Content

Chapter 1 Introduction

1.1 Research Background

With the rapid development of modern transportation, part of the prestressed reinforced concrete structure has become the most commonly used structural form in bridge engineering, especially in the medium and large span bridges have a pivotal position. 1928, the famous French engineer Freyssinet to reduce the stress loss rate and improve the tension stress began to use high-strength steel wire to apply prestress to the concrete structure, which means that prestressed concrete structures began to enter the practical stage [1]. In the early stages of structural application, members were generally designed according to fully prestressed concrete, i.e. no tensile stresses were allowed in the concrete under the most unfavourable combination of all loads. However, after a long period of practice, it was found that the fully prestressed concrete structural members have a large reverse arch, poor ductility, poor performance and other problems, especially when the pre-stressing stress is too large, the fully prestressed concrete structure will also appear too large cross-section and along the longitudinal prestressing steel cracks that can not be recovered [2]. In order to improve the above shortcomings, Austrian engineer Fritz Emperger proposed the use of partial prestressing steel to replace the amount of ordinary steel. 1951, the British engineer Abeles combined with its earlier series of engineering practice, formally proposed the use of ordinary steel and prestressing steel mixed with the "partial prestressing The concept of "partial prestressing", i.e. allowing the concrete at the bottom of the beam to develop tensile stresses and even micro cracks under all loads. Since then, countries around the world have made initial provisions for partially prestressed concrete (PPC) and carried out a lot of engineering practice and theoretical research. 1970, the International Prestressing Association FIB and the European Concrete Board CEB at the International Conference on Prestressed Concrete clearly distinguished between partially prestressed concrete and ordinary reinforced concrete, proposing to determine the degree of prestress according to the degree of applied prestress prestressed concrete grade, and it was officially included in the European Code [3]. Since then, partially prestressed concrete structures have flourished and been used in industrial plants, civil houses, highway bridges, railway sleepers and marine platforms and other engineering structures, of which the most widely used in bridge engineering [4].

It is generally believed that the prestressed concrete structure has the characteristics of high concrete strength and good compactness, and at the same time, due to the presence of prestressing effect, the cracks of prestressed concrete structure can be easily closed, and it is generally difficult for external harmful media to invade, thus relatively good durability. As a major structural form of bridge structures, prestressed reinforced concrete structures are often subjected to frequent repeated loads, such as vehicle loads, random wave forces, and intra-cycle pressures, in addition to static loads, during their service life. Under the action of long-term repeated loads, the fatigue process often results in crack development in structural members under the action of load levels smaller than the static load capacity of the members, and generally

speaking, fatigue damage does not occur without the extension of cracks [5]. In the corrosive environment in which the concrete bridges across rivers and seas are located, the cracks generated by fatigue will accelerate the corrosion of the prestressing strands, and the corrosion of the prestressing strands will accelerate the fatigue damage deterioration of the prestressed concrete structures. Some prestressed reinforced concrete bridge structures subjected to fatigue loading for a long time, in addition to possible fatigue cracks, in the actual construction of prestressed members due to the need to go through multiple processes, such as the production of bellows, filling of pipes, anchoring of force bars, etc., problems in any of these links may lead to the presence of cavities, moisture and chloride ion residues in the prestressing orifice, laying hidden dangers for the corrosion of PC strands[6].

The fracture of PC strands can lead to brittle failure of prestressed concrete members without warning or even catastrophic failure of the whole bridge causing huge casualties and economic losses.

In November 2001, Zivanovic et al. also briefly summarized the main causes of prestressing tendon corrosion in terms of both design defects and construction defects in an international conference on the durability of post-tensioned prestressing strands held at the University of Ghent, Belgium[7]. In 1953, a single-span post-tensioned prestressed concrete bridge over the River South Wales in the UK, which had been in service for six years, collapsed. The investigation revealed that the accident was caused by de-icing salt seeping into the longitudinal and transverse post-tensioned prestressing tendon apertures along the bridge deck joints, causing severe corrosion of the PC strands [8].

In 1998, a prestressed concrete viaduct in Slovenia had a serious corrosion damage accident, the investigation results showed that: the bridge deck structure in addition to the existence of many cracks, the longitudinal beams of the non-prestressed reinforcement direction there are a number of paratenon Cracks, and the longitudinal beam in the PC strands also appear different degrees of corrosion, serious section loss rate of more than 40%, and even some have been rusted off [9]. In Mumbai, India, also due to severe corrosion of prestressing steel, the first post-tensioned prestressed concrete bridge built on the Tana River had to be replaced and rebuilt in advance, however, the new bridge after the rebuilding of the prestressing tendons in the atmosphere before the installation of salt contamination, less than ten years of the new bridge of all ordinary reinforcement, prestressing tendons and their casing and suffered serious corrosion damage. 2007. A highway bridge crossing the Mississippi River in Minnesota, USA suddenly collapsed during peak traffic hours. The investigation report showed that the bridge had signs of corrosion near the bridge bearings and bridge frame joints, and fatigue damage at the approach bridge sections.

Faced with the combined effects of maritime climate with wind and wave impacts, and fatigue loads from increasingly busy traffic vehicles, the damage deterioration mechanism of concrete bridges is more complex. For some prestressed concrete bridge members where cracks are allowed to appear, the cracks generated by fatigue loads create conditions for corrosion of reinforcement in an aggressive environment, thus accelerating the fatigue damage of the structure. As the most widely used prestressing reinforcement, the steel strand has a small wire cross-sectional area and is often at a

high stress level. After some of the prestressed concrete beams are subjected to fatigue loading to produce cracks, they are prone to fatigue damage caused by rusting and fracture of the strand in an eroding environment. And the strand from the beginning of corrosion to fracture is often a relatively fast process, the components are usually no aura of brittle damage, this damage will often cause huge economic losses and social impact. Examples include the Nielsen Strait Bridge in the United States, the Saint Stefano Bridge in Italy and the pedestrian bridge at Lowe's Motor Speedway in North Carolina[10, 11, 12] and the sudden collapse of the Ynys-yGwas Bridge [13].

However, the fatigue performance of some prestressed concrete beams, which has been widely studied by the academic and engineering communities in recent years, is still mainly focused on the damage mode of fatigue fracture of non-prestressed steel bars, and there is almost no research on the damage mode of fatigue fracture of steel strands that may occur in corrosive environments starting from rusting. Therefore, it is of great importance to carry out research on the fatigue performance of prestressed concrete beams with corroded strands to provide technical support and guidance for the rational design and evaluation of the performance of bridge structures in service in corrosive environments.

1.2 Current status of research on corrosion and fatigue problems in PC structures
1.2.1 Research on the performance of corroded prestressing strands.

Over the past three decades, the detrimental effects on pc strands of the corrosion process have been deeply investigated by many authors. The main effects of corrosion have been attributed to loss of cross-sectional area, reduction in bond strength, and deterioration of the ultimate tensile properties.

Kondo et al.[14] have simulated the reduction in the cross-sectional area of PC steel strands due to corrosion by artificially cutting the steel strands. Tensile tests were carried out on the cut and corroded strands separately to compare the differences in performance between them. The test results showed that as compared with the corroded PC steel strand, the maximum load of the cut steel strand had a linear relationship with the elongation when the cross section of the cut steel strand was reduced less.

The mechanical properties of corroded PC strand were reported by Kitano et al.[15]. According to the corrosion degree in this test, the steel strand was divided into four categories: less than 1%, 1%-2.5%, less than 10% and more than 10%. The influence of corrosion degree on the tensile strength, yield strength, elastic coefficient, and elongation of the steel strand was observed respectively. The report indicated that even if the mass loss rate is the same, the mechanical properties of the steel strand with different corrosion characteristics are different. The steel strand with slight surface corrosion was similar to the steel strand without corrosion, but the performance of the steel strand with pitted corrosion deteriorates obviously. The tensile and yield strengths of corroded PC steel strand decreased with the increase of mass loss, and similar conclusions can be obtained by showing the section loss.

Tanaka et al.[16] used the electrified accelerated corrosion method to corrode steel strand embedded in concrete, set seven corrosion levels; 0%, and 10% to 40%, and carried out tensile tests to analyze the effect of corrosion on the maximum tensile strength, yield strength, stiffness and elongation rate of steel strand. They have found that the maximum tensile strength and yield strength decreased with the increase of

corrosion degree.

In aggressive environments, PC steel strands were more prone to corrosion under high stress conditions [17]. However, most of the earlier studies ignored the promotion of prestress on the corrosion of steel strands in the actual working condition especially under prestressing situation. Jeon et al.[18] tested the prestressing strand taken from the existing bridge. The cross-sectional shape after corrosion was divided into three types and the method of calculating the cross-sectional area by corrosion depth for different types was proposed. The tensile loading tests were conducted on these specimens to study the tensile properties of the steel strand after corrosion, and the results showed that the decrease in tensile strength become larger than the decrease in the reduction in cross sectional area, and the decrease of fracture strain was large enough to be cautious.Then he made further studies on the tensile properties of corroded steel strand[19], and based on the test results, proposed the tensile strength and ductility of corroded steel strand empirical equations for the tensile strength and ductility of corroded strands. And it was found that even if two strands have the same degree of maximum cross-sectional area loss, the degree of maximum cross-sectional area loss of the wire may be very different, and the most corroded wire determines the mechanical properties of the strand. Zhang et al.[20] used artificial climate corrosion method to corrode steel strands with prestressing applied to investigate their mechanical properties and have found that corrosion resulted in a significant reduction in the ultimate strain of the strands, leading to brittle damage. In contrast, the effect of corrosion on the elastic modulus and yield strength was not obvious in the previous study. For instance, Wang et al. [21] also used artificial climate corrosion method to corrode the PC steel strands, analyzed the shape of corrosion and its mechanical properties, and have found that high stress level can promote the expansion of corroded microcracks on the surface of steel strands. Finally, the corrosion was divided into slight and severe conditions, and a constitutive model was proposed to predict the stress-strain curve of these corroded PC strands.

Vecch et al. [22] applied 3D scanning technique to measure the cross-sectional area of steel strands after corrosion and used the measurements to validate the three methods proposed by Jeon et al. [18] for calculating the cross-sectional area after corrosion based on corrosion depth and a new method for the evaluation of the sample average pit depth was proposed. Lee et al. [23] based on Chi-Ho Jeon's proposed finite element model was developed based on the three cross-section types，and then based on the FE analysis results, a nonparametric surrogate model is constructed using Gaussian process regression. Finally, the ultimate strength and strain of the corroded steel strands are predicted probabilistically by conducting a Monte Carlo simulation with a theoretical strand model. Based on the prediction results, appropriate probabilistic distributions for the ultimate strength and strain are studied.

As the fundamental feature for the estimation of its residual strength capacity, the corrosion morphology of steel strands has attracted more and more attention. Jeon et al. [18] defined three types of pitting configurations for the description of the shapes of corroded strands based on the measured maximum pitting depth. However, as pointed out by Wang et al.[21], irrational results could be obtained when the morphology of pitting was not completely defined only evaluated by depth and width. To this aim, Wang et al. [21] carried out an experimental campaign by analyzing a total of 119 pittings coming from prestressing strands artificially corroded. They classify the pitting as spheroidal, saddle, and pyramidal, and it provided a new relevant parameter for the design and maintenance procedures.

Chen et al.[24] investigated the effect of the direction of the outermost steel wire corrosion pitting on the mechanical properties of the strand by finite element analysis and found that The stress concentration factor, maximum stress, maximum plastic deformation, maximum contact pressure and loading capacity of the strand all increase first and then decrease with the direction angle of the corrosion pitting increase, while After that, Chen et al.[25] established a high-precision finite element model of steel strand with different corrosion directions on the basis of the original one to study the effect of corrosion pitting direction on the mechanical properties of the strand, and came to similar conclusions as the first one The maximum von Mises stress, maximum plastic strain, stress concentration factor, maximum contact pressure and the decrement of bearing capacity did't decrease with the direction angle of the corrosion pitting increase.

1.2.2 Influence of strand corrosion on structural static properties.

As one of the main effects caused by corrosion, the deterioration of bond performance has also been studied in detail by scholars.Wang et al.[26] conducted pull-out tests on 20 beams with corrosion-induced concrete cracking to investigate the effect of corrosion-induced cracks on the bond performance between the strand and concrete. It was found that Corrosion-induced concrete cracking decreases the maximum bond stress between strand and concrete. while Li et al.[27] made 12 pull-out specimens and exposed these specimens to a mixture of chloride and indoor and outdoor natural climates to approximate the actual effects of corrosion. The results of the pull-out tests revealed that corrosion mainly affected the ultimate tensile properties of the strand rather than the bonding properties. Then He fabricated specimens for fatigue pulling tests on the strand in corrosion using fatigue loading[28] and found that corrosion-fatigue life decreased with increased corrosion current density under a constant fatigue action, and the decrease rate also was slower and slower with a trend of exponential function relation.

Li zhao Dai[29], proposed A global model to predict prestressed concrete(PC) cracking induced by strand corrosion. The proposed model considers the three stages: micro-crack formations, cover cracking initiation, and crack width growth. Result show that the critical corrosion loss at the three stages increases with increasing concrete tensile strength and concrete cover, and decreases with an increasing strand diameter and rust expansion ratio.

The effect of prestressing tendon corrosion on the static performance of concrete structures is also manifested in damage morphology, bearing capacity, and deformation, and many related studies have been conducted by scholars.

Zeng, Y Hong[30] fabricated nine post-tensioned concrete (PC) beams and corroded them by applying direct current to them. The damage modes and damage mechanisms of corroded PC beams were investigated by monotonic loading tests. The test results showed that the higher the corrosion rate of PC strands, the lower the cracking, yielding and ultimate bearing capacity of prestressed concrete beams. The PC strands are more prone to corrosion in beams with poor grouting conditions, and the corrosion leads to a severe reduction in the bond strength of concrete and PC strands, which greatly reduces the stiffness of the beam. lei Wang[31] also conducted an experimental study on the effects of inadequate grouting and strand corrosion on the flexural performance of prestressed concrete beams. He designed eight prestressed beams with different degrees of corrosion for four-point bending loading. The results showed that corrosion of the strands in the ungrouted pipes resulted in loss of pretension and reduced the cracking

load of the beams. Different degrees of strand corrosion had different effects on cracking. When the corrosion loss was relatively small (<10%), the number of cracks increased, the crack spacing decreased, and the beams had similar load-crack width behavior. With further corrosion of the strand, the number of cracks decreases, the crack spacing increases, and the main cracks expand faster within the beam. For relatively small corrosion losses (<10%), strand corrosion has a small effect on bending performance and damage modes. In contrast, severe corrosion of the strands resulted in significant degradation of the post-cracking stiffness and ultimate strength of the beams and produced different damage modes.

Xuhui Zhang[32] conducted flexural degradation tests on eight post-tensioned bonded concrete beams with different degrees of corrosion. The effects of corrosion on concrete cracking, stiffness, ultimate strength, strain, damage modes and ductility are discussed. The experimental results surface:Strand corrosion accelerates the shifting of neutral axis and decreases depth of compressive concrete, reducing markedly the ultimate As the corrosion loss increases, the damage mode of the beams changes from concrete crushing to shearing, and the ductility decreases sharply. For mild and moderate corrosion beams, the effect of wire fracture on beam ductility during the test was more significant than that of beam ultimate strength.

Qian-Qian Yu [33] prepared six post-tensioned concrete beams by accelerated corrosion and tested under four-point bending. Variables including the corrosion degree, reinforcement ratio and corrosion of non-prestressed rebars were considered.that, corrosion of PC strands led to a deteriorated flexural bearing capacity of a beam. The cracking load, yield load, and ultimate load all decreased with the corrosion degree. Thereafter, a theoretical approach based on the stress–strain model of corroded steel tendons was proposed to predict of flexural behavior of corroded prestressed concrete beams. Good agreement with experimental results of current study and from literature was observed.

Many scholars have also developed new models or improved existing models based on experiments to simulate more accurately the effect of strand corrosion on the mechanical properties of prestressed beams.

Giuseppe Campione[34] developed a simplified bending model for simply supported beams and introduced the effect of pitting corrosion into the model. The simulation results showed that the corrosion of strands reduce the bearing capacity of the viaducts with prestressed beams especially and because of the reduction of strain capacity of steel strand, arises a risk of brittle collapse under service conditions due to the strand failure.

Zhao-Hui Lu[35] sumrised a total of 70 experimental flexural tests of corroded post-tensioned prestressed concrete (PC) beams were gathered from the Meanwhile, the empirical models for calculating the residual flexural strength of the corroded PC beams proposed by Lin, Li, Qin, Wang were also gleaned and contrasted with the published literatures. It turns out that three of the four existing empirical models underestimate the It turns out that three of the four existing empirical models underestimate the flexural capacity. that the corroded post-tensioned PC beams' residual flexural capacity is affected most by the corrosion ratio.

1.2.3 Fatigue performance of prestressed concrete flexural members

Since the 1970s, many scholars have conducted various experimental studies on the fatigue performance of prestressed concrete structures, and obtained test results on the effects of various factors on the fatigue performance of partially prestressed concrete flexural members, such as fatigue load level, prestressing degree, pre- or post-tensioning

construction, steel strand and concrete bonding, beam section shape, and fatigue load form.

Benneet[36] et al. conducted fatigue tests on partially prestressed concrete beams with post-tensioning with bonding. The tests showed that with high prestressing degree (0.5-0.7) and low fatigue load levels (0.27-0.55), the partially prestressed concrete beams experienced 4 × 106 repeated loadings without fatigue damage and no reduction in static load strength after fatigue.

Abels et al. [37, 38], conducted static load and fatigue tests on partially prestressed concrete beams with low reinforcement ratios. The effects of reinforcement condition, degree of bond, prestressing reinforcement, and non-prestressing reinforcement on the fatigue life of partially prestressed concrete beams were analyzed. The results showed that the non-prestressed reinforcement was beneficial to improve the crack distribution and bond conditions and to increase the effect of bearing fatigue loads, that the degree of bond between the strand and the concrete had an effect on the fatigue strength of the test beams, and that the effective prestress in the test beams would gradually decrease under cyclic loading.

Fauchart et al. [39] conducted isometric fatigue tests on rectangular and shaped partially prestressed concrete beams and concluded that the fatigue damage pattern was related to the shape of the cross section. And et al. obtained the opposite conclusion by high stress equal amplitude fatigue tests on shaped test beams.

Harajli et al. [40] investigated the effect of reinforcement index on the fatigue performance of pretensioned partially prestressed concrete test beams and concluded that increasing the reinforcement ratio of non-prestressed steel bars improved the ductility of the test beams and reduced the fatigue stiffness decay.

EI shahawi et al. [41] fatigue loading tests were conducted on root post-tensioned bonded shaped beams with the test parameter of prestressing degree, varying from 0.2 to 1.0. The results showed that (1) the crack width and dawn degree had a development pattern of initial growth, medium-term stability, and sharp increase at the later stage with the increase in the number of cycles, and the damage of the test beams began with the fatigue fracture of the non-prestressed reinforcement; (2) the partial prestressed (2) in concrete members, reasonable reinforcement of non-prestressed reinforcement can improve the ductility and fatigue deformation capacity of the members, too much prestressing and too little prestressing will lead to early fatigue damage, the value of prestressing degree is 0.3-0.6, and 0.4 is the best value of prestressing degree; (3) the crack width is between 0.85-1.2 of the average crack width.

Yongxiao Du [42] tested the fatigue behavior of prestressed concrete (PC) beam used in a heavy-haul railway under constant-amplitude and variable- amplitude fatigue loading.

The experimental result shows that the fatigue failure mode of PC beam is the fatigue fracture of bottom tensile steel bar in the pure bending section. fatigue characteristic parameters (stiffness, displacement and strain of concrete in compression zone) of variable-amplitude fatigue test beams The fatigue characteristic parameters (stiffness, displacement and strain of concrete in compression zone) of variable-amplitude fatigue test beams exhibit the multi stage development law due to the addition of multi-level fatigue load. Further, on the basis of the fatigue characterization model of classical materials and the stress analysis of fatigue cracking cross-section, a nonlinear numerical analysis method for the whole fatigue process is Further, on the basis of the fatigue characterization model of classical materials and the stress analysis of fatigue cracking cross-section, a nonlinear numerical analysis method for the whole fatigue process is proposed.

1.3 Inadequacy of existing research

The corrosion of PC strands affects the serviceability and safety of prestressed concrete structures, especially under fatigue loading.
Therefore, it is very important to study the deterioration of the performance of prestressed concrete structures caused by the corrosion of prestressing strands, but the current work in this area is not deep enough.

(1) Prestressing tendon corrosion is one of the most important factors to reduce the durability of prestressed concrete structures. At present, the research mainly focuses on the residual properties of PC strands after corrosion, while the research on the effect of corrosion on PC strands in working condition is less, and there is a lack of tests for direct research. And for corrosion pit shape on the mechanical properties of the strand less research.

(2) Although there are more studies on the mechanical properties of prestressing flexural members after corrosion, and there are more summaries of the corrosion degree and damage mode, but because it is difficult to determine the force state of the strand after corrosion, for different degrees of corrosion of the prestressing beam, it is difficult to accurately determine the type of damage and determine the timing of strand fracture.

(3) There are fewer studies on the fatigue performance of prestressed concrete structures after PC strand corrosion, and even fewer studies on the residual performance of beams after fatigue loading.

1.4 Research significance

(1) This paper innovatively combines a relaxation machine with a conventional electrically accelerated corrosion system to simulate the corrosion of steel strands in working state, and to study the effect of corrosion on prestressing force deterioration. The test results are also analysed and explained from the viewpoint of fracture type and corrosion pits.

(2) Corrosion tests on PC beams were carried out with conventional methods, and based on the results of previous innovative research on PC strand corrosion, a new method was used to calculate and study the prestressing force deterioration of PC strands in PC beams.

(3) Although static load tests on PC beams after PC strand corrosion have been carried out by common methods. However, different from previous studies, this paper is based on the previous research on prestressing deterioration and fracture type of corroded PC strands. and combines the deterioration law of corroded PC strands to analyse the role of corroded PC strands in the loading process of PC beams with the corroded PC strands. The failure mode of the beams were analysed from the fracture type of the strands and the fracture of the strands was predicted based on the displacements.

(4) Corrosion before fatigue tests were conducted to simulate the corrosion of beams after the appearance of small cracks due to fatigue loading, and to study the effect of corrosion on the subsequent fatigue damage process. After fatigue loading to a certain number of times, the specimen was subject to static loading, and the test results were compared with those of the specimen directly subjected to static testing, to analyse the reasons for the deterioration of the residual performance of the specimen due to fatigue loading. The results of the previous study were used to predict the specimens after fatigue loading test with strand fracture in the static load test, and the calculated results were compared with the actual results to analyse the

effect of fatigue on the fracture of the PC strands.

1.5 Main research contents

In this paper, the prestressing force after corrosion of PC strands in working condition and its residual mechanical properties are studied, and static and fatigue test research and analysis of prestressing beams after corrosion of PC strands are also carried out, and the main research contents and results are as follows:

(1) The deterioration law of the internal prestressing force of PC strands under working condition and the causes of deterioration were analyzed. The relationship between prestressing tendon mass loss and prestressing stress loss established, tensile tests on corroded PC strands, and the relationship between the degree of corrosion and ultimate tensile strength are summarized. On this basis, the effect of fracture type on prestress loss and ultimate tensile strength is studied, and the reasons for the occurrence of different fracture types are investigated by analyzing the section types.

(2) The relationship between prestress deterioration and corrosion degree in beams, and the effect of different corrosion locations on the initial cracking load and flexural performance are studied. It is proposed to predict the mid-span deflection of the prestressed beam at the time of strand fracture based on the specimen deflection, strand prestress deterioration, ultimate tensile performance of the strand after corrosion, shape of the corroded section of the strand, and then analyze the damage pattern of the specimen through different degrees of corrosion.

(3) To study the effect of the degree of corrosion at different locations on the stiffness deterioration and damage morphology of prestressed beams after corrosion and to compare the effect of different corrosion locations.

(4) After the fatigue test, the specimens after fatigue damage were loaded statically and compared with the specimens with the same degree of corrosion but without fatigue damage to study the effect of fatigue damage on the static load performance of the beam.

In order to reduce the influence of other factors in the research process and to study the effect of corrosion of prestressing strands on prestressed beams more clearly, a specimen beam with a simple structure was designed. Although such simple prestressed structures are seldom used in actual engineering projects. The results of the experimental study can provide a reliable theoretical basis for the subsequent study of more complex prestressed members.

Chapter 2 Corrosion test of PC strands

2.1 Introduction

Corrosion of prestressing strands is one of the most significant factors that reduce the durability of prestressed concrete structures. While previous studies have mainly focused on the mechanical properties of prestressing strands after corrosion, the effect of corrosion on the internal prestressing force of the strands has been ignored. Prestress, as an important parameter of prestressed members, has an important influence on the mechanical properties of prestressed mechanical members, but the loss of prestress in steel strands due to corrosion was mainly theoretical speculation in the previous research.

Resmi et al. [43] predicted the flexural performance of PC beam with corroded PC strands by modeling the loss of cross-sectional area of the strand, but only the prestress loss due to relaxation was considered, and not the prestress loss due to corrosion, which has been proven in previous tests to be much more serious than the prestress loss due to relaxation. Zhang et al.[32] found a reduction in the initial cracking load when they investigated the flexural behavior of bonded post-tensioned concrete beams under strand corrosion and inferred the loss of prestress by calculation. The effect of corrosion on prestress in PC strand needs to be further studied.

The objective of the present study is to investigate the effect of corrosion on prestressing force in PC strands and the mechanism of the stress redistribution in the strand. This paper innovatively combines an electrochemically accelerated corrosion device with a relaxation test machine, which can directly observe the change of prestress during the corrosion process. To study the effect of corrosion on the deterioration of prestressing, to analyse the effect of different section types, fracture types on prestressing and ultimate load carrying capacity, and to provide a theoretical basis for the study of damage analysis of prestressed beams after corrosion in Chapter 3.

2.2 Experimental overview
2.2.1 Details of specimens

In this section, first the material properties are introduced, then the special electrochemically accelerated corrosion test is explained. Herein, combining relaxation test machine and traditional electrochemically accelerated corrosion test, the PC strand in the working status were investigated regarding the prestressing force, the elastic modulus was measured. After conduction the corrosion test, the tensile test was conducted for some corroded prestressed steel strands which was not raptured during the corrosion tests.

Specimens were fourteen 15.2 mm diameter 7-wire steel strands. The length of strand sample was set as 2.5 m to adapt the relaxation loading test machine. The material performances of strand are given in **Table 2.1**.

Table 2.1   Material properties of steel strand.

Type	Nominal diameter	Cross-section area	The weight per meter	Tensile strength	Range of ultimate tensile capacity	Elongation
1×7	15.2 mm	140 mm^2	1101 g/m	1860 MPa	260-288 kN	≥ 3.5%

Note: The ultimate tensile capacity standard of 15.2mm 7 wires strand is from 274kN to 280kN, in this test the ultimate tensile capacity of specimen was 265kN, when one specimen was used.

2.2.2 Accelerated corrosion test

In order to measure the change of prestressing force and elastic modulus of PC steel strand in the corrosion process under working condition, the relaxation testing machine WSC-300 and electrochemically accelerated corrosion device were combined in the test. Tension steel strands to simulate high prestressed working condition of strand in PC beam, and the prestressing force in the strand was continuously measured. The relaxation test machine used here as shown in **Fig. 2.1**. The anchorage end on both sides of machine were used to fix the steel strands, and the side show in Fig.2.1(b) can move to stretch strands, and it stops moving when prestressing force reached target values. The displacement of two anchorage end kept constant, during the test process.

In general, the accelerated corrosion methods can be divided into three conditions: the electrochemical accelerated corrosion, dry-wet alternating corrosion and artificial climate box corrosion. The strands were corroded more evenly by using electronic accelerate method than steel strands in natural environment. In most situations, the effect of cross-sectional area loss caused by two corrosion method on strand properties can be regarded as same.

Due to the existence and limitation of relaxation machine, the latter two methods are difficult to use, and the electrochemically accelerated corrosion method has the advantages of simple operation, short corrosion cycle, low cost, accurate control of corrosion degree, and the most important thing is that it can be more convenient to combine with relaxation testing machine test.
Fourteen corroded steel strand specimens were used to study the influence of corrosion on the prestress and mechanical properties of steel strands. Faraday's electrolysis law was used to calculate the corrosion time, and specimens with different corrosion degrees were obtained by controlling the corrosion time and current intensity. Faraday's first law of electrolysis can be expressed as

$$\Delta w = \frac{M}{NF} IT \tag{2.1}$$

where Δw is mass of metal corrosion; I is current intensity; M is Atomic mass of metal; F is Faraday constant, $1F = 96485$; N is The number of valence electrons lost by oxidation of a metal; T is corrosion time.

Faraday's law is used to calculate the theoretical mass of metal corrosion. The Eq.(2.1) can be translated into Eq. (2.2) to calculated mass loss as corrosion degree.

$$n = \frac{M}{NFm_0} IT \tag{2.2}$$

where, n is a calculated mass loss of the corroded steel stands, m_0 is an initial mass of the corroded steel stands.

Eq. (2.2) can be written as $\frac{nNFm_0}{MI} = T$ to calculated corrosion time

The test device is shown in **Fig. 2.2** and the diagram of test setup is shown in **Fig. 2.3**, respectively. The $100*100*500$ or $100*100*300$ mold is installed in the center of the relaxation test machine as a tank filled with water to corrode the steel strands at 500 mm or 300mm in the middle. The corrosion system consisted of the direct current galvanostatic, the strand anode, and the stainless-steel plate cathode submerged in the 5% saline solution.

Drill holes on the lower part of both sides of the tank so that the strand passes through it, apply structural adhesive to the side of the holes between the strand and the mold to prevent sodium chloride solution from leaking out, and wrap the non-corroded

part of the strand with transparent tape to prevent the solution from flowing out along the internal pores of the strand. The fixed steel plate was installed on the steel strand has a displacement along with the elongation of the steel strand. The displacement of the steel plate in the test process is measured by the sensor, that is, the longitudinal deformation of the steel strand, as shown in **Fig. 2.4**. The initial distance of the sensor was set as 1m, and the initial tension distance of the relaxation machine was set as 1.5m, and the anchorage device was shown in **Fig. 2.5**. Epoxy resin is applied to the anchor end of the relaxer to prevent the anchor end from corrosion. To ensure that the current will not affect the normal operation of the relaxer, the corrosion current was smaller at 0.5 A or 0.35 A. When the prestressing load reached the target load, the displacement of the tensile end was kept constant until the end of the test.

| (a) | (b) |
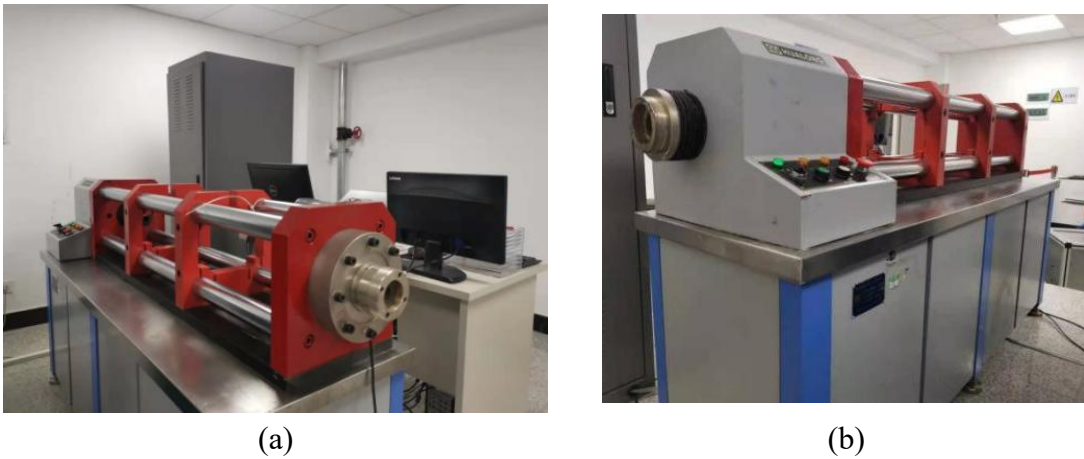
Fig. 2.1   Microcomputer controlled tensile stress relaxation testing machine WSC-300
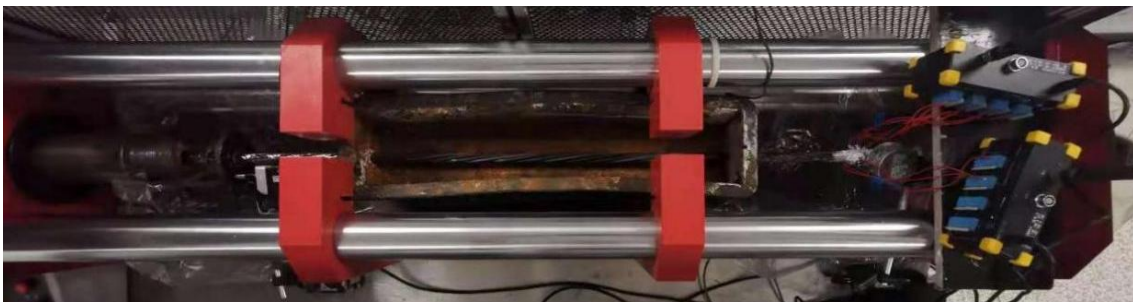
Fig. 2.2   Corrosion test setup with a relaxation test machine
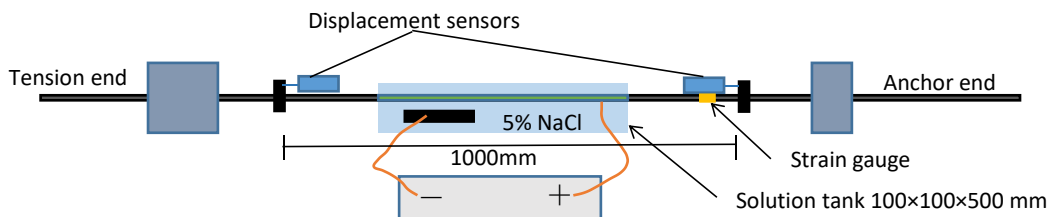
Fig. 2.3   Outlines of corrosion test under sustain tensile loading

Fig. 2.4 Steel plate and displacement sensor

Fig. 2.5 Anchor device

2.2.3 Tensile loading test

A tensile loading test was carried out on 9 steel strands which showed without fracture during the previous corrosion test. The electric hydraulic servo universal testing machine as shown in **Fig. 2.6** was used to tension the steel strand. To facilitate the tensile test, the test strands were cut to 1000 mm (including the corroded section) and protected at both ends with clamps. In the tensile test, two end sides of the strand are held by the grip. If the grip wedge contacts, the surface of a strand directly, crack can be propagated from the wedge earlier than the tensile strength of the wire due to stress concentration. For this reason, Kim et al. (2014) suggested to wrap the end parts with a silica-coated aluminum sheet to protect the end parts. This method was adopted in this study. The loading speed was controlled by displacement, and was set at a rate of 1 mm/min. The load data was automatically read by the tension tester.

Strand was considered to reach the ultimate tensile force once the steel wire was reputed as stipulated in the Chinese Standard (China GB/T 5224-2014 2014). The failure modes of specimens with different corrosion degree were compared to investigate the fracture mode of steel wire under different corrosion losses. The relationship between the ultimate tensile strength and corrosion degree curve was drawn to summarize the effect of corrosion on the tensile capacity of the strand. For the steel strand failed in tension test, the corroded section was re-intercepted after test, cleaned with 12% hydrochloric acid, and measured the weight to calculate the mass loss of the corroded steel wires. The tested wires in the PC strand are shown in **Fig. 2.7** as a sample.

Fig. 2.6 SHT4106G microcomputer control electro-hydraulic servo universal testing machine

Fig. 2.7 Disassembled corroded steel wires

2.3 Effect of corrosion on prestressing force
2.3.1 Specimen group

The detailed specimens' group of the first test is shown in **Table 2.2**. In order to study the influence of different corrosion degrees on the steel strand of different prestress grades, the specimens are divided into two series: 70- series and 50-series.

The initial tension stress of the strand was used to reflect the prestress level in the present study. The initial tension stress of series 70 and 50 were 70% and 50% of σ_s, respectively, where σ_s is the tensile strength of the steel strand. The 70-series contained 3 groups, and the 50-series contained 2 groups. Each group consisted of three strand samples except 70-2, it only includes 2 specimens.

Table 2.2　Grouping of specimens

Series	Symbol	Target corrosion degree %	Corrosion time/h	Stress level
70-series	70-0-1	0	0	$0.7\sigma_s$
	70-2-1	2	30	
	70-2-2	2	30	
	70-5-1	5	75.20	
	70-5-2	5	75.20	
	70-5-3	5	75.20	
	70-10-1	10	150.42	
	70-10-2	10	150.42	
	70-10-3	10	150.42	
50-series	50-0-1	0	0	$0.5\sigma_s$
	50-5-1	5	75.20	
	50-5-2	5	75.20	
	50-5-3	5	75.20	
	50-10-1	10	150.42	
	50-10-2	10	150.42	
	50-10-3	10	150.42	

Note: σ_s is the tensile strength of the steel strand. When tensile force reached target values,most specimen start corrosion test, the 70-10-2, 70-10-3 and 50-10-1 start corrosion test after tension 10 hours, during the corrosion test, the distance between the two anchorage ends remains constant.　The corrosion tests were terminated when wires were fractured or specimens reached a target corrosion degree.

Table 2.3　Corrosion test result

Specimen No.	Prestress degree	Mass loss %	Max mass loss %	Prestress loss %	Test series the wire was raptured
70-0-1		0.00	0.00	0.76*	-
70-2-1		2.00	2.70	2.20	T
70-2-2		1.90	3.70	2.36	T
70-5-1	70% (182 kN)	6.00	6.24	2.80	T
70-5-2		4.54	4.95	3.50	T
70-5-3		4.46	5.30	3.15	T
70-10-1		9.00	10.5	7.40	C
70-10-2		8.20	9.50	5.66	C
70-10-3		5.80	9.60	3.30	C
50-0-1		0.00	0.00	0.66*	-
50-5-1		5.60	5.85	3.20	T
50-5-2	50% (130 kN)	5.10	6.24	3.50	T
50-5-3		7.15	7.50	3.60	T
50-10-1		8.54	9.90	4.54	C
50-10-2		7.80	8.80	3.65	T
50-10-3		8.40	9.10	4.00	T

Note: Max mass loss means mass loss of the fractured wires. Test series the wire was raptured: C means failure in the corrosion test, T means failure in the tensile loading test. *Prestress loss caused by relaxation (the prestress loss of 70-0-1 and 50-0-1 were calculated by the data of 96th hours).

(a) 70 series　　　　　　　　　(b) 50 series
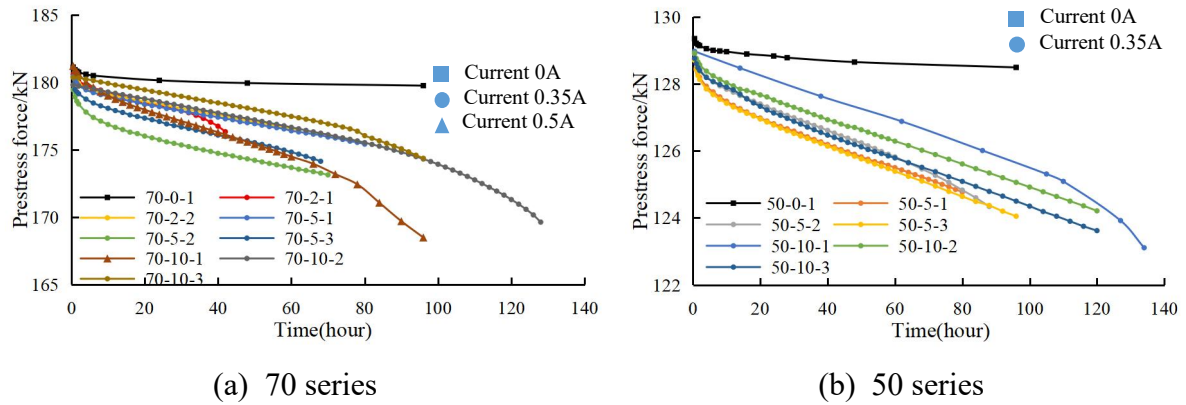
Fig. 2.8　Prestressing force versus corrosion time curve

2.3.2 Results of corrosion tests

Fourteen steel strands were subjected to electrochemically accelerated corrosion under the action of corresponding tensile stress, and the test results are shown in **Table 2.3**. Due to effect of bond stress and concrete cracks, there are some difference of prestress loss which caused by corrosion between the PC strands and PC structures. The mass loss and maximum cross-sectional loss of strand or a wire are generally two main parameters to reflect the corrosion level. The mass loss in this study presents the average corrosion level of the PC strand, which is more suitable for the uniform corrosion or global corrosion of samples. In contrast, the maximum cross-sectional loss can reflect the severity of local corrosion and is suitable for reflecting pitting corrosion of samples. In the experiments, the fracture of steel wires was a sign of the failure of PC steel strands, so the mass loss of fractured steel wire can better reflect the damage of steel strand than the mass loss of the whole strand.

Consider the three specimens 70-10-1, 70-10-2 and 70-10-3 which were corroded to fracture as an example. The mass loss was quite different, but the difference of fracture wires' mass loss was quite small. However, the prestressing force was influenced by the properties of the whole steel strand, and the mass loss of the whole strand has a better correlation with loss of prestress. Therefore, the mass loss of whole strands was focused on to express the corrosion degree in this study.

2.3.3 Prestressing force versus corrosion time

The prestressing force of the specimen with two prestress levels was measured during the corrosion test and is summarized in **Fig. 2.8**. For uncorroded specimens 70-0-1 and 50-0-1, the prestressing force decrease rapidly at early hours, due to relaxation properties, and then almost never decreases again. As for corroded specimens, the prestressing force of both groups declined continuously as the corrosion time goes by. Among them, specimen 70-10-1 used a corrosion current of 0.5 A., which corroded faster, so the prestressing force dropped faster than the other specimens. The prestressing force of most of the specimens decreased rapidly in the initial stage of the corrosion test, which was due to an effect of the relaxation of the steel strand. While specimens 70-10-3, 70-10-2, and 50-10-1 were corroded after 10 hours under tension, the effect of relaxation properties on prestressing force almost disappeared and did not show a stage of the rapid decline of prestressing force at the initial stage, but declined steadily in a linear relationship with the growth of corrosion time. For the specimens 70-10-1, 70-10-2, 70-10-3, and 50-10-1 which were finally fractured during the corrosion test, as the increase of corrosion time, prestressing force was decreased rapidly. In addition, the maximum cross-sectional area loss was serious, and the strand

16

tensile properties were reduced when the plastic deformation occurred at the section of corrosion pitting, resulting in an accelerated decline in prestress. Specimens 70-10-1 and 70-10-2 had large deformation at the corrosion pitting, and the prestressing force dropped severely during the destruction stage, while specimens 70-10-3 and 50-10-1 had a small deformation at the corrosion pitting, and the prestressing force reduced relatively small.

Table 2.4   Measured and calculated mass losses (corrosion degrees)

Specimen No.	70-2-1	70-2-2	70-5-1	70-5-2	70-5-3	70-10-1	70-10-2	70-10-3
Measured mass loss (%)	2.00	1.90	6.00	4.54	4.46	9.00	8.20	5.8
Calculated mass loss (%)	2.80	4.10	5.30	4.65	4.50	9.10	8.50	6.38
a	0.71	0.46	1.13	0.98	0.99	0.99	0.96	0.91

Specimen No.	50-5-1	50-5-2	50-5-3	50-10-1	50-10-2	50-10-3
Measured mass loss (%)	5.60	5.10	7.15	8.54	7.80	8.40
Calculated mass loss (%)	5.32	5.85	6.38	8.90	8.00	8.00
a	1.05	0.87	1.12	0.96	0.98	1.05

2.3.4 Calculated corrosion degree

One of the significant advantages of the widely used accelerated corrosion method is that the theoretical mass of steel strand corrosion can be calculated according to Faraday's first law of electrolysis based on the current intensity and corrosion time.

According to the Eq. (2.2), the time history of corrosion degree was calculated by corrosion time and current intensity, and the relationship between prestressing force and time was transformed into the relationship between prestressing force and corrosion degree.

Comparison between the measured and calculated mass losses due to the corrosion are summarized in **Table 2.4**. It is found that the calculated values of most specimens are close to the measured values. According to the Eq. (2.2), it can be found that the corrosion degree is linearly related to the corrosion time. In the previous section mentioned that the prestressing force with the increase in corrosion time linear decline, so it can be considered that the prestressing force with the increase in the degree of corrosion linear decline. The accuracy of Faraday's law is affected by a variety of factors, such as chloride ion concentration, current density, temperature, etc. In this test, the calculated values of some specimens differ greatly from the actual values due to the crystallization cleaning of the corrosion tank and the change of weather and temperature.

However, it can be seen from **Fig. 2.8** that the relationship between prestressing force and corrosion time is also linear for specimens with different calculated values

and measured values, so it can be assumed that the relationship between corrosion time and corrosion degree is also linear, but the slope is different. Thus, Eq. (2.2) can be written as;

$$n = a \frac{M}{NFm_0} IT \tag{2.3}$$

where, a is a variable parameter for each specimen and obtained as the measured mass loss divided by the calculated mass loss based on Eq. (2.2).

2.3.5 Failure mode of corroded strands in the corrosion tests

The failure modes of the raptured steel strand during the corrosion test are analyzed. The failure conditions of the four corroded strands are summarized in **Fig. 2.9**. It can be found from the figure that different from the uniform corrosion of steel bars in the state without prestressing [44, 45]. The corrosion on the surface of the steel strand was not uniform despite the electrochemically accelerated corrosion method was adopted. The corrosion of steel wire around the fracture was severe, and the corrosion pitting was occurred wide and deep, while the corrosion degree of other parts of the steel strand was slight, and the fracture position of the steel strand is random, and the steel wire becomes slender at the fracture point, and the fracture is either neat or staggered. It is because that after corrosion the steel strand produced micro-cracks and its local tensile performance decreased, and the high prestress level damage to the weak position further strengthened the corrosion effect. The steel strand deformation occurred in the place where the cross-sectional area loss was greater, and the corrosion condition at the fracture position is more serious than other position.

(a) 70-10-1   9.2%   (b) 70-10-2   8.8%

(c) 70-10-3   5.8%   (d) 50-10-1   9.5%
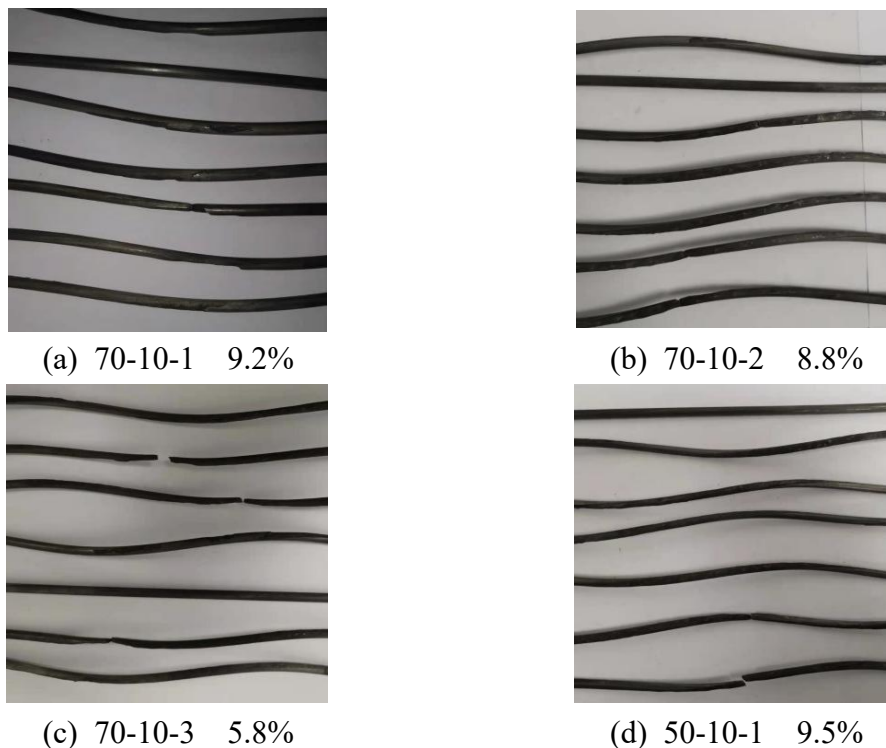
Fig. 2.9   Corrosion condition of the steel wires

| Cup and cone type | Milling cutter type | Split type | Milling cutter-Split type |

Fig. 2.10   Fracture type of corroded steel wires

Table 2.5   Fracture condition of corroded steel wires after corrosion test

Specimen NO.	Fracture section	Fracture type	Necking degree	Mass loss %	Prestress loss %
70-10-1		Milling cutter type	Severe	9.00	7.46
70-10-2		Milling cutter type Cup and cone type	Severe	8.20	6.29
70-10-3		Split type	None	5.80	3.67
50-10-1		Milling cutter type Split type	Slight	8.54	4.54

All the fracture type can be divided into three basic fracture types: cup and cone type, milling cutter type, split type and their combination. Macroscopic photos of various fracture type are shown in **Fig. 2.10.** Cup and cone fracture type consists of cup and cone conjugate. A cup consists of a bottom and a wall (also known as a clipped lip). Some have a wide, flat bottom, while others have a narrow, v-shaped bottom. The milling cutter fracture type consists of many "small ridges" radially distributed along the transverse radius line. Split fracture is composed of several split surfaces, the color is relatively bright.

Necking phenomenon appears near both cup and cone fracture type and milling cutter fracture type (the necking degree of the cup and cone type is relatively light), Both are ductile failure. There is no obvious necking phenomenon near split type and split - milling cutter type, which belong to brittle failure.

The cross-sectional conditions of the four specimens are shown in **Table 5**. it can be found that 70-10-1 is milling cutter fracture, and 70-10-2 were milling cutter fracture and milling cutter-cup and cone fracture. Both of them showed necking phenomenon near the fracture, they were ductile fracture; for 70-10-3 and 50-10-1, they were splitting fracture and Split - milling cutter type, respectively, they are not obvious necking phenomenon near the fracture, belong to the brittle fracture. Therefore, the steel wire in the corrosion strand could occur both ductile fracture and brittle fracture.

2.3.6 Effect of corrosion on prestressing force

The relationship between corrosion degree calculated by Eq. (2.3) and prestressing force are shown in **Fig. 2.11** in which the parameter of *a* for each specimen was calculated separately. It can be found from the figure that the prestressing force decreases continuously with the increase of corrosion degree, but this graph does not remove the effect of relaxation property on prestress, so it can be found that the prestressing force of the strand except for specimens 70-10-3, 70-10-2 and 50-10-1 decreased rapidly at the initial stage, and after 5-6 hours. After corrosion degree reached around 0.8%, the effect of relaxation property on prestressing force almost disappeared,

prestressing force decreased linearly with the increase of corrosion degree. As the corrosion of the strand increased, the cross-sectional area decreased, and a large amount of plastic deformation occurred. When the corrosion became severe, the prestressing force decreased rapidly until the specimen was failed.

In order to compare the prestress deterioration of specimens with different prestress degree, a prestress ratio, $Pc/P0$ that is a ratio of prestressing force of corroded strands to that of uncorroded strand is defined in the present study, and is shown in **Fig. 2.12**. Comparing the prestress ratios of 70-series and 50-series, the deterioration pattern of prestressing force is the same for both prestress levels of strand, while the loss of prestressing force in the strand at the 70-series prestress level is more severe than in the 50-series with the same degree of corrosion, and the difference is increasing as the corrosion degree continues to rise, the maximum difference is 64.3%.

Figure 2.13 is summarized the prestress loss versus corrosion degree when corrosion test were terminated. A similar pattern can be observed so that the prestress loss became larger as the corrosion degree increased, although the prestress loss was slightly larger in 70-series than in 50-series at the corrosion level of around 8% or more. This is because when the strand is severely corroded, the corrosion pits produced a large amount of plastic deformation and the prestressing force decreased rapidly.

(a) 70-series   (b) 50-series
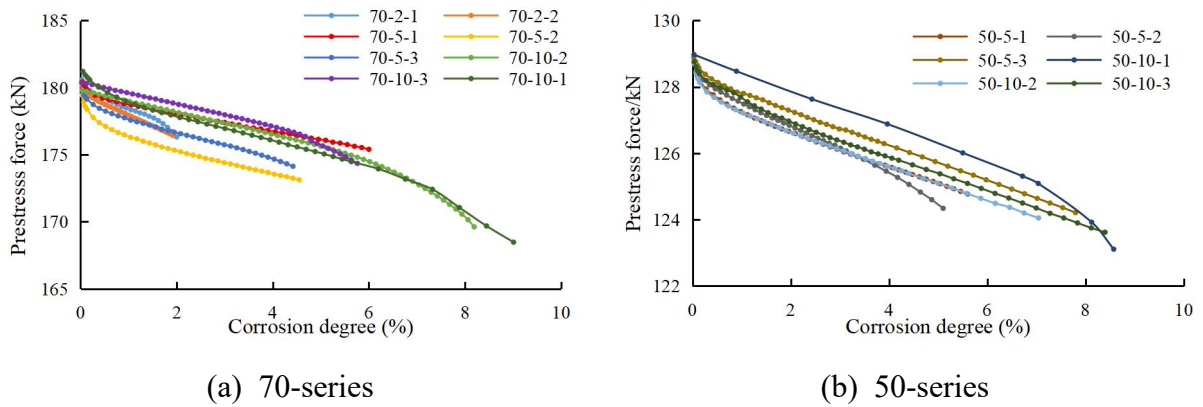
Fig. 2.11   Prestressing force versus corrosion degree
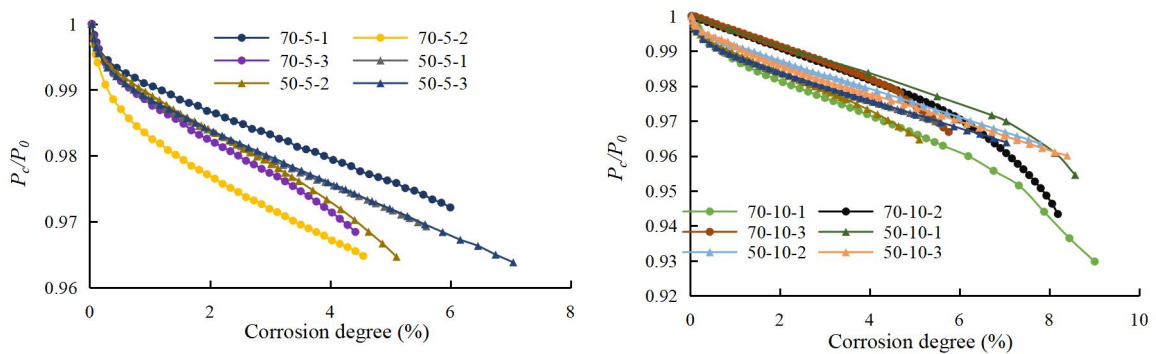
Fig. 2.12   Prestress ratio versus corrosion degree
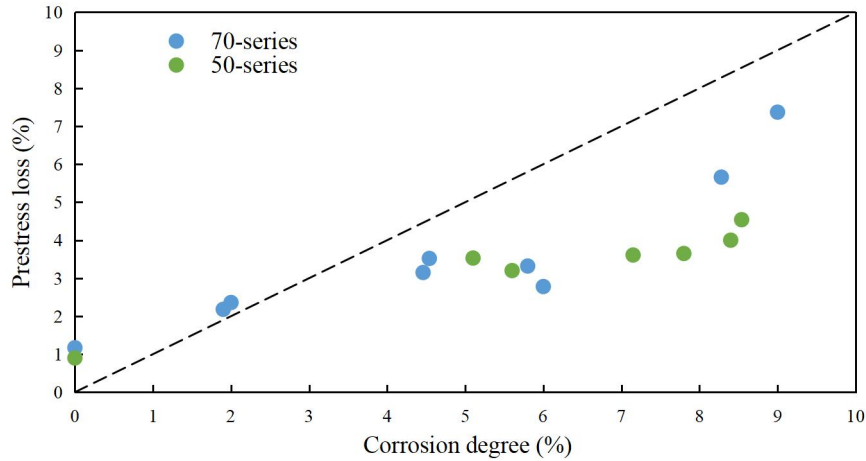
Fig. 2.13   Relationship between prestress loss and corrosion degree

2.3.7 Reduction process for prestressing force of corroded PC strand

The whole process of prestressing force with increasing corrosion degree can be divided into three stages, as shown in **Fig. 2.14** for specimen 70-10-1 as an example. In the first stage, the prestressing force decreases rapidly due to an influence of relaxation properties and corrosion. In the second stage, the strand relaxation properties have almost no effect on the prestressing force, and the prestressing force decreases linearly under the action of corrosion. As for the third stage, with the increase the degree of corrosion, the maximum cross-sectional area of the strand is severely reduced. In this stage, the tensile properties are reduced. When the yield strength is reduced to less than the prestress, the strand shows the plastic deformation, and then the prestressing force is significantly reduced. The specimens that are not corroded severe do not reach this stage. This phenomenon occurs in electronic accelerate corrosion method. The strand was corroded more uniformly by using electronic accelerate method than that under natural environment. Thus, if the strands which were corroded by two method have same mass loss, the cross section loss of strand which were corroded in natural environment is more severe than that were corroded by electronic accelerate method. The prestress deteriorated process of steel strands under natural environment needs further study.

The first stage therefore ends when the effect of strand relaxation performance on the prestress disappears, independent of the degree of corrosion, 70-10-2, 70-10-3 and 50-10-1 three specimens do not have this stage because corrosion began 10 hours after tensioning, while the second stage is completely caused by corrosion to reduce the prestressing force of the strand, and the relationship between them is linear. The reason for the emergence of the third stage is severe corrosion cause plastic deformation of steel strands, it makes prestressing force is decreased rapidly. It was observed that the fracture was occurred in the most corroded and deformed wires. Therefore, as compared with the mass loss of the whole strand, the expression of corrosion degree by the mass loss of fractured steel wire can more accurately reflect the degradation law of prestress in third stage.

The corrosion law of fractured wires can be assumed to be correspond to the Faraday's first law of electrolysis in this study. The degree of mass loss of fractured wires at each time was calculated by Eq. (2.3) to show the process of mass loss during the corrosion test, as show in **Fig. 15**. It can be seen from this figure that the beginning of the third stage of prestressing force was more regular when corrosion degree was expressed by the mass loss of fracture wires. The mass loss of the fractured wires at the

beginning of the third stage is defined as the critical mass loss in this study. The critical mass loss was concentrated between 7.5% and 8.5% of the fracture wires' mass loss. In addition, although 70-10-3 occurred brittle failure, its fracture type was the split type, no necking phenomenon, and its deformation was the smallest, thus, prestress loss of 70-10-3 seemed to be the least in third stage.
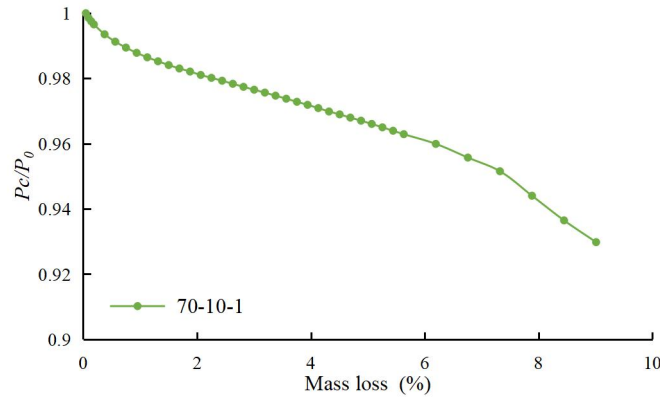
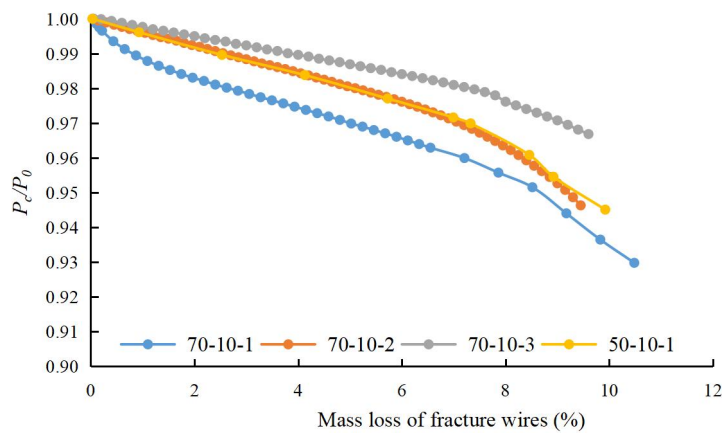Fig. 2.14   Reduction process of prestressing force of corroded steel strand

Fig.2.15   Prestress ratio versus corrosion degree obtained by Eq.(2.3) for corroded steel strands which was fractured during the corrosion test

2.3.8 A model for predict prestressing force of corroded PC strands

The three stages of prestress decline, the first stage mainly affects the prestress reduction factors are the relaxation performance of the strand as well as corrosion, while the relaxation performance of the strand is only related to time and has nothing to do with the degree of corrosion. In the third stage, the prestressing force is reduced due to a large amount of plastic deformation of the wire at the corrosion pit. The deformation depends on the different fracture modes of the strand, which occur randomly, so the prediction of the reduction of prestressing force becomes difficult. Therefore, this paper mainly studies the linear relationship between the second stage of prestressing force and the degree of corrosion. Separate interception of two prestress level specimens after 24 hours of corrosion time, and the strand did not occur in the third stage of the test data are summarized in **Fig. 2.16**. According to the figure, the model of prestressing force and corrosion degree relationship is assumed to be a liner equation. The test data for the 70-series and 50-series specimens were fitted and calculated.

$$P_c/P_0=-0.45n+1.0 \tag{2.4}$$

where, P_c is the prestressing force of the steel strand after corrosion; n is the corrosion degree of the steel strand; P_0 is the prestress load at 24 hours of corrosion time.

It can be seen from **Fig. 2.16** that the test data were used for verification and the proposed model had a good prediction accuracy, which can be employed to predict the prestress-corrosion degree curve of corroded PC steel strands.
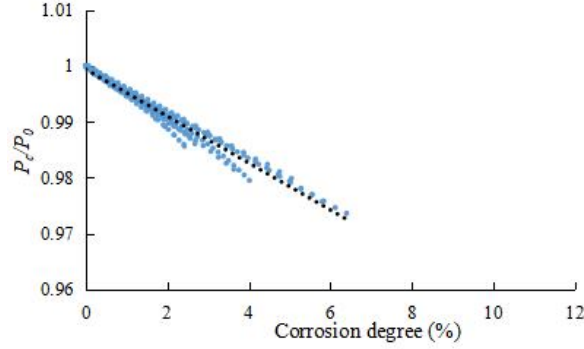
Fig.2.16　Relationship between prestressing force and corrosion degree

2.3.9 Nominal elastic modulus

Regarding how corrosion reduces the prestress of the strand, it is conjectured that corrosion leads to a reduction in the elastic modulus of the strand, which deforms and reduces its prestress. The modulus of elasticity of the test strand was calculated by the following equation.

$$E = \frac{\sigma}{\varepsilon} = \frac{F/A}{\Delta L/L_0} \tag{2.5}$$

where, F is the prestressing force; A is an initial cross-sectional area which is not reduced due to corrosion; ΔL is an elongation; L_0 is an original length of specimens.

The follow equation is elastic calculation formula.

$$K = F/\Delta L \tag{2.6}$$

where, K is elasticity coefficient.

According to the Eqs. (2.5) and (2.6), the formula of elasticity coefficient and elastic modules of PC strand can be written as;

$$K = E \cdot A/L_0 \tag{2.7}$$

Corrosion caused the cross section loss and nominal elastic modules declined. When the mass loss of steel strands is same , it can be assumed that average cross-sectional area loss is same. According to the Eq(2.7), the lower elastic modules, the lower elasticity in this test, when cross section area is same and initial length is constant. This decrease in elasticity leads to prestress loss. Thus, with the decrease of nominal elastic modules, the the prestress decreases continuously.

The ratio of the elastic modulus after corrosion to the elastic modulus before corrosion of specimens with different corrosion degrees is used to represent elastic properties. When corrosion test terminated, measure the mass loss and calculate the ratio of elastic modulus. the influence of corrosion degree on the elastic modulus is observed, as shown in **Fig. 2.17**. The results include the elastic modulus ratio of uncorroded strand in this figure. The results show that there is a small decrease in the modulus of elasticity with increasing corrosion degree for both 70-series and 50-series while that of 70-series decreased further at the corrosion degree of around 8% or more.
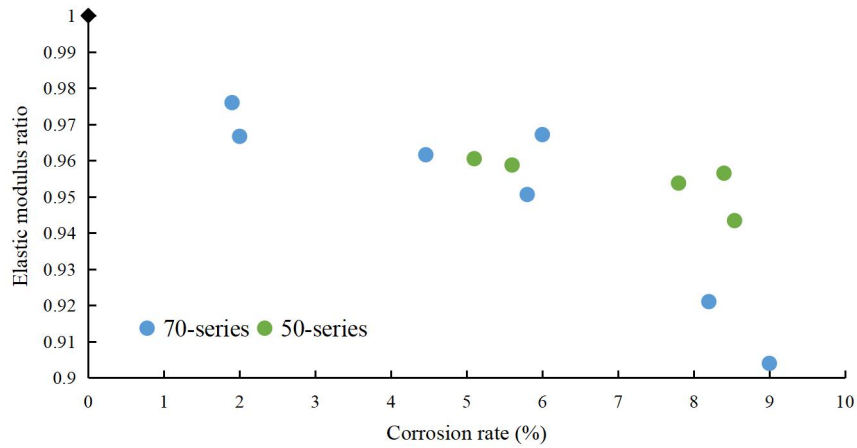
Fig. 2.17   Relationship between elastic modulus ratio and corrosion degree

2.4 Results and discussion of tensile loading tests
2.4.1 Failure mode

The tensile loading test was carried out on the nine steel strands that was not raptured during the corrosion test. The fractography on the fracture surfaces of corroded steel wires with different corrosion degrees were conducted after the tensile loading tests. The fracture surfaces are shown in **Fig. 2.18**. The fracture surface of uncorroded steel wire exhibits a necking phenomenon, which can be considered as a ductile fracture. After the corrosion test, the maximum tensile strength of steel strand decreases, and also the failure mode changes from ductile failure to brittle failure. There is no obvious necking phenomenon at the fracture of steel strand. The results of tensile test indicated that the corroded strands failed at the location with minimum cross-sectional area. Thus, the corrosion degree in the tensile test section is indicated by the mass loss of fracture wires which is closer to the maximum cross-sectional area loss.

| Uncorroded (0%) | 70-2-1 (2.67%) | 70-2-2 (3.68%) | 70-5-1 (6.24%) | 70-5-2 (4.95%) |
| 70-5-3 (5.33%) | 50-5-1 (5.85%) | 50-5-2 (6.24%) | 50-5-3 (7.53%) | 50-10-2 (8.82%) |
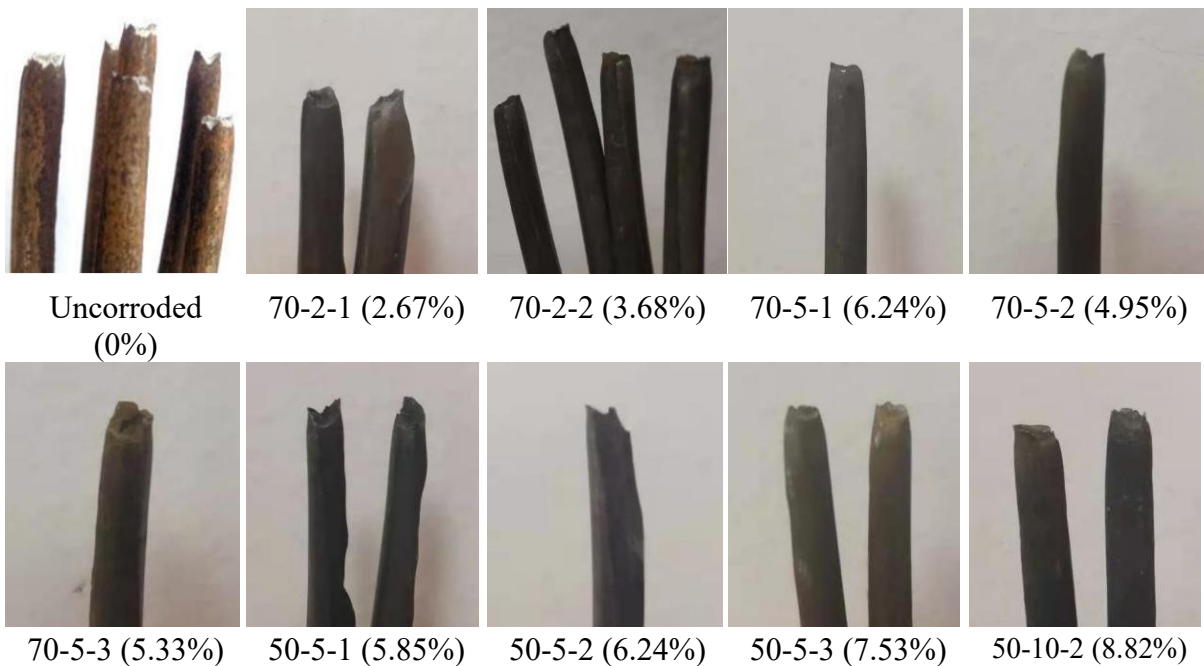
Fig. 2.18   Fracture section of corroded steel wires after tensile loading test

24

2.4.2 Ultimate tension capacity of corroded strand

The tensile test results are summarized and the relationship between the ultimate tensile capacity and the corrosion degree for the steel strand is shown in **Fig. 2.19**. Compared with the uncorroded steel strand (0%) of which the ultimate tensile capacity was 274 kN, the tensile capacity of the corroded steel strand was obviously decreased, but there was no obvious rule in the change of ultimate tensile properties with the increase of the mass loss of the fracture wires. The fracture section of specimens and ultimate load for each specimen are summarized in **Table 2.6**, in addition to the max mass loss as a corrosion degree.

According to **Table 2.6**, the corrosion degree of 70-2-1 was 2.67% and the ultimate tensile capacity was only 187 kN; the corrosion degrees of 70-5-1 and 50-5-2 are both 6.24%, but their ultimate tensile loads differ by 6.5%. Observing the fractures, it can be found that 70-2-1 and 50-5-2 are split type, which is a brittle fracture; 70-5-1 is a milling-cup cone type, which is a ductile fracture.

The ductile fracture originates from the plastic deformation that occurs first at the corrosion pitting. Subsequently, a more sufficient redistribution of stress and strain occurs in each section in which the corrosion pitting occurred in the wire. In contrast, brittle fracture originates from cracking caused by localized plastic deformation at the bottom of the corrosion pitting. And once cracked, rapid destabilization extends to full section fracture, namely the initial fracture and limit fracture occur almost simultaneously. Therefore, the ultimate tensile strength of the wire with a split fracture is lower than other fracture types. When the corrosion degree is the same, the ultimate tensile capacity of the strands which occurs in brittle failure with Split fracture type is lower.

Therefore, the fracture mode determines the ultimate tensile resistance of the steel strand. The different fracture modes of corroded steel wire in the strand depend on the fracture effect characteristics of the corrosion pitting, and the characteristics of fracture effect depend on the geometric characteristics of corrosion pitting. However, corrosion is random, it is a probabilistic problem that corrosion pits lead to split fractures. Therefore, the relationship between corrosion degree and ultimate tensile capacity was not obvious for this test.
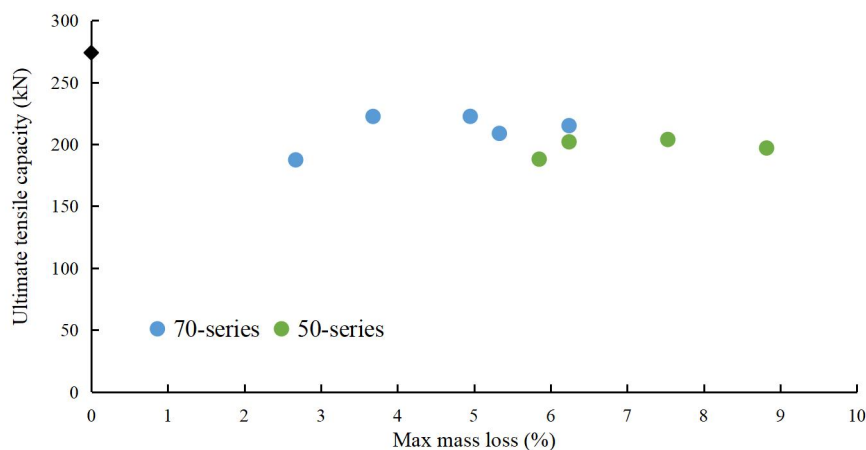
Fig. 2.19　Relationship between ultimate tensile capacity and corrosion degree (Max mass loss)

Table 2.6　Fracture condition of corroded steel wires after tensile loading test

Specimen NO.	Fracture section	Fracture type	Necking degree	Max mass loss %	Ultimate tensile capacity kN
70-2-1		Milling cutter-Split type	Slight	2.67	187
70-2-2		Milling cutter type	Severe	3.68	223
70-5-1		Milling cutter type	Severe	6.24	215
70-5-2		Milling cutter-Split type	Severe	4.95	223
70-5-3		Milling cutter-Split type	Slight	5.33	208
50-5-1		Split type	None	5.85	188
50-5-2		Split type	None	6.24	202
50-5-3		Milling cutter-Split type	Medium	7.53	204
50-10-2		Milling cutter type	Severe	8.82	197

2.5 Mechanism of reduction on prestressing force of corroded PC strands
2.5.1 experimental program

The relationship between mass loss due to corrosion and the prestressing force has been investigated in first series tests. However, the wires fractured as an initiation of the failure, and the mechanism of loss of the prestressing force due to the corrosion and its tension capacity needs further study.

The test was performed on a total of 16 strands to study the effect of corrosion on the wire and the changes in the wire during the corrosion process. Calculated using Faraday's law, by controlling the corrosion time and current strength to control the degree of corrosion of the specimen, according to the target corrosion degree of the specimen into three groups. The initial tension stress of the strand was used to reflect the prestress level in the present study. According to the previous study, it was found that the higher the prestress level of the strand the easier it is to fracture again at lower corrosion levels. In order to investigate the effect of corrosion on the steel strand, it is necessary to make the steel strand more corrosion graded and more severe corrosion before failure, so this test chose a lower prestress level, the prestress level was set as 50% of σs, where σs is the tensile strength of the steel strand. According to the target corrosion level, specimens were divided into three groups, using Faraday's law to calculate the corrosion time and current strength, by controlling the corrosion time and current strength to control the degree of corrosion of the specimens, the specific grouping is shown in **Table 2.7**

Figure 2.20 shows the diagram of test setup. The 100×100×300 plastic tank was installed in the center of the relaxation test machine as a tank filled with 5% sodium chloride solution to corrode the steel strands at 300 mm in the middle of steel strands. The corrosion system consisted of the direct current galvanostatic, the strand anode, and the stainless-steel plate cathode submerged in the 5% saline solution. Cut holes in the lower part of both ends of the corrosion tank so that the strand can pass through it. To prevent the solution from leaking out, the pores between the strand and the corrosion

Table 2.7   Grouping of specimens.

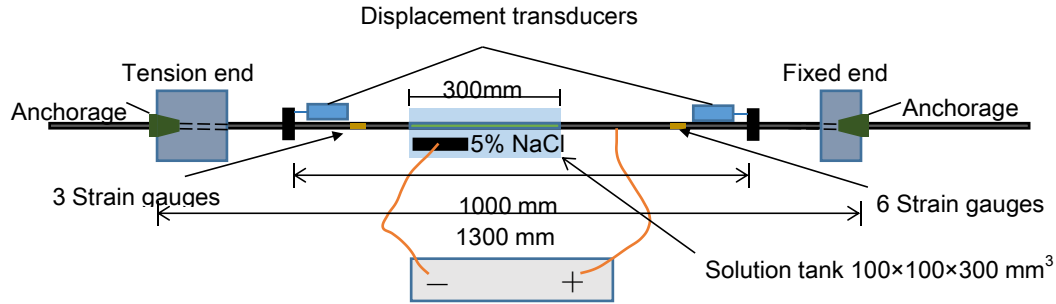| Series	Symbol	Target corrosion degree (%)	corrosion time (h)	Prestress level
0	50-0-1	0	0	$0.5\sigma_s$
5	50-5-1 ~ 6	5	52.6	(130kN)
7	50-7-1 ~ 5	7	73.7	
10	50-10-1 ~ 5	10	105.3	

Fig. 2.20   Outlines of corrosion test under sustain tensile loading

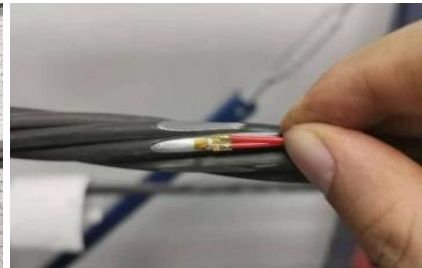Fig. 2.21   Steel plate and displacement transducer

Fig. 2.22   Anchorage device

Fig. 2.23 Pasted strain gauge

tank were sealing and the non-corroded section of the strand was wrapped with adhesive tape to prevent the solution from flowing out along the pores inside the strand. The strand on both sides of the corroded part was fixed steel plates and displacement transducers were set to measure the change in elongation of the strand during corrosion, as shown in **Fig. 2.21**. The initial distance of the displacement transducers was set as 1000 mm. The distance between the two anchor points before tension was 1300 mm, and the anchorage device was shown in **Fig. 2.22**. Before corrosion test started, the outer ring wires of the strand were marked and numbered as No.1 to No.6, and strain gauges were pasted on the uncorroded section of the outer ring wire between the displacement transducers, as shown in **Fig. 2.23**. Six gages on the right and three gages on the left as a supplement was set to measure the strain change in each wire of the outer ring during corrosion.

Epoxy was applied to the anchored end of the relaxation machine to prevent the machine from rusting. To ensure that the current would not affect the normal operation of the relaxation machine, the current was set as smaller at 0.5A. When the prestressing load reached the target load, the displacement of the tensile end was kept constant until the end of the test. For the first 12 hours after the PC strands has been stretched, the strand relaxation has a great influence on the prestressing force. In order to avoid the effect of strand relaxation on the loss of prestress, the corrosion test was started 20 hours after tensioning. At this time, the relaxation of the strand has almost ignorable effect on the loss of prestress. When the wire fractured or reached the corrosion target, the corrosion test was terminated. After the corrosion test, the 300 mm corroded section

of the strand where the wire was fractured was cut off and cleaned with 12% hydrochloric acid

2.5.2 Tensile loading test

The tensile tests were conducted with a universal testing machine. A total of ten steel strands which did not fracture in the corrosion test were used in the tensile loading test. The displacement control method was adapted and tested until the specimen was fractured in the loading test. The loading speed was set to 5 mm/min. As the first occurrence of fracture of one steel wire was the failure sign of a specimen, the loading test stopped when a wire was raptured. In order to let the specimen has enough length for a tensile test, the length of the strand was cut to 1000 mm of which the corrosion section of 300 mm was at the middle part. In the tensile test, two end sides of the strand are held by the grip. To prevent cracks in the part of the grip wedge in contact with the strand end due to stress concentration before the strand reached its ultimate tensile strength, tests were used with the method proposed by Kim et al.[46] wrapping the end parts with a silica-coated aluminum sheet to protect the end parts. The corroded part of the specimen was cut off after loading test and washed with 12% hydrochloric acid to measure the residual mass of the wires to calculate the mass loss.

2.5.3 Measurement method for the cross-sectional area loss of the strand

The mass loss and maximum cross-sectional loss of a strand or a wire are generally the two main parameters to reflect the corrosion level. The mass loss can be directly weighed and calculated, while the maximum cross-sectional area loss was measured and calculated by using the method of Jeon et al.[18]. The method calculates the cross-sectional area loss of the strand by measuring the corrosion depth, and divides three types of corrosion pitting as shown in **Fig. 2.24**. Vecch [22] used 3D scanning technology to verify this method, and found that the calculated results are very close to the size of the actual cross-sectional area loss. The depth of the strand corrosion pitting was measured by means of an instrument shown in **Fig. 2.25**. The loss of sectional area can be calculated through Eqs. (2.8) to (2.13).

$$\text{Type 1: } A_{sl1} = 2r^2(\theta_1 - \sin\theta_1\cos\theta_1) \quad \text{for} \quad 0 \le d_p \le 2r \qquad (2.8)$$

$$\theta_1 = \arccos\left(1 - \frac{d_p}{2r}\right) \qquad (2.9)$$

$$\text{Type 2: } A_{sl2} = r^2(2\theta_2 - \pi - 2\sin\theta_2\cos\theta_2) \quad \text{for} \quad 0 \le d_p \le 2r \qquad (2.10)$$

$$\theta_2 = \arccos\left(-\frac{d_p}{2r}\right) \qquad (2.11)$$

$$\text{Type 3: } A_{sl3} = r^2(\theta_3 - \sin\theta_3\cos\theta_3) \quad \text{for} \quad 0 \le d_p \le 2r \qquad (2.12)$$

$$\theta_3 = \arccos\left(1 - \frac{d_p}{r}\right) \qquad (2.13)$$

where, A_{sl1}, A_{sl2}, and A_{sl3} are the loss of sectional area according to the types of pitting configuration, r is the radius of a wire, and d_p is the pitting depth measured by depth gauge at the deepest location.
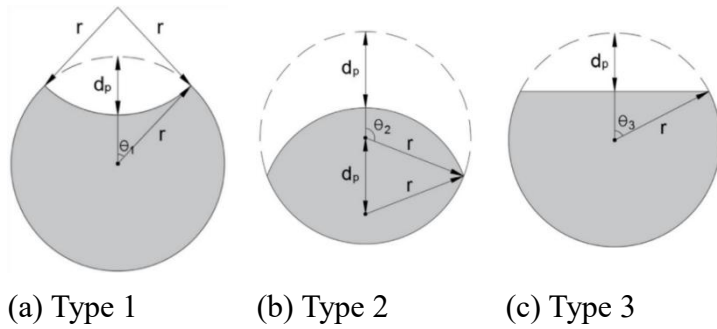
(a) Type 1　　　　(b) Type 2　　　　(c) Type 3

Fig. 2.24　Pitting configurations (Jeon et al., 2019)

Fig. 2.25 Depth measuring instrument

Table 2.8　Results of corrosion tests

Specimen No.	Mass loss (%)	Maximum cross-sectional loss (%)	Prestress loss (%)	Test series which the wire was ruptured [*1]
50-5-1	7.2	22.3	2.1	T
50-5-2	6.6	21.8	1.9	-
50-5-3	3.7	7.8	0.8	T
50-5-4	6.9	24.3	1.9	T
50-5-5	6.6	26.4	2.1	-
50-5-6	4.1	15.3	1.4	T
50-7-1	10.5	30.1	3.2	T
50-7-2	11.2	30.3	2.9	T
50-7-3	11.4	31.9	3.6	T
50-7-4	10.7	31.4	3.2	T
50-7-5	8.4	35.1	3.1	C
50-10-1	12.0	35.9	4.1	C
50-10-2	10.1	47.1	3.3	C
50-10-3	14.7	40.6	4.7	C
50-10-4	7.2	26.5	2.6	C
50-10-5	10.8	37.3	4.0	C

*1 Test series the wire was ruptured: C means failure in the corrosion test and T means failure in the tensile loading test. '-' means wires was not ruptured.

2.5.4 Results of corrosion tests

Sixteen steel strands were subjected to electrochemically accelerated corrosion under the action of corresponding tensile stress, and the test results are shown in **Table 2.8**. The maximum cross-sectional area loss of the PC strand can reflect the corrosion degree of the strand at a certain corrosion pitting, while the mass loss presents the average corrosion level of the PC strand, which reflects the uniform corrosion condition of the steel strands. The fracture of a steel wire in tension will occur in the most severely corroded corrosion pits, and the maximum cross-sectional area loss can better reflect the ultimate tensile performance of the strand, while the prestress loss of the strand is related to the corrosion degree of the whole section of the strand, so the mass loss has a better correlation with the prestress loss of the strand. The phenomenon of PC strands corrosion has a little randomness. There may be one deep corrosion pit on the surface of the PC strand, or there may be multiple shallow corrosion pits. It can be found from **Table 2.8** that 50-10-1 and 50-7-5 have similar cross-sectional area loss, but the mass loss of 50-10-1 is greater than that of 50-7-5, and its prestress loss is also

greater. It is also found that 50-10-2 has a greater maximum cross-sectional area loss as compared with 50-10-1, but it has a smaller mass loss and a smaller prestress loss. However, this randomness is minimized when the corrosion conditions are the same. The relationship of mass loss and max cross section area loss was shown in Fig.8. According to **Fig. 2.26**, it can be found that there is a good correlation between mass loss and maximum cross-sectional area loss. With the mass loss increase, the max cross section area loss increase roughly linearly.
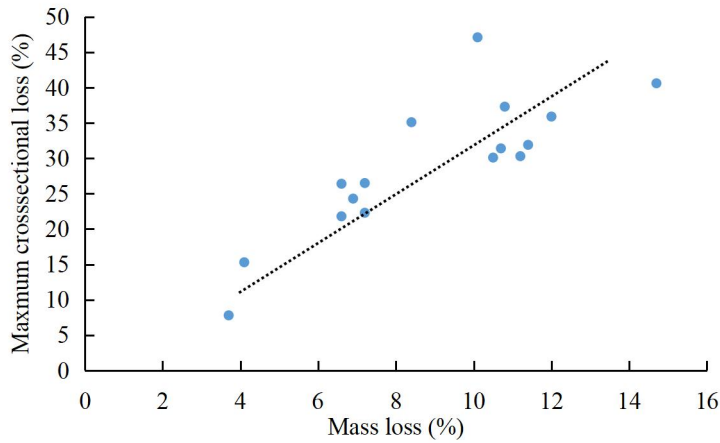
Fig. 2.26   Mass loss versus maximum cross-sectional area loss of the PC strand

Table 2.9   Fracture type and results of the corrosion tests

Specimen No.	Fractured section	Fracture type	Corrosion pitting	Necking degree	Mass loss (%)	Cross-sectional area loss of wires (%)	Prestress loss (%)
50-7-5		S		Slight	14.2	53.4	3.1
50-10-1-1		S		Medium	19.2	59.0	4.1
50-10-1-2		M		Sever	13.9	55.2	
50-10-2		M		Medium	10.8	59.7	3.3
50-10-3-1		S		Slight	17.0	62.1	4.7
50-10-3-2		S		Slight	18.1	58.4	
50-10-4		S		None	8.6	55.2	2.6
50-10-5-1		M		Sever	11.0	57.9	4.0
50-10-5-2		M		Sever	13.4	61.7	

Note: Fracture types are S: Split type, M: Milling cutter type.

| Cup and cone type | Milling cutter type | Split type | Milling cutter-Split type |
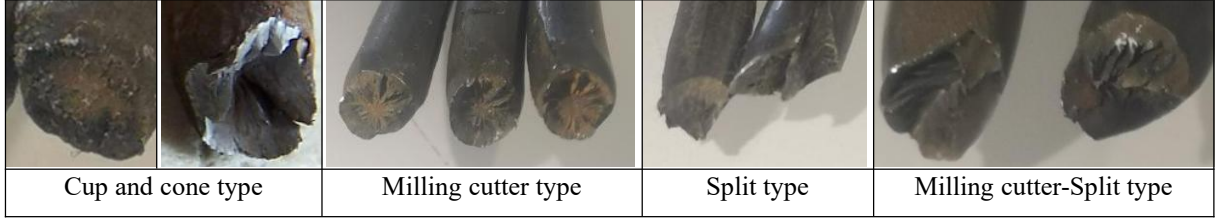
Fig. 2.27   Fracture type of corroded steel wires[47]

2.5.5 Failure mode of corroded strands in the corrosion tests

The failure modes of the ruptured steel strand during the corrosion test are analyzed. The fracture of wires is a sign of failure of PC strands, the conditions of the 9 fractured wires in the 6 corroded strands are summarized in **Table 2.9**. All the fracture types can be divided into three basic fracture types: cup and cone type, milling cutter type, split type, and their combination. Macroscopic photos of various fracture type are shown in **Fig. 2.27**, and those pictures were taken in previous study[47]. The necking phenomenon appeared near both the cup and cone fracture type and the milling cutter fracture type (the necking degree of the cup and cone type is relatively light), which shows ductile failure. There is no obvious necking phenomenon near the split type and split-milling cutter type, which shows brittle failure. It can be found from Table 4 that the fracture types of 50-10-1, 50-10-2, and 50-10-5 are all the milling cutter type, with a more obvious necking phenomenon belonging to ductile failure.

It should be noted that during the corrosion process, although hydrogen generated at the cathode and hydrogen ions in the solution may enter the strand from the cracks created by corrosion, it is difficult to determine whether hydrogen embrittlement was one of the causes of strand fracture. In this study, it is assumed that the degradation of the tensile capacity of strands due to a loss of cross-sectional area caused by corrosion is a main reason for the fracture of steel wires.

2.5.6 Prestress force deterioration process

The test results of the previous investigation[47] show that the prestress of strand wires decreases linearly with the increase of its mass loss, and the calculation formula of mass loss is proposed as follow:

$$n_{mass\ measured} = 1 - \frac{M_c}{M_0} \tag{2.14}$$

$$n_{mass} = a\frac{M}{NFM_0}IT \tag{2.15}$$

where, $n_{mass\ measured}$ is the measured mass loss of corroded strand, M_0 is the initial mass of strand, M_c is the mass of corroded steel strand of which was measured after the corrosion test, and n_{mass} is the calculated mass loss of the corroded steel stands, a is an empirical parameter for each specimen, M is the atomic mass of metal, N is the number of valence electrons lost by oxidation of a metal, F is Faraday constant; $1F = 96485$ C/mol, I is a current intensity, T is a corrosion time.

In order to express the change of prestress in corrosion, the prestress loss, P_{loss} was used to express the change of prestressing force.

$$P_{loss} = 1 - \frac{P_c}{P_0} \tag{2.16}$$

where, P_0 is the initial prestressing force, P_c is the prestressing force of corroded steel strand.

According to the Eq. (2.16), the relationship between mass loss and prestress loss in this test was obtained, as shown in **Fig. 2.28**.
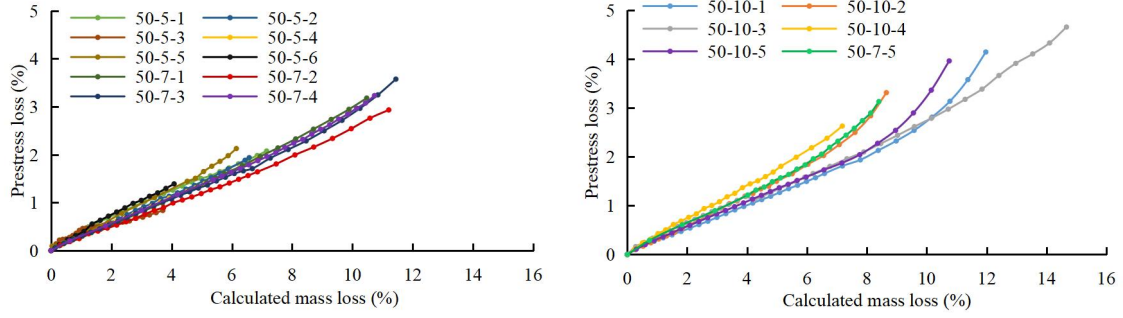
(a) PC strand not fractured during corrosion test   (b) PC strand fractured during corrosion test

Fig.2.28   Calculated mass loss versus prestress loss

Since the test started at about 20 hours after the tensile loading applied, the effect of relaxation properties on the prestress has been reduced to a negligible level, and the tensile load on the strand was mainly concentrated between 127.9-129.2 kN at this time. According to **Fig. 2.28(b)**, it can be found that the specimens with higher corrosion degree its deterioration process of prestressing force with increasing corrosion degree can be divided into two stages. In the first stage, the prestress decreased linearly with the increase of the overall corrosion level of the strand with increasing the corrosion degree. Once the prestressing-corrosion degree curve shows an inflection point at which the slope of the curve increases, it is assumed to start the second stage. At this time, the strand indicated the plastic deformation, and the prestressing force was rapidly reduced until the specimen was ruptured. In the second stage, the plastic deformation due to the yielding of the steel wire and finally the wire was ruptured, both of which are related to the maximum cross-sectional area loss of the strand. Therefore, the maximum cross-sectional area loss, $n_{area\,max}$ was assumed be according to that of the fractured wire and calculated by Eq. (2.17). In this study, $n_{area\,max}$ was selected as the corrosion degree to evaluate the second stage as a prestress degradation.

$$n_{area\,max} = 1 - \frac{A_c}{A_0} \tag{2.17}$$

where, A_0 is the initial cross-sectional area of the wires, A_c is the cross-sectional area of the fractured wire.

The maximum cross-sectional area loss increased roughly linearly with mass loss as shown in Table 3, although specimens with the same mass loss have different maximum cross-sectional area losses due to the random behavior of corrosion. Corrosion in the natural environment, the positive and negative electrodes formed at the corrosion pits and the uncorroded portion led to the speeding up of the corrosion speed at the corrosion pits. In the electrically accelerated corrosion test, the external power supply provides stable positive and negative poles, and the accelerated corrosion effect of the corrosion pit is almost negligible, so the corrosion of the specimen in the electrically accelerated corrosion test is more uniform than that of the natural environment corrosion, and the corrosion velocity at the corrosion pit is almost constant. Thus, it is assumed that the cross-sectional area loss, n_{area} also has a linear relationship with a corrosion time. Thus, Eq. (2.18) could be gotten to calculate the velocity of loss of the maximum cross-sectional area.

$$n_{area} = b\,T \tag{2.18}$$

where, b is an empirical parameter to fit the loss of the measured maximum cross-sectional area of the fractured wire, T is the corrosion time (hours).

The maximum cross sectional area loss of fractured wires was calculated by Eq. (2.18) after the corrosion test was terminated as show in **Fig. 2.29**. The values of b for each specimen were also summarized in **Table 2.10**

Table 2.10　　Maximum cross-sectional area loss of the fractured wire and prestress loss

Specimen No.	50-7-5	50-10-1	50-10-2	50-10-3	50-10-4	50-10-5
$n_{area\,max}$ (%)	41.7	46.9	44.6	50.5	41.2	45.8
Corrosion time when the wire is fractured (hour)	61	80	66	104	56	72
b	0.68	0.59	0.68	0.49	0.74	0.63
Prestress loss in 1st stage (%)	2.05	2.32	2.25	2.97	2.38	2.28
Prestress loss in 2nd stage (%)	1.08	1.82	1.06	1.68	0.25	1.68
n_{area} when the 2nd stage is started	32.2	35.2	36.5	36.9	38.3	35.6
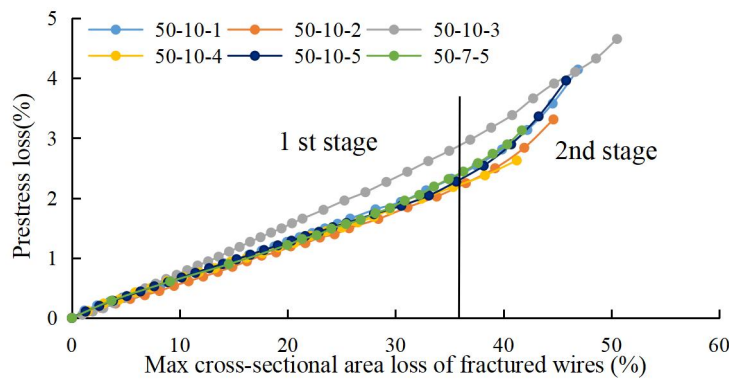
Fig. 2.29　　Prestress loss versus cross-sectional area loss of fractured wires

It can be found that when the corrosion degree is expressed by the cross-sectional area loss of the fractured wires, a clear law of prestress deterioration emerges, and the second stage of prestress deterioration (the rapid decline stage) begins when the cross-sectional area loss reaches around 36%. The prestress deterioration trend is almost the same, while the prestress reduction rate of 50-10-3 is significantly faster than the other specimens, which is due to the fact that when the maximum cross-sectional area loss is similar, its overall corrosion is much higher than the other specimens, and when it was failure, its mass loss is at least 22.5% higher than the other specimens. Due to the lower internal prestress relative to the other specimens, when the maximum cross-sectional area loss reaches around 36%, The wires' deformation due to cross section area loss is lower, the prestress degradation rate of 50-10-3 is slower than others in second stage.

According to **Fig. 2.28** and **Fig. 2.29**, comparing the second stage of each specimen, it can be found that the second stage of 50-10-1, 50-10-2 and 50-10-5 develops longer and the prestress loss is more serious than that of 50-10-3, 50-10-4 and 50-7-5, which is due to the fact that the second stage of prestress deterioration is directly related to the deformation of the wire after yielding, and different fracture types have different failure modes that can directly affect the deformation of the wire in this stage.

According to **Table 4**, the fracture of 50-10-1, 50-10-2 and 50-10-5 showed the milling cutter type, and their failure mode was ductile, while the fracture types of 50-10-3, 50-10-4 and 50-7-5 were the split type or milling cutter split type, and the failure mode was in brittle. In the case of the ductile failure, after yielding, necking

occurred and the steel wire was deformed at the fracture, resulting in an accelerated drop in prestress, whereas in the case of brittle failure, the steel wire was only slightly necked or no necked before fractured, and there was no obvious deformation at the fracture, and the prestress loss is low. Therefore, the second stage of prestress deterioration is more obvious and serious for the steel strand with ductile failure, and the second stage of prestress deterioration is shorter and the prestress loss is less for the steel strand with the brittle failure.

2.5.7 Strain loss of wires and strand at the uncorroded portion

The immersion of the solution during corrosion and the rusting of the strand surface made it difficult to measure the strain in the corroded portion of the strand. the test measured the strain in the six wires in the outer ring of the uncorroded portion of the strand under tension. **Figure 2.30** shows the strain loss versus mass loss for 50-5-5 and 50-7-1 during corrosion. **Figure 2.31** shows the average prestress loss versus mass loss during corrosion of the outer ring wires of the strands except 50-10-3 and 50-10-4 since the strain gauges were failure in the corrosion tests. It can be found that with the increase in mass loss of the outer ring wire strain have occurred in varying degrees of reduction. The strain loss of specimens 50-10-1 and 50-10-2 is much higher than the other specimens, which is presumably related to the characteristics of the specimens themselves, as the deformation of each wire is not the same everywhere, and therefore the strain change is much higher than the other specimens.

(a) 50-5-5   (b) 50-7-1
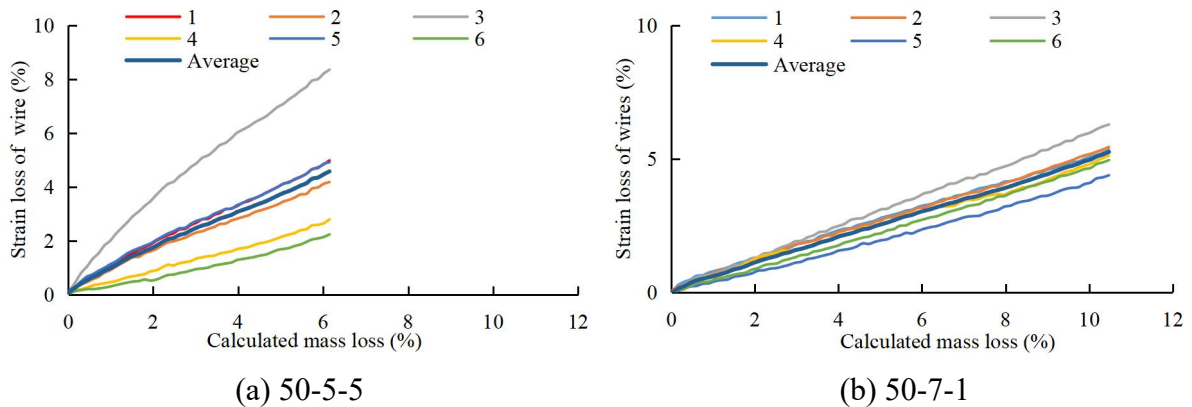
Fig. 2.30   Example of strain loss of 6 wires in the out ring versus calculated mass loss

(a) Series of 5 and 7   (b) Series of 10
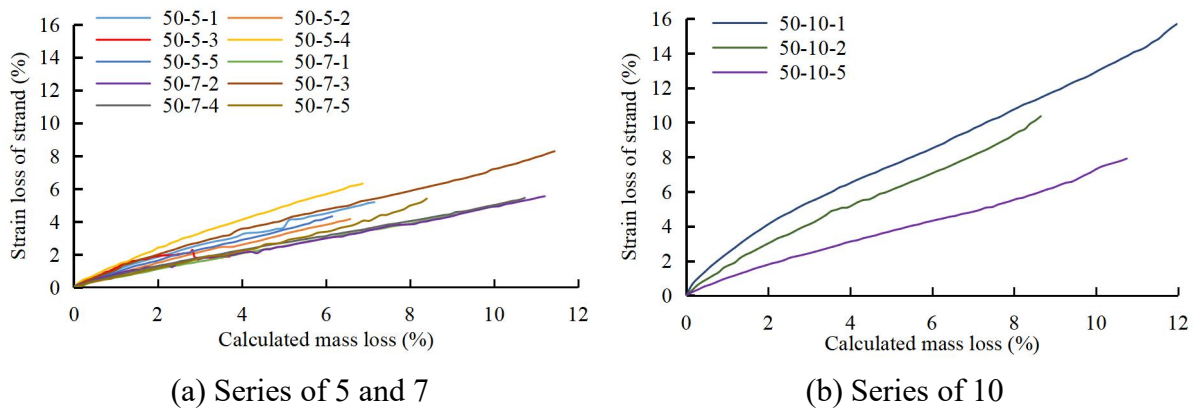
Fig.2.31   Strain loss of strand versus calculated mass loss

The strain loss at the uncorroded portion mass loss of each wire was plotted against the mass loss of wires as shown in **Fig. 2.32**. The regression line of the overall

strain loss of the strand was added to show that the data were mainly concentrated in the upper part of the regression line and the strain loss of the outer ring wire was almost always higher than the overall strain loss of the strand. From these results, the average value of the strain loss in the outer ring of the strand was calculated and the relationship between the average strain in the outer ring and the mass loss of the strand was plotted as shown in **Fig. 2.33**. The average strain loss of the outer ring of the strand increases roughly linearly with the increase in mass loss. And they are higher than the overall strain loss of the strand. It is presumed that during the corrosion of the outer ring wire, the uncorroded central wire was gradually subjected to more load.

The strain loss of the strand as a whole at the strain gage is calculated by Eq. (2.19).

$$\varepsilon_{loss\ uncorroded} = 1 - \frac{\varepsilon_c}{\varepsilon_0} = 1 - \frac{P_c/(E\,A_c)}{P_0/(E\,A_0)} \tag{2.19}$$

where, ε_0 is the initial strain of strands, ε_c is the strain of steel strand at the uncorroded portion after the corrosion was occurred.

Here, there is no corrosion at the location where the strain gauges were attached, the cross-sectional area is assumed to be constant. Therefore, Eq. (2.19) can be written as same formula of Eq. (2.16). Then the strain loss of PC strand at the uncorroded part was calculated from Eq. (2.16) and (2.19), and drawn as shown as Eq. (2.20).

$$\varepsilon_{loss\ uncorroded} = 1 - \frac{P_c}{P_0} \tag{2.20}$$

From Eq. (2.20), the strain loss versus mass loss is shown in **Fig. 2.34**. The strain loss of the strand which presents as an entire behavior of the 7 wires was presented. It can be found that the strain of the steel strands in the uncorroded part decreases continuously with the decrease of prestress, and the overall relationship is linear. The regression line of prestress loss and overall strain loss of the strand is obtained by linear fitting.
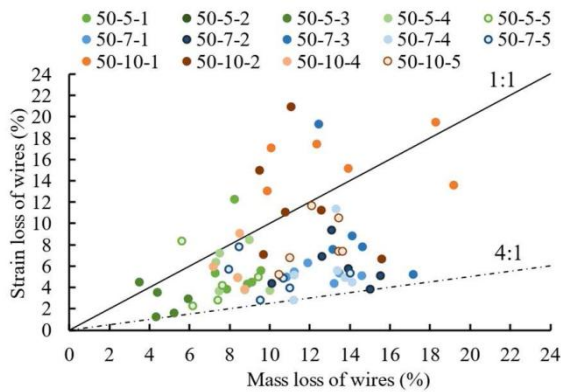
Fig. 2.32   Strain loss of each wire
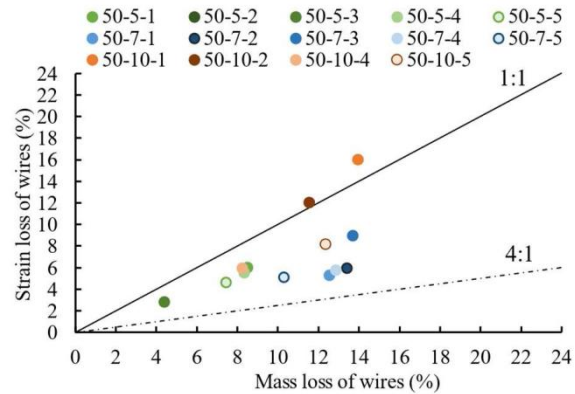
Fig. 2.33   Average strain loss of out ring wires

2.5.8 Strain change at the corroded portion

The stain of the steel strand after the tensile force was applied showed a decrease in the uncorroded section, while the results of the displacement measured at two points including the corroded section of the PC strand showed that the deformation increased, which is presumed to be an increase in the deformation of the corroded section of the steel strand. Since the strain of the strand in the corroded section strain is difficult to measure directly, it was calculated by Eqs. (2.21) and (2.22).

$$\varepsilon_{loss\ corroded} = 1 - \frac{\Delta L_{300}}{L} \tag{2.21}$$

$$\Delta L_{300} = -\Delta L_{700} + \Delta L_d \qquad (2.22)$$

where, ΔL_{300} is the deformation of strands including the corroded portion, and ΔL_{700} and ΔL_d are the deformations of strand at the uncorroded portion and at the measuring points, 1000 mm, L is an initial length of strand at the corroded portion; 300 mm in this study.

Here, ΔL_{700} was shortening deformation and obtained by multiplying length of 700 mm by the strain measured using the strain gages located at the uncorroded portion of PC strand. In addition, ΔL_d was measured by the displacement transducers attached at the distance of 1000 mm, previously shown in **Fig. 2.20**

The strain loss of corroded part was calculated according to Eq. (2.21), and the strain increase of PC strand at the corroded portion versus mass loss was shown in **Fig. 2.35**. It can be found that unlike the uncorroded portion, the strain in the corroded portion of the PC strand indicates in negative value and increased linearly with increasing corrosion degree, namely, the elongation of the corroded section of the strand linearly increased. This is because as the cross-sectional area of the corrosion pit decreases when the strand was corroded, it was deformed and elongated at the corroded portion to reach a balanced equilibrium state. The total length of the strand between the anchors of each end is assumed to keep constant after the tensile loading was applied, and consequently, the corroded part elongates, and simultaneously the uncorroded part shortens. This balanced condition of the internal force leads to a decrease in the prestressing force until the tensile force in the corroded section increased and reached that in the uncorroded section. In other words, the deterioration of the prestressing force of the strand leads to an imbalance in the overall tensile force of the strand, and the result of the balance is a reduction in prestressing force.
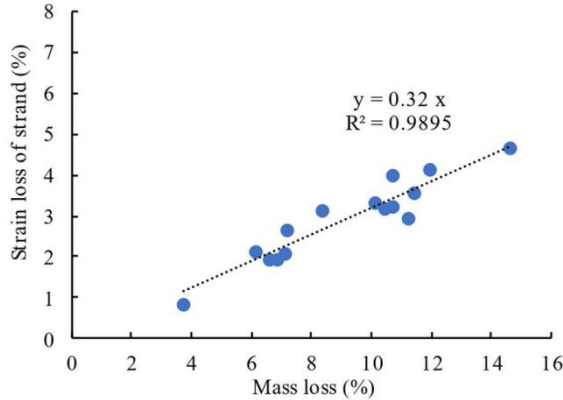
Fig. 2.34   Strain loss of PC strand at the uncorroded portion
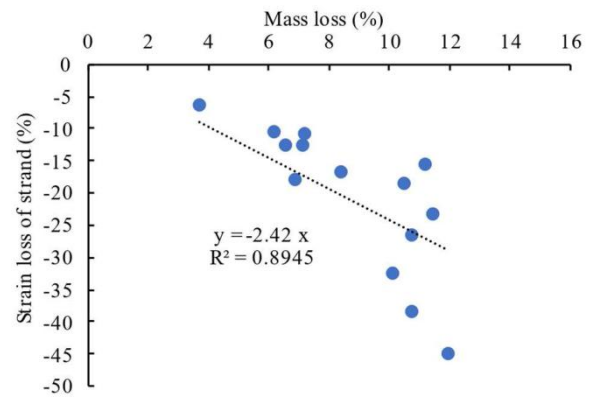
Fig. 2.35   Strain increase of PC strands at the corroded portion

To confirm the measurement accuracy of displacement transducers and strain gages, the elongation of the corroded portion obtained by Eq. (2.23) is shown in **Fig. 2.36**. ΔL_{1000} was obtained by multiplying only the strain measured using the strain gages by the length of 1000 mm which was of the uncorroded portion between the anchors of each end, 1300 mm. The result indicates that the elongations obtained by the two measurement procedures agreed with each other.

$$\Delta L_{300} = -\Delta L_{1000} \qquad (2.23)$$

In this study, the strain change of the strand at the corrosion part and uncorroded part has been investigated, while the degradation of prestress is closely related to strand corrosion and the deformation of the strand at the uncorroded sections. It is possible to predict the prestress loss in PC members by measuring the strain changes at different

locations of the strand considering the influence of factors such as bonding properties and based on the results of this study.
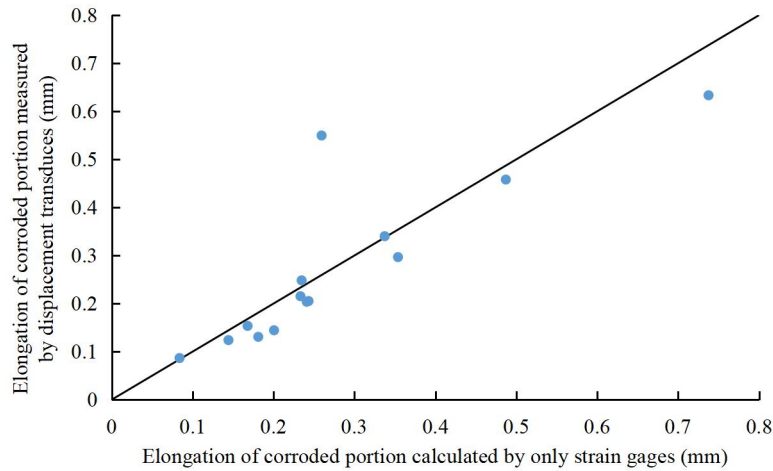
Fig. 2.36   Measurement accuracy for the elongation of corroded portion of PC strand obtained by displacement transducers and by only strain gages

2.5.9 The relationship between the strain loss of out ring wires' uncorroded part and prestress loss

The reduction of strain in the uncorroded section of the strand is caused by the reduction of prestress in the strand, and the relationship between the average strain loss in the outer ring of the wire and the loss of prestress in the strand is shown in **Fig. 2.37**. Theoretically, under the same load, the deformation of the outer ring wires of the strand should be the same, but in the actual test process, due to the differences between the specimens themselves, such as the size of the wire, the friction coefficient, etc., different steel strand outer ring wires under the same load bears a different load, the deformation occurs differently, the average strain loss and the prestress loss in the strand had two trends, six specimens conform to the trend 1, and three specimens conform to the trend 2. According to the **Fig. 2.37**, the average strain of the outer ring wires in all two trends decreases as the prestress decreases, only the magnitude of the decrease is different, according to the calculation method of strain loss, it is presumed that the initial strain of the outer ring wire has a great relationship with the initial strain of the outer ring wire. The initial average strain of the first trend is 4044-4765, and the initial average strain of the second trend is 3870-4272. The modulus of elasticity of the wire is generally 200 kN/mm2, and the prestress after relaxation will decay to about 128.5 kN, assuming that the force on the seven wires of the strand is the same, the calculation shows that the theoretical value of the initial average strain of the outer ring wire is 4676, but in fact the center The load on the wire is slightly greater than that on the outer wire, so the actual value of the initial average strain on the outer wire is slightly less than 4676. Fitting trend 1 and trend 2 to obtain Eq. (2.24).

$$\text{Prestress loss} = 2.1n^2 + 0.36n \tag{2.24}$$

where n is average strain loss of out ring steel wires.

The prestress loss can be calculated more accurately by the loss of strain on the outer wires according to the Eq. (2.24). The accuracy of the prediction was verified by the test data.
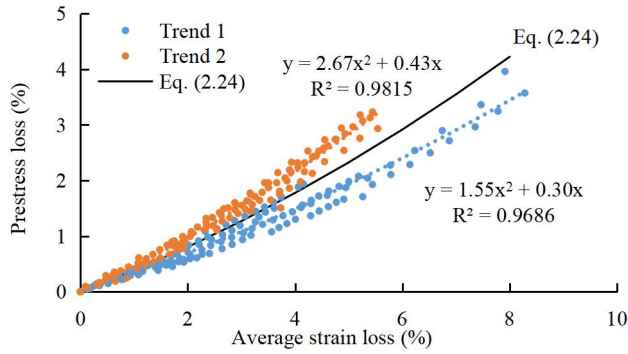
Fig. 2.37   The average strain loss versus prestress loss

2.5.10 Corrosion length

The overall corrosion degree (mass loss) and corrosion length have a direct effect on the tensile capacity of the strand. When the overall corrosion of the specimen is greater, the greater the average cross-sectional area loss, the lower the tensile capacity. And when the corrosion degree is the same, the longer the corrosion length, the lower the tensile capacity of the strand, This is because the increase of corrosion length increases the absolute corrosion mass loss value at the same mass loss rate. Therefore, the corrosion length also has a significant effect on the prestressing loss. The test data of the strand with a corrosion length of 500 mm are summarized with the present test data in **Fig. 2.38.** Comparing the specimens with different corrosion lengths, it can be found that the prestress loss of the strand with a corrosion section length of 500 mm is more severe than that of the strand with a corrosion section of 300 mm, which is about 1.2% higher on average, under the same prestress level and corrosion degree.
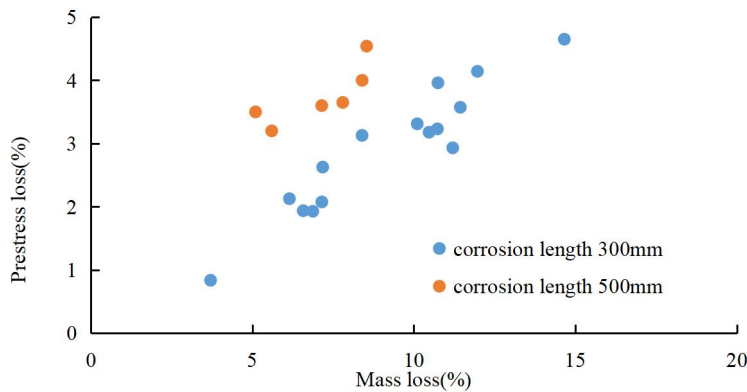
Fig. 2.38 Effect of corrosion length on prestress loss of PC strand

2.5.11 A model for predict prestressing force of corroded PC strands

In the second stage, the prestressing force is reduced due to a large amount of plastic deformation of the wire at the corrosion pit. The deformation depends on the different fracture modes of the strand, which occur randomly, so the prediction of the reduction of prestressing force becomes difficult. Therefore, This paper mainly studies the linear relationship between the first stage of prestressing force and the corrosion degree. Test data of first stage are summarized in **Fig. 2.39(a)**. According to the figure, the model of prestressing force and corrosion degree relationship is assumed to be a liner equation.

$$P_c/P_0 = -0.27n + 1 \qquad (2.25)$$

where, P_c is the prestressing force of the steel strand after corrosion; n is the corrosion degree of the steel strand; P_0 is the prestress load at before corrosion. 0.27 is verify parameter can be written as a.

The previous study also summarized the prestress force linear decrease stage with the mass loss increase, as shown in **Fig.2.39(b).** And the equation (2.26) was gotten.

$$P_c/P_0=-0.45n+1 \qquad (2.26)$$

where, the 0.27 and 0.45 are verify parameter, they can be represent as a, the equation can be written as follow:

$$P_c/P_0=-an+1 \qquad (2.27)$$

It can be found that the ratio of a is same as ratio of corrosion length.

| (a) 300mm | (b) 500mm |
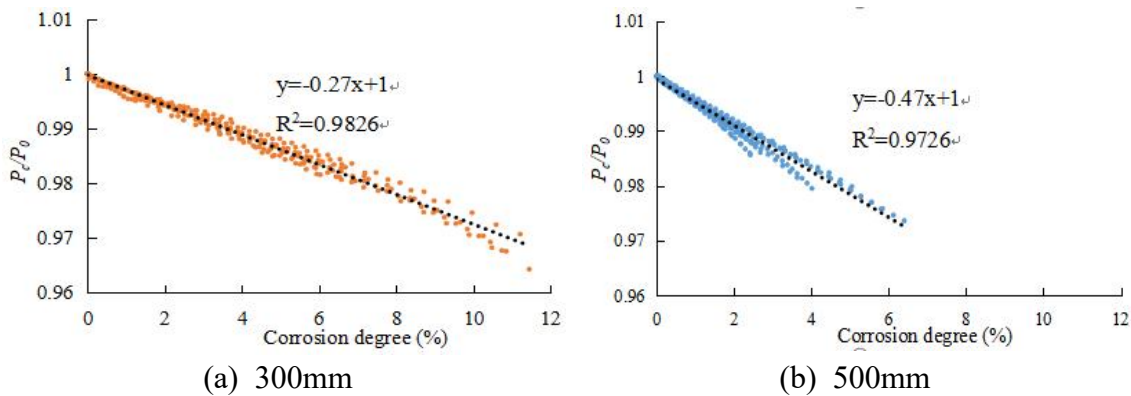
Fig.2.39   Relationship between prestressing force and corrosion degree
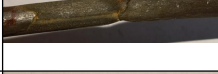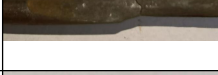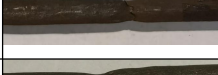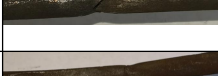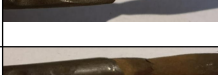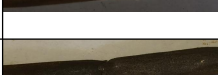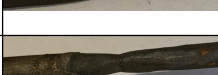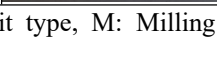
2.6 Effect of pitting characteristic on ultimate tensile capacity of corroded PC strands

2.6.1 Failure mode and fracture type

The tensile loading test was carried out on the nine steel strands that was not ruptured during the corrosion test. Since the tensile performance of the strand is directly related to the cross-sectional area loss, the maximum cross-sectional area loss of the strand is used to express the corrosion degree when studying the ultimate tensile performance of the strand. Due to the pitting corrosion steel strand in each steel wire etching pitting shape, size and distribution of the different make it in the static tension of each wire does not break at the same time, so that the tensile curve in each fractured wire step down, and the strand in the first occurrence of fracture of the wire to reach its ultimate tensile load. Therefore, the tensile test was terminated after the first fracture of the wire. The fractography on the fracture surfaces of corroded steel wires with different corrosion degrees were conducted after the tensile loading tests, and they were summarized in **Table 2.11.**

It can be found that the corrosion of the strand will occur after the ductile failure and brittle failure in two ways, for the corrosion of the lighter degree of steel strand usually occurs ductile failure, fracture types were milling cutter type and cup and cone type, and has an obvious necking phenomenon, while for the corrosion of the higher degree of specimens, the failure mode will change from ductile to brittle failure, fracture type to split type or split-milling cutter type.

Table 2.11   Fracture type and results of the tensile loading tests

Specimen No	Fracture	Fracture type	Corrosion pitting	Necking degree	Tension capacity (kN)	Cross-sectional area loss of wire (%)
50-5-1-1		S		None	200.9	40.8
50-5-1-2		M		Medium		29.6
50-5-1-6		M		Medium		32.5
50-5-3-1		M		Severe	238.3	13.6
50-5-4-1		S&M		Slight	168.6	47.2
50-5-6-1		M		Severe	216.7	27.6
50-5-6-6		M		Severe		21.7
50-7-1-4		S		None	143.5	45.7
50-7-1-5		S		Slight		42.4
50-7-2-6		S&M		Slight	174.2	42.9
50-7-3-4		S		None	136.0	36.9
50-7-3-5		S		None		49.0
50-7-4-4		S		None	149.7	47.2
50-7-4-5		S		None		40.8

Note: Fracture types are S: Split type, M: Milling cutter type and S&M: Split-Milling cutter type, respectively.

2.6.2 Ultimate tension capacity of corroded strands

The tensile test results are summarized and the relationship between the ultimate tensile capacity and the corrosion degree for the steel strand is shown in **Fig. 2.40.** Compared with the uncorroded steel strand (0%) of which the ultimate tensile capacity was 265 kN, the tensile capacity of the corroded steel strand was obviously decreased. From **Fig. 2.40(a)**, the ultimate tensile strength decreased approximately linearly with the loss of the maximum cross-sectional area of the strand. When the maximum cross-sectional area loss was less than around 30%, the linear relationship between the maximum cross-sectional area loss and the ultimate tensile capacity of the strand was more obvious, and when the maximum cross-sectional area loss of the strand reached around 30%, the ultimate tensile strength distributions of the specimens were more scattered, which was related to the change of the failure mode due to the high corrosion of the specimens.

It can be seen from the tests, the maximum tensile strength of the corroded steel strand appears in the first fracture of the wire, the steel strand as a tensile specimen, its maximum tensile strength but only depends on the first fracture of the corroded steel

wire. Therefore, the failure of the test piece and the maximum cross-sectional area loss of a fractured wire has a close relationship, with the maximum cross-sectional area loss of the ruptured wire represents the degree of corrosion, the ultimate tensile strength and the relationship between the degree of corrosion as shown in **Fig. 2.40(b)**. It can be found that the deterioration process of the maximum tensile strength can be divided into two stages; when the corrosion level is less than around 40%, the ultimate tensile strength of the specimen and the corrosion level have an obvious linear relationship, while when the corrosion level exceeds around 40%, the ultimate tensile strength of the specimen with the corrosion level decreases significantly. It is found that the fracture type of the wires in the three specimens in the first stage was the milling cutter type and that in the second stage, the fracture type was changed from the milling cutter type to the split-milling cutter type with a slight necking phenomenon or the split type. In addition, the failure mode was changed from ductile to brittle failures.

The different failure modes of the wire led to the deterioration of the ultimate tensile capacity of the strand dividing it into two stages, and the wires which occurred brittle failure had lower ultimate tensile capacity. It's because when the wires indicated ductile failure, the plastic deformation at the corrosion pitting occurred, and then a more adequate stress and strain redistribution may occur in the cross-section at each wire's corrosion pitting, the cross-section as a whole undergoes plastic deformation and necking phenomenon occurs. The ultimate tensile strength of the strand continued to increase in this process until the wire circumferential slip separates and fractures formed a milling cutter fracture type. On the other hand, brittle fracture originated from cracking caused by localized plastic deformation at the bottom of the pitting, and once cracked, the rapid instability expansion to full-section fracture, that is, the initial fracture and ultimate fracture occurring almost simultaneously, without the process of ultimate tensile strength increased. Thus, the ultimate tensile capacity of specimens which indicated the split-milling cutter type showed higher than that of specimens with split type because the split-milling cutter type had a slight necking phenomenon, and that indicated increasing the ultimate tensile capacity.
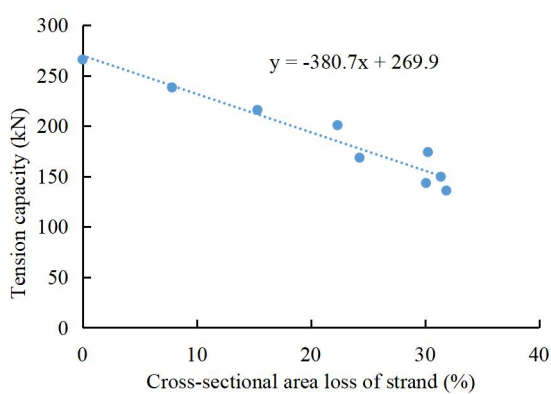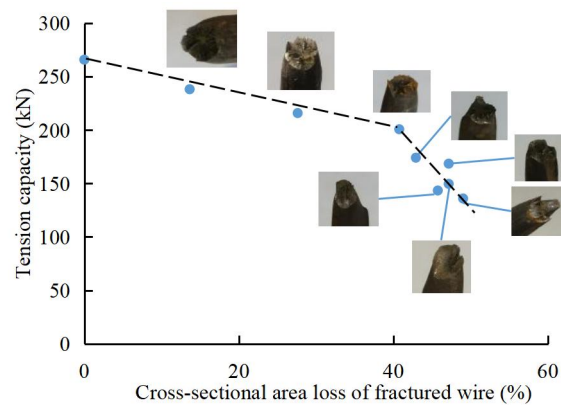
(a) Cross-sectional area loss of PC strand   (b) Cross-sectional area loss of fractured wire
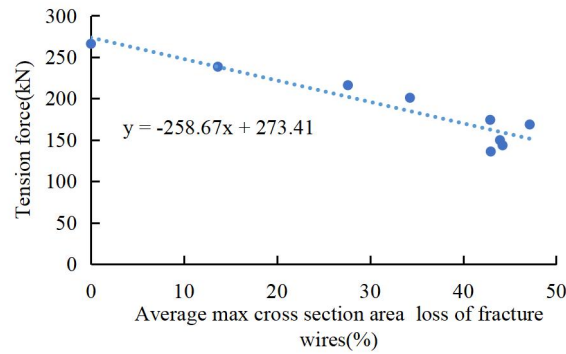
(c) Average cross-sectional area loss of fractured wire

Fig. 2.40   Relationship between ultimate tensile capacity and cross-sectional area loss

2.6.3 Elongation of corroded strands

Before the start of the tensile test, the corroded section of the strand was marked with a red marker pen for 300 mm. The elongation wasmeasured after tensile test finished by vernier callipers fromthe distance between markers, the relationship between elongation and the maximum cross-sectional area loss of broken steel wire is shown in **Fig. 2.41**. This elongation included the elastic shortening, therefore, the calculation of the elongation is a bit low. The higher elongation of 50-5-1 was due to the fact that the test was not stopped in time when the first wire fractured. It can be noticed that the elongation of the strand continues to decrease as the maximum cross-sectional area loss of the broken wire increases, with a trend almost identical to the decrease in load. As the loss of cross-sectional area reduces the tensile capacity of the strand, unlike uncorroded strands, corroded strands may fracture just before reaching the yield stage. When corrosion is severe, the wire may even fracture at the elastic stage, when the strand is less deformed and has a lower elongation.
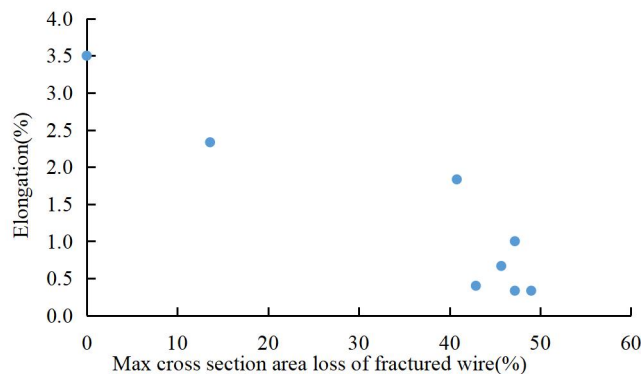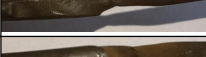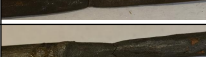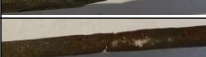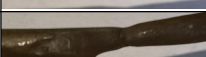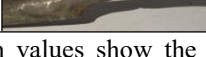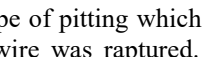

Fig.2.41   Elongation of strands versus max cross section area loss of fractured wires

2.6.4 Influencing factors of strand fracture type

The fracture type of the wire determines the failure mode of the strand and has an important influence on the deterioration process of the prestressing force and the ultimate tensile capacity, so it is particularly important to study the fracture mechanism of the strand. The shorter one of the strands that fractured into two pieces is set as the left part and the longer one is set as the right part. The cross-sectional area loss and the cross-sectional types which explained previously in **Fig. 2.27** were measured and observed at six points on the left and right, centered on the location of the fracture point, with a distance of 5 mm between each point. The measured data of corrosion near the

Table 2.12   Cross-sectional area loss and cross section type of pitting of fractured wires at each section

No.	Fracture type	Corrosion pitting	Left (mm)						C	Right (mm)					
			30	25	20	15	10	5	0	5	10	15	20	25	30
			Cross-sectional area loss (%) / Cross section type of pitting												
5-1-1	S		0.0	0.0	0.6	3.8	6.8	13.3	40.8	28.4	26.1	25.4	18.5	21.8	19.8
			-	-	1	1	3	3	2	2	2	2	2	2	2
5-1-2	M		3.6	0.0	16.5	19.5	30.9	32.6	29.6	28.6	22.3	18.8	19.0	16.5	16.5
			2	3	2	2	2	2	2	2	2	2	2	2	2
5-1-6	M		0.0	0.0	3.1	14.8	19.7	31.4	32.5	23.6	24.9	20.8	19.0	14.4	7.5
			-	-	1	3	3	2	2	2	2	2	2	2	2
5-3-1	M		0.0	0.0	0.0	6.7	7.5	12.6	13.6	11.8	9.0	10.0	11.6	11.3	7.5
			-	-	-	2	2	2	2	2	2	2	2	2	2
5-4-1	S&M		0.5	1.3	6.5	10.2	20.6	44.4	47.2	41.5	21.6	11.8	9.8	4.9	12.9
			-	1	3	3	3	2	2	2	2	2	2	2	2
5-6-1	M		2.8	2.8	3.9	5.7	14.9	21.6	22.2	17.0	19.0	9.5	8.2	9.0	8.2
			3	3	3	3	2	2	2	2	2	2	2	2	2
5-6-6	M		10.6	10.0	7.5	11.8	13.6	22.3	27.6	17.7	38.1	7.5	9.8	9.3	7.5
			2	2	2	2	2	2	2	2	2	2	2	2	2
7-1-4	S		1.3	15.0	18.2	17.3	27.6	31.9	45.7	43.0	27.9	19.3	15.4	14.7	10.0
			-	3	3	3	3	3	2	2	2	2	2	2	2
7-1-5	S		0.0	0.0	0.0	0.0	0.0	16.4	42.4	38.1	20.0	15.7	12.1	9.5	7.5
			-	-	-	-	-	3	2	2	2	2	2	2	3
7-2-6	S&M		24.3	17.2	27.1	20.3	24.9	36.6	42.9	36.9	30.4	21.0	22.3	16.5	12.4
			2	2	2	2	2	2	2	2	2	2	2	2	2
7-3-4	S		0.0	4.1	2.8	7.7	8.5	9.3	36.9	13.6	10.0	9.0	10.3	10.0	9.8
			-	-	-	-	3	3	2	3	2	2	2	2	2
7-5-3	S		15.0	28.8	25.4	37.4	33.9	53.3	53.4	37.2	24.0	23.6	17.1	29.4	24.6
			3	3	2	2	3	2	2	3	3	3	3	2	2
7-3-5	S		0.0	7.5	19.9	24.7	25.2	47.6	49.0	44.7	33.9	28.1	21.3	8.8	4.9
			-	1	3	3	3	3	2	3	2	2	2	2	2
7-4-4	S		0.0	0.0	12.9	16.9	25.0	40.2	47.2	44.9	37.6	30.9	14.1	7.2	9.5
			-	-	3	3	3	3	2	2	2	2	3	3	2
7-4-5	S		0.0	0.0	3.4	8.0	8.2	20.8	40.8	42.3	22.3	22.6	28.1	31.1	22.3
			-	-	2	2	2	3	2	2	2	2	2	2	2
10-1-1	S		4.1	16.2	24.7	28.8	30.0	42.0	59.0	43.3	40.7	36.7	30.5	28.5	11.6
			2	3	3	3	3	3	2	3	3	3	3	3	2
10-1-2	M		3.6	35.1	42.5	51.8	54.0	56.3	55.2	48.5	29.1	16.5	11.8	10.6	7.7
			2	2	2	2	2	2	2	2	2	2	2	2	2
10-2-5	M		0.8	2.1	7.0	27.8	50.7	57.0	59.7	55.8	49.5	34.9	19.5	21.3	23.3
			-	2	2	3	2	2	2	2	2	2	2	2	2
10-3-1	S		0.0	0.0	0.0	0.8	45.9	49.7	62.1	58.8	54.2	50.2	44.9	44.7	44.9
			-	-	-	1	2	3	2	2	2	2	2	2	2
10-3-2	S		0.0	7.7	16.2	36.2	54.9	58.3	58.4	40.2	45.4	44.7	49.0	47.8	43.0
			-	3	3	3	2	2	2	3	2	2	2	2	2
10-4-6	S		2.3	0.0	1.7	0.0	34.9	38.7	55.2	41.5	34.1	30.9	26.4	23.1	15.7
			1	2	1	/	2	3	2	2	2	2	2	2	2
10-5-4	M		0.0	4.5	16.4	22.4	30.2	51.1	57.9	45.7	38.8	24.3	21.3	19.8	18.0
			-	1	3	3	3	2	2	2	2	2	2	2	2
10-5-5	M		0.0	0.0	2.1	9.5	17.1	53.3	66.7	48.8	42.7	21.6	27.4	36.1	40.1
			-	-	2	2	3	2	2	2	2	2	2	2	2

Note: The upon values show the cross-sectional area loss, and the lower numbers: 1, 2, 3 show the cross-section type of pitting which was explained in Fig. 2.24. As for the measurement location, C is the section of the wire was raptured. Fracture types are S: Split type, M: Milling cutter type and S&M: Split-Milling cutter type, respectively.

fracture were summarized in **Table 2.12**. From the visual observation, it was found that when the corrosion degree of steel wire was slight, its cross-sectional shape was categorized as type 1 or type 2 in **Fig. 2.27**, while as the corrosion degree increased, type 3 appeared when wires were corroded significantly. It was found that the corrosion around the fracture point of the wire had an important effect on the fracture type of the wire.

When the cross-sectional area losses of a wire at the fracture point and each adjoining end were different significantly, and the cross-sectional type closest to the fracture point was indicated as type 3, the wire was fractured as the split type. On the other hand, when the corrosion on both sides of the fracture point was more uniform, and the cross-sectional type near the fracture point was type 2, it is found that the wire fracture type was the milling cutter type or the split-milling cutter type. Comparing the geometry shape of type 2 and type 3, it can be found that the cross-section of type 2 was more uniformly corroded than that of type 3, so type 3 was more prone to stress concentration, leading to brittle failure of the specimen and the appearance of split fracture type.

As for the specimen fractured in the tensile test, when the wire cross-sectional area loss was significant, even if the cross-sectional type adjacent to the fracture point was type 2, the stress concentration occurred at the corrosion pitting resulting in partial cracking. The residual part of the wires rapidly carried out stress-strain redistribution, and the cross-sectional deformation occurred necking phenomenon. The tensile capacity of the residual cross-sectional area was particularly small relative to the applied tensile force, therefore, the residual part of the wire instantly fractured to form a milling cutter type.

2.7 Chapter conclusions

The corrosion test and tensile test for thirty 1×7 PC steel strands were carried out to study the prestressing force and the residual properties of the corroded steel strand. The following conclusions were drawn:

1. The degradation of prestressing force of the strand during corrosion test can be divided into two stages after the effect of relaxation. In the first stage the prestress decreases linearly with the mass loss of the strand due to the corrosion, and the second stage starts when the maximum cross-sectional area loss of the corroded wire in the strand reaches around 40%.
2. The second stage of prestress loss is greatly related to the way the wire is damaged. Compared with specimens with brittle damage, specimens with ductile damage have a longer second stage of deterioration and higher prestress loss.
3. During the corrosion process, the corroded part of the strand decreases in tensile properties due to loss of cross-sectional area and increases in deformation and strain, resulting in loss of prestress in the strand. The uncorroded part has an overall strain reduction due to the loss of prestress. Therefore, both the mass loss of the corroded part and the corroded length have a significant effect on the prestress loss.
4. The deterioration of the ultimate tensile properties of the strand after corrosion can be divided into two stages, which are basically the same as the deterioration stage of prestressing. When the maximum cross-sectional area loss of fractured wire is less than around 40%, the ultimate tensile capacity decreases linearly with the increase of the maximum cross-sectional area loss, and the fracture type is milling cutter type with ductile damage. When the maximum cross-sectional area loss of the fractured wire exceeds around 40%, the wire fracture type changes to the split type or split-milling cutter type with brittle damage, and the ultimate tensile capacity of the specimen with the fracture type of split-milling cutter type is slightly higher than that of the specimen with the fracture type of split type.
5. The fracture type of steel wire and stress distribution, affected by the corrosion shape, when the corrosion around the most serious point corrosion degree changes more, and cross-sectional shape for type 3, the fracture is usually split type. When

the corrosion around the most serious point corrosion degree changes less, corrosion is more uniform, and cross-sectional shape for type 2, the fracture is usually milling cutter type, when Specimen corrosion degree is higher, and by the external force of tensile, cross-section type will change from milling cutter type to split - milling cutter type brittle damage.

Chapter 3 Corrosion test of PC beam

3.1 Introduction

This chapter introduces the design and production process of the specimen and the corrosion test of the PC beam. Investigates the effect of corrosion of prestressing strands on deterioration of the average strain of the steel wire, deflection during initial loading and initial crack load.

3.2 Specimen production
3.2.1 Specimen design

A total of 24 post-tensioned concrete beams were designed and manufactured for this project to investigate the effect of prestressing strand corrosion on beam performance. The beams are reinforced with two 8 mm plain bars at the bottom, two 12 mm deformed bars at the top, and 8 mm stirrups with 90 mm spacing. To prevent corrosion of the longitudinal and hoop reinforcement, an epoxy resin coating was applied to the longitudinal and hoop reinforcement prior to casting. The beams are casted with a 32 mm concrete duct. The duct is formed by dragging out the embedded rubber rod after concrete casting. The cross section and reinforcement of the beams are shown in **Fig. 3.1**.
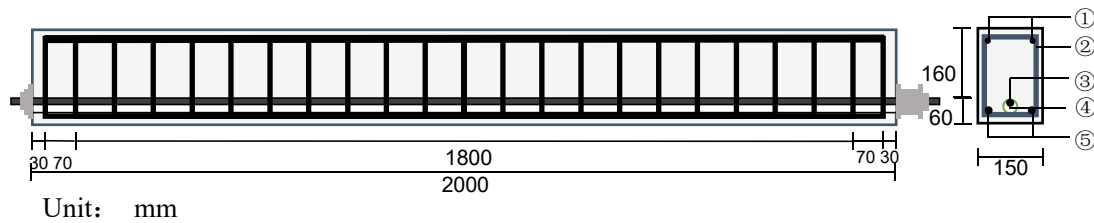
Note: ① 2⌀8 steel bars, ② Φ8@90 stirrups, ③Φ15.2 1×7 strand, ④ Φ32 duct, ⑤ 2⌀12 steel bars

Fig. 3.1   Beam detail

3.2.2 Mechanical properties of the test materials

The design strength of the concrete for the test beam was chosen as C40, which is commonly used in engineering, and the concrete was obtained from Ningxia Commercial Mixing Station, Details of the concrete mix ratio are shown in as shown in **Table 3.1**. The age and mechanical properties of the concrete are shown in **Table 3.2** The mechanical properties of the reinforcement, strand used in the test beam are shown in **Table 3.3**. and **Table 3.4**

Table 3.1   Proportions of concrete mixes

NO.	Water	Cement	Fine Aggregates	Coarse Aggregates	Water Reducers
C40	160kg/m³	400kg/m³	758kg/m³	1137kg/m³	7.4kg/m³

Table 3.2 Mechanical properties of the concrete

Age	compressive strength	Flexural strength	Splitting strength
7d	42.00MPa	4.65MPa	2.70MPa
28d	49.60MPa	5.29MPa	3.22MPa

Table 3.3 Mechanical properties of reinforcement

Type of reinforcement	Diameter	Yield strength	Elastic modulus
Deformed bars (HPB335)	12 mm	335 MPa	110 GPa
Plain bars (HRB 235)	8 mm	235 MPa	210 GPa

Table 3.4 Material properties of steel strand.

Type	Nominal diameter	Cross section area	The weight per meter	Tensile strength	Range of ultimate tensile capacity	Elongation
1×7	15.2 mm	140 mm^2	1101 g/m	1860 MPa	260-288 kN	≥ 3.5%

Note: The ultimate tensile capacity standard of 15.2mm 7 wires strand is from 260kN to 288kN, in this test the ultimate tensile capacity of specimen was 265kN, when one specimen was used.

3.2.3 Fabrication process of the test beam

The reinforcement cage was tied. To prevent corrosion of the longitudinal bars and hoop reinforcement during the test, anti-corrosion paint was applied to the surface of the cage after tying as shown in **Fig 3.3**. To measure the internal strain in the concrete, 100aa strain gauges were attached to the plastic 'I'-plates and the surface was covered with waterproof structural adhesive to prevent damage to the gauges during casting as show in **Fig 3.2**. After the pour was completed, the 'I' plastic plate was embedded in the concrete and deformed as the concrete deformed. The corrugated pipe was not buried inside the test beam to prevent the strand from being difficult to corrode. After the tied cage was formed, a 2.5m long, 32mm diameter pvc pipe was fixed to the position of the strand and then casteded. After the concrete had first set, the pvc pipe was pulled out to form the prestressing strand aperture. Tension is applied at one end and the age of the concrete exceeds 28 days at the time of tensioning. The tensioning end and the anchoring end are simultaneously pre-buried with a steel mat to withstand the local pressure. Strain gauges affixed to the outer ring of the strand were attached to the strand before tensioning and tested for strain changes during the tensioning process. The tensile prestress σ was taken to be 915 MPa for all test beams, which is approximately 50% of the yield stress. Finally, grouting was carried out and the results are shown in **Fig. 3.4**

(a) 'I' plastic plate with concrete strain gage

(b) Install in reinforcement cage

Fig 3.2 Embedded concrete strain gage

Fig. 3.3　Anti-corrosion paint is applied　　Fig.3.4　Grouting condition

3.2.4 Strain gauge distribution

The internal strain gauges paste position as shown in **Fig. 3.5**. The concrete strain gauges are embedded in the geometric centre of the beam and at a distance of 450mm from the centre and 10mm from the strand. The strand strain gauges are positioned at the mid-span and at a distance of 500mm from the mid-span, depending on the location of the corrosion. To prevent errors and damage to some of the strain gauges, strain gauges were attached to the bottom two longitudinal bars in the same position, at the midpoint, below the loading point and 45° below the loading point diagonally.
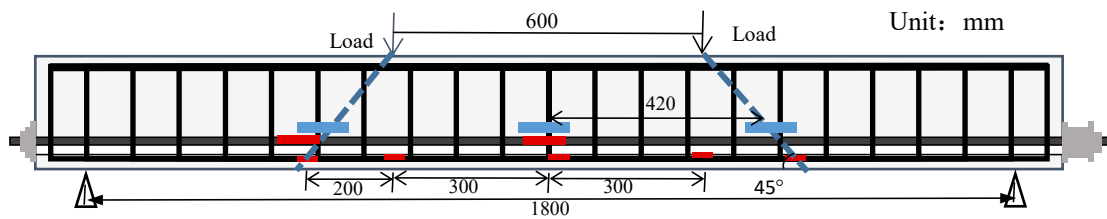

Fig. 3.5 Strain gauge distribution diagram

3.3 Overview of the accelerated corrosion test

The test uses the current acceleration method to corrode the specimen, and controls the corrosion time and current strength to control the degree of corrosion of the strands in the beam. The short side of a 500mm length basin is cut into a U-shaped opening and taped to the corroded position of the beam, a 5% NaCl solution is added and soaked overnight so that the solution penetrates into the concrete to contact the steel strand, after which the stainless-steel plate is placed in the basin and converted from domestic 220v AC to constant DC by using the UTP3315TFL-ll Regulated DC power supply. The positive terminal is connected to the strand and the negative terminal to the stainless-steel plate, forming a circuit. Due to the different circuit resistance of different specimens and the limited voltage, the corrosion current of each specimen is its maximum value, taking into account the test time. The strain change in the outer ring of the steel strand is tested during the corrosion process. All beams were divided into two groups according to the corrosion location, with some beams corroding in the middle of the span and some beams corroding on the side of the beam, as shown in **Fig 3.6.** In order to prevent the corrosion of the strand surface from affecting the strain measurement, and the effect of corrosion on the strand strain can be measured more accurately. The 1aa strain gauge is affixed to the 6 outer wires of PC strand 250mm away from the corrosion edge. The corrosion system picture is shown in **Fig. 3.7.**
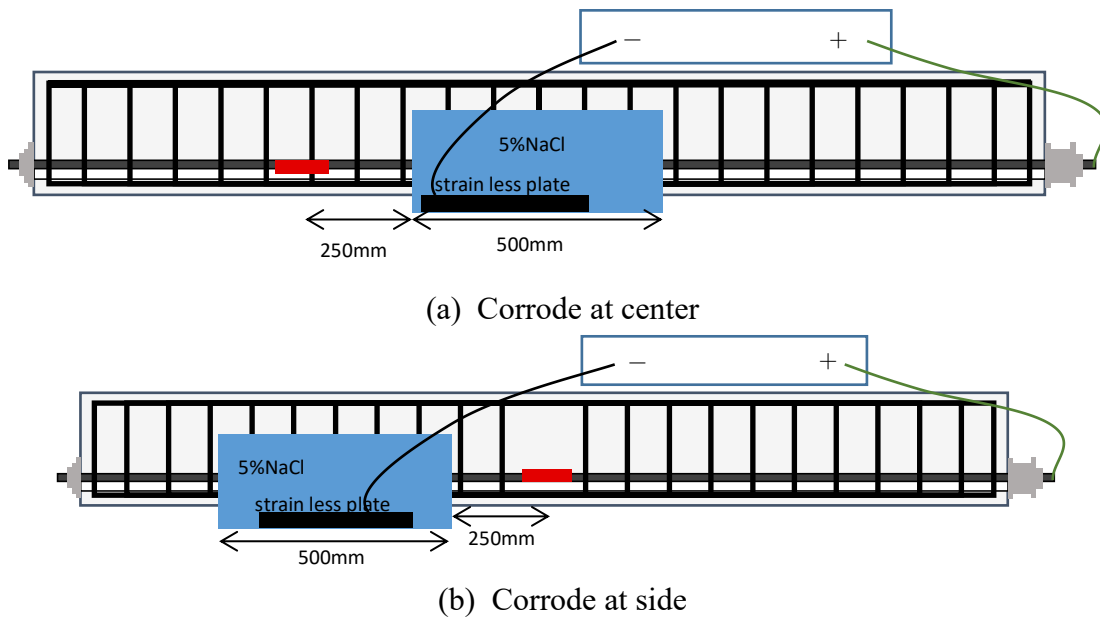
48

(a) Corrode at center

(b) Corrode at side

Fig. 3.6   Corrosion system diagram
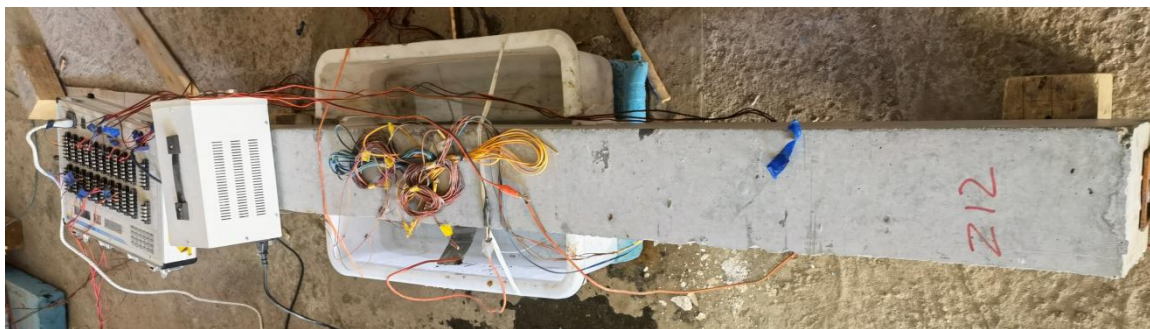
(a) Corrode at center

(b) Corrode at side

Fig. 3.7   Corrosion picture

3.4 Analysis of corrosion test results.
3.4.1 Test result

The strain of the outer ring steel wires of the PC strands was measured during the corrosion process, and the strain loss was calculated for the average value of the strain in the outer ring steel wires. The strand corrosion loss in each beam was measured by the destructive method. After the mechanical tests, the corrosion section of the beam was cut down with a concrete cutting machine. The concrete cover was stripped off, strands were taken out and the grout on their surface was removed. Then, the corroded strands were cleaned by 12% hydrochloric acid solution and neutralized by the acid with alkali. The mass of each group of strands after complete descaling was weighed

separately with an electronic scale to calculate the actual mass loss of the corroded strands. The strand is separated into wires and the corrosion is observed. The corrosion focused almost at the external wires, the corrosion of the central wire is very slightly. Following this, the corrosion depth of the strands was measured and the maximum cross-sectional area loss of the strands was calculated according to the previous research method which has been mentioned in chapter 2. **Table 3.5** shows the mass loss, maximum cross-sectional area loss, strain loss during corrosion, and cracking load for all specimens. The specimens in the table include the specimens of static load test and the specimens of fatigue test, where the specimens of fatigue test are performed and the test results will be used in the subsequent research. The S-B-12-2 have two mass loss value, the 10.65%* is calculated value at wires fracture, the 12.85% is the measured value after test. In the specimen No., 'S' represents the specimen will be carried out static loading test, 'F' means the specimen will be carried out fatigue loading test. 'UC' represents uncorroded, 'A' means corrosion position is at the center of beam, 'B' means corrosion position is at side of beam. As a example, 'S-B-12-2 The first number '12' shows the mass loss value of specimen; the second number '2' is specimen number, when specimens have same mass loss value.

Table 3.5   Corrosion test result

Specimen No.	Mass loss /%	Max cross section area loss /%	Strain loss/%	Cracking load/kN
S-UC	/	/	/	42
F-UC	/	/	/	44
S-A-1	1.83	1.6	1.04	44.8
S-A-3-1	3.69	5.09	2.09	32
S-A-3-2	3.73	5.71	-	32
S-A-6	6.37	11.25	2.89	38
F-A-1	1.29	2.1	0.79	39
F-A-7-1	7.25	18.64	-	34
F-A-7-2	7.34	11.7	6.44	35
S-B-6	6.63	20.44	3.68	37.86
S-B-7	7.28	33.42	7.49	38
S-B-9	9.37	24.3	-	28
S-B-11	11.43	23.47	6.14	-
S-B-12-1	11.93	17.4	-	30
S-B-12-2	10.65*/12.85	39.19	8.57	22.8
S-B-13	13.7	22.1	11.83	35
F-B-6	6.40	16.47	4.05	35
F-B-5	5.168	19.42	2.24	35
F-B-12	12.73	30.07	8.19	32

Figure 3.8 shows the corrosion condition of S-B-6 and S-B-12 in bottom of beam, PC strands, stirrups and longitudinal steel bars. It can be found that due to the anti-corrosion paint applied to the stirrups and longitudinal bars, the surfaces of the stirrups and longitudinal bars are almost free from corrosion regardless of whether the corrosion level of the strands is high or low. Observing the corrosion zone at the bottom

of the specimen, it can be found that when the corrosion degree is high, longitudinal cracks will appear at the bottom of the specimen.

(a) S-B-6

(b) S-B-13

Fig 3.8   Corrosion condition of PC strands, reinforce bars and stirrups

3.4.2 Strain loss

According to a previous study[47], the mass loss has a better correlation with strain loss. Thus, in this paper, the mass loss of strand is used to represent the corrosion degree to analyse the relationship between the strain loss of outer ring wires and the corrosion degree. The average strain loss in the outer ring steel wires during the PC strand corrosion tests (which have been mentioned in Chapter 2), and that of the PC strands in the PC beam corrosion tests are shown in **Fig. 3.9**. Since the distance from the corrosion location to the strain gauge attachment location is the same for both A and B series, the bonding action is almost the same. Although the corrosion locations are different, their strain loss regularity is almost the same. And the PC strands inside the PC beams were subjected to bonding forces due to the grouting. It was found that the strain loss in both bonded and unbonded PC strands increased with the increase of corrosion, and the trend of increase was similar in both cases. Comparing the strain loss of these PC strands, it can be found that the strain loss of the PC strands bonded in concrete is very close to that of the PC strand unbonded. However, it is noted that the corrosion length of the PC beam was 500mm, which is larger than that of unbonded PC strands. Consequently, the

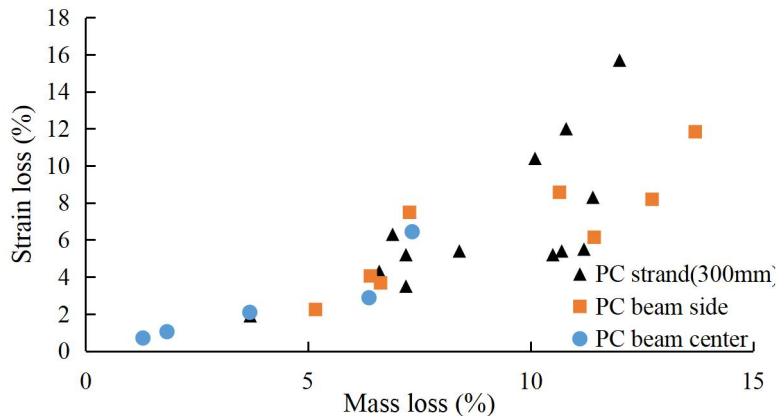bond property between the PC strand and concrete in the beams decreases the strain loss due to the corrosion.

Fig.3.9   Strain loss versus mass loss

3.4.3 Cracking load

The relationship between cracking load and mass loss is shown in Fig. 3.10. It can be found that the specimen cracking load decreases with the increase of mass loss. It is due to the mass loss which leads to reduction of prestressing force in strand which in turn causes the cracking load to decrease. Comparing the centre-series and side-series, it can be found that the trend of the reduction of the initial cracking load with the degree of corrosion is almost the same, which indicates that the corrosion location has a lower influence on the prestressing deterioration. According to the deterioration law of prestressing with mass loss, the cracking load decreases linearly with the increase of mass loss, and the cracking load decreases faster when the mass loss is higher.
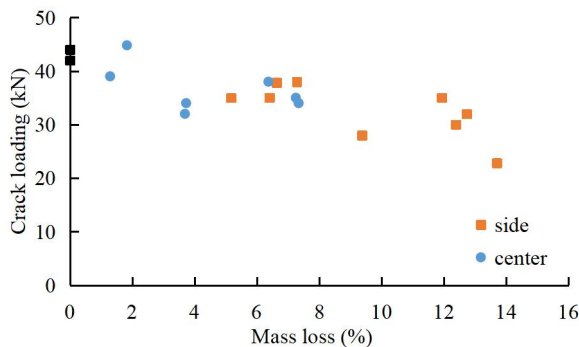

Fig. 3.10   Crack load versus mass loss of strand

3.4.5 Prestress loss

Figure 3.11 shows the prestress loss of PC strands in the PC beams calculated by the strain loss according to Eq. (2.24) in chapter 2. The results from the figure show that the trend of prestress loss of PC strands in the beams due to corrosion agrees with the results of the PC strand corrosion tests; the deterioration process can be divided into two stages. In the first stage, the prestress loss increases linearly with increasing mass loss. When the corrosion degree is higher, the second stage begins, and the speed of prestress loss increases. Since the beginning of the second stage of prestress deterioration is associated with the maximum cross-sectional area loss[48], it is difficult to determine the

stage of prestress deterioration by mass loss. When the mass loss is small the maximum cross-sectional area loss is usually also relatively small, therefore, by narrowing down the selection (mass loss less than 7%), selecting the data with a high probability of being in the first stage of prestress deterioration for fitting. The regression line as show in Fig. 10, its regression equation as follows:

$$P_c/P_0 = -0.23n + 1 \tag{3.1}$$

where, P_c is the prestressing force of the PC steel strand after corrosion; n is the corrosion degree of the steel strand; P_0 is the prestressing force before corrosion occurred.

Make a comparison with corrosion test of PC strands which has been mentioned in Chapter 2 Eq (2.25), it can be found that the a of PC beam is less than PC strand, even if the corrosion length of PC beam is larger than that of PC strand. Thus, the bonding between the strand and concrete can effectively inhibit prestressing loss.
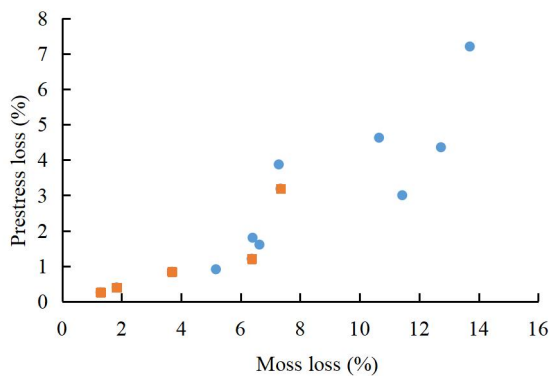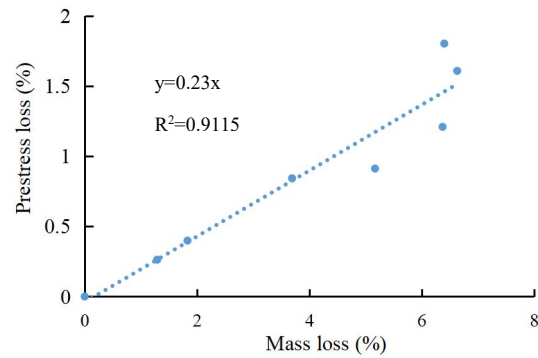
Fig. 3.11   Prestress loss versus mass loss   Fig. 3.12   Prestress loss in first stage

3.4.5 Initial loading and displacement

Figure. 3.13 illustrates the load-deflection curves for the static and fatigue tests at initial loading from 0 to 30kN. Comparing the specimens with different corrosion degree at the same corrosion location, it is found that the higher the corrosion degree, the larger the deflection under the same load, because in the early stage of loading before cracking occurs, when the external load is small, the initial prestress has a greater influence on the deformation of the beam, and according to the conclusions of the previous tests[47], the higher the corrosion degree of the strand, the greater the prestress loss. In addition, when the corrosion degree is higher, the expansion of corrosion products will lead to the cracking of the concrete cover to reduce the bond performance, resulting in a larger deflection of the specimen. Comparing the uncorroded and slightly corroded specimens, it can be found that the deflection of the specimen with slight corrosion is smaller under the same load, it is due to the fact that the effect of slight corrosion on the prestressing force is very low, and the expansion of the corrosion products did not lead to cracking of the concrete, but instead, it strengthened the bonding properties, which resulted in lower deflection of the specimen. Comparing the A series with the B series, for the same degree of corrosion, centre corrosion has a greater effect on the mid-span deflection of the beam than edge corrosion. The reason for this is that the middle of the beam is where the bending moment is greatest during four-point loading, and the loss of bending resistance and deterioration of bond properties of the strands is more significant here than at other locations.
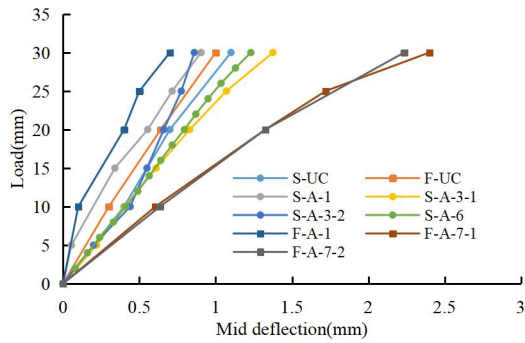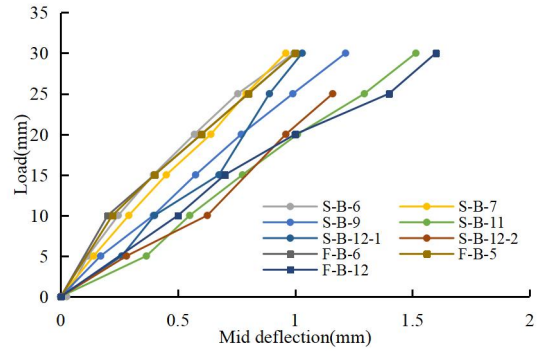
(a) A-series   (b) B- series

Fig. 3.13   Load- deflection curve (0-30kN)

3.5   Chapter conclusions

1. In prestressed beams, the effect of corrosion on prestressing deterioration remains significant and bond performance can be effective in preventing prestressing deterioration. The prestress loss of PC beam show the same regulation with that in corrosion test of PC strand. In the first stage, the prestress loss increase linearly with mass loss increase, in the second stage, the speed of prestress loss increase.

2. In the loading stage before concrete cracking, the initial cracking load decreases linearly with increasing strand mass loss, and the deflection of the specimen increases with increasing strand mass loss. Corrosion location in the centre has a greater influence.

Chapter 4 Effect of corrosion of PC strands on bending behaviour of PC beams under static loading

4.1 Introduction

Corrosion of prestressing strand, the impact on the force performance of prestressed concrete members is mainly manifested in three aspects: (1) the internal prestressing force of the strand decreases. (2) The cross-sectional area of the strand is reduced, the tensile properties are weakened and deformation is more likely to occur. (3) Corrosion pits on the surface of the strand, will produce stress concentration phenomenon, in the state of high stress is prone to brittle fracture. (4) Corrosion products lead to volume expansion, weakening the bond between the prestressing strand and the concrete.

This chapter investigates the effect of corrosion of prestressing strands on the damage patterns of stressed members, and predicts and prevents sudden damage of prestressed beams after corrosion by analysing the role played by the strands in the beam loading process after corrosion.

4.2 Static loading test program

The specimens of this test is S series of Chapte 3 after the accelerated corrosion. **Fig. 4.1** shows the schematic arrangement of the dial gauges and the strain gauges. The vertical deflections in the span, at the loading point and at the support settlement were measured by means of five electronic digital micrometers. Resistance strain gauges were installed in the mid-span section to measure the concrete strain. Each side of the figure beam was painted white and marked with a 50mm metre grid to facilitate detection of cracks.
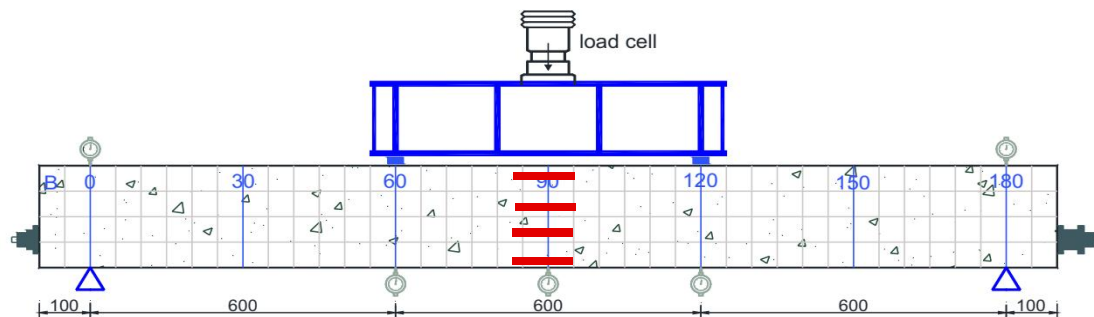

Fig. 4.1   Loading diaram

The beams were simply supported and subjected to four-point bending. Each beam had a clear span of 1800 mm and a shear span of 600 mm. The test was carried out using a 500T screw type electro-hydraulic servo loading tester JAW-500A. In order to eliminate the gap between the loading equipment and the test beam, to check the normal operation of the apparatus and to reduce the measurement error, the test was preloaded twice before the final test and the load control value was taken as 10kN. The final loading process was divided into two stages. The first stage is controlled by the load until the peak load of the beam is reached. For light and slightly corroded beams, the load is applied gradually at a rate of 5 kN/min. Severely corroded beams have a lower load carrying capacity and are loaded at a rate of 2 kN / min. The second stage is carried

out in displacement controlled mode with loading increments of 2 mm per step and a loading rate of 2 mm/min. The loading test is stopped when the load carrying capacity drops to 80% of the peak load or when physical deterioration of the beam is evident. At the initial stage of loading, cracks are observed by eye to appear and the initial crack load is recorded, after which up to 40 or 50 kN, the width of each crack is measured starting until the load reaches its peak.

4.3. Test result and discussion
4.3.1 Static load test results

In order to study the flexural performance of prestressing strands after corrosion of PC strands, a four-point flexural loading test was carried out on 14 beams. A summary for the flexural test results is listed in **Table 4.1**. The corrosion loss, ultimate strength, and failure mode are included in this table.

According to the table it can be found that for strands corroding within the beam, when the corrosion is more severe, the strand corrosion is not uniform and is more random, which results in a greater difference in the maximum cross-sectional area loss when the mass loss of both strands is the same.

The mass loss of S-B-12-1 and S-B-13 are both large at 11.93% and 13.7% respectively and that of S-B-7 is only 7.28%. However, the cross sectional area loss of S-B-7 is 31.87%, much greater than the 17.4 for S-B-12-1 and 22.1 for S-B-13. And since the change in mass loss has a more pronounced effect on the prestress in the strand, the mass loss expresses the degree of corrosion in a way that better reflects the relationship between the degree of corrosion and the initial cracking load. The ultimate load and damage type of the beam are more influenced by the maximum cross-sectional area loss. The table shows that the ultimate load of the strand is significantly reduced when the corrosion is relatively severe.

Table 4.1　Static loading test result

Specimen No.	Mass loss(%)	Max cross-section area loss(%)	Ultimate strength(kN)	Failure mode
S-UC	0	0	121.1	CC
S-50-A-1	1.83	1.6	118.5	CC
S-50-A-3-1	3.69	5.09	111.2	CC
S-50-A-3-2	3.73	5.71	115	CC
S-50-A-6	6.37	11.25	110	CC+CS
S-50-B-6	6.63	20.44	115	CC
S-50-B-7	7.28	33.42	100	WR+SCC
S-50-B-9	9.37	24.3	115	WR+CC
S-50-B-11	11.43	23.47	115	CC
S-50-B-12-1	11.93	17.4	115	CC
S-50-B-12-2	12.85	39.19	95	WR(PRE)+SCC+CS
S-50-B-13	13.7	22.1	110	WR+CC+CS

Note: CC means concrete crushed, WR means wires rupture. CS means concrete spalling, WR(PRE) means wires rupture before loading test. SCC means slight concrete crush

4.3.2 Specimen failure patterns position

Figure 4.2 shows the failure condition of the specimen and the area of corrosion. When loaded to about 30% of the ultimate load, the first crack appeared in the span of

the uncorroded beam S-UC-1, with increasing cracks in the pure bending section and bending shear zone as the load increased, when loaded to about 60% of the ultimate load, the cracks were not increasing but developing wider as the load increased, with a more uniform distribution of cracks in the span and fine cracks due to the presence of the bond. Under the load, the test beam was eventually over-deformed due to the yielding of the non-prestressed tendons, and the strain on the concrete in the compression zone increased sharply, resulting in the concrete being crushed as a typical reinforced beam failure.
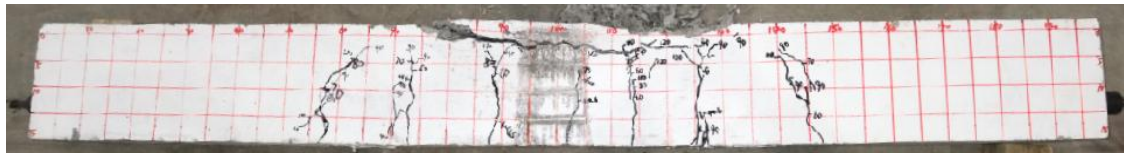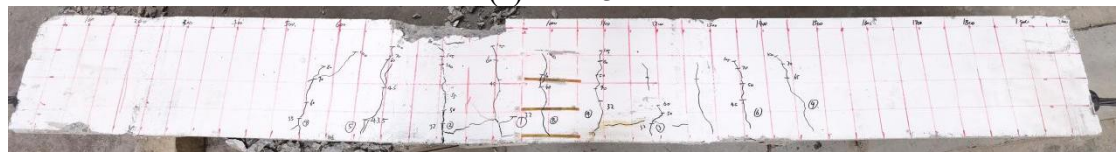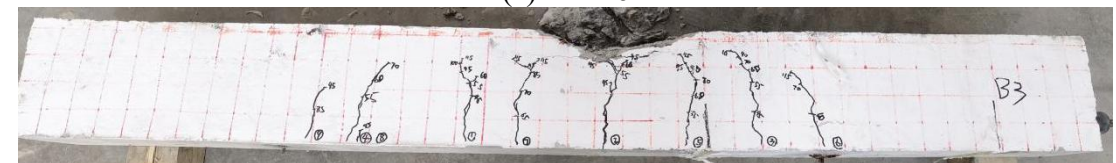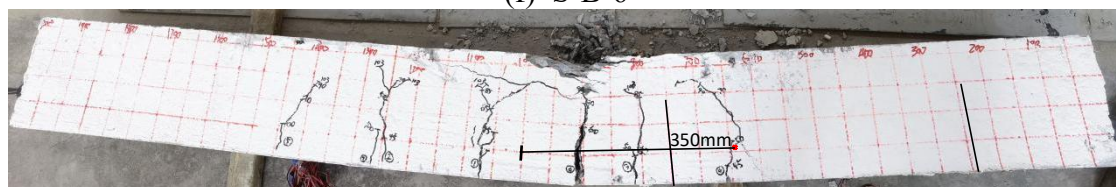

(a) S-UC

(b) S-A-1
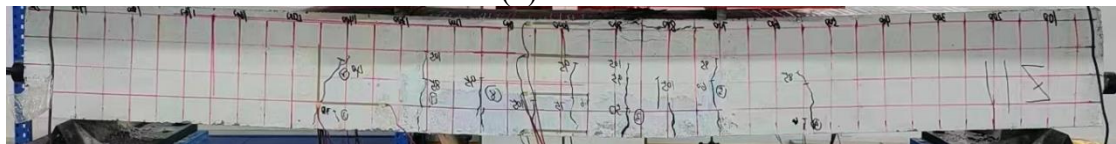
(c) S-A-3-1

(d) S-A-3-2

(e) S-A-6

(f) S-B-6

(g) S-B-7

Fig. 4.2   Specimen failure mode

(h) S-B-9

(i) S-B-11
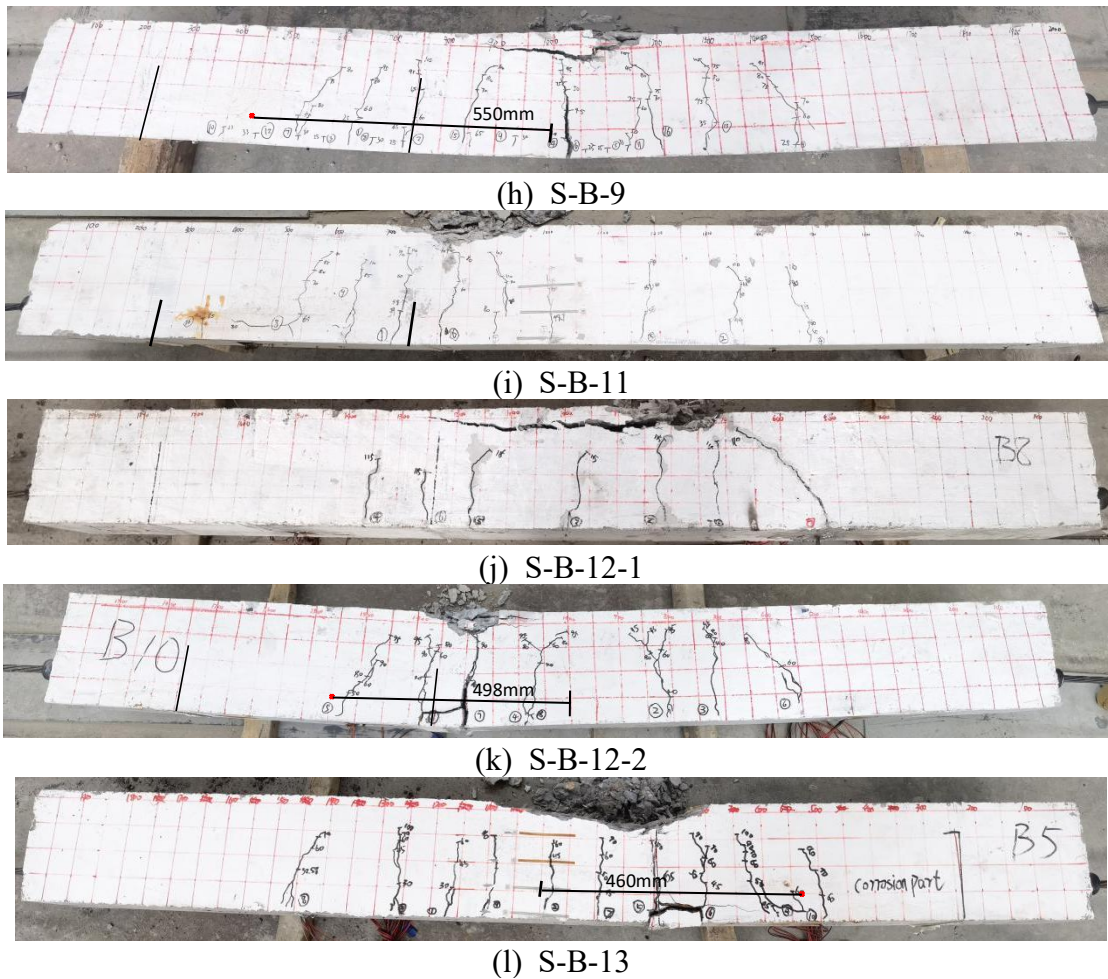

(j) S-B-12-1

(k) S-B-12-2

(l) S-B-13

Fig. 4.2   Specimen failure mode

The specimens S-A-1, S-A-3-1, S-A-3-2, S-B-6, S-B-11 and S-B-12-1 were all failure due to the cracking of the concrete in the compression zone at the top of the beam, of which S-A-1, S-A-3-1 and S-A-3-2 were failure due to the low level of corrosion and the expansion of the corrosion products did not lead to concrete cracking, but rather to The bonding properties are enhanced, resulting in finer cracks compared to the uncorroded beams.

In the remaining specimens, due to the relatively high level of corrosion, the volume expansion of the corrosion products causes the surface of the concrete protection layer to crack, longitudinal cracks appear, the bond strength decreases and the width and spacing of the cracks in the beams increase with the level of corrosion. In S-A-6, the longitudinal cracks occurred in the purely curved section of the beam and intersected with the longitudinal cracks during loading, resulting in interlocking longitudinal and vertical cracks in the concrete at the bottom of the purely curved section of the test beam and leading to spalling of the concrete at the bottom. At the same level of corrosion, this did not occur in the B series due to the location of the corrosion at the edge of the beam, only in S-B-12-2 and S-B-13 did the concrete crack and spall in the bending shear zone due to the high level of corrosion. The strands of specimens S-B-7, S-B-9, S-B-12-2 and S-B-13 all fractured, the fracture location has been marked in **Fig. 4.2**, and show the distance from center of beam to fracture point.However, but the failure mode of S-B-9 and S-B-13 was different from that of S-B-7 and S-B-12-2. Due to the severe loss of cross-sectional area of the strands in S-B-7 and S-B-12-2, the strands fractured before the beam reached the yielding stage,

58

resulting in a lower ultimate load carrying capacity of the beam. Continued loading of the beam resulted in successive fractures of the strands, a continuous reduction in the load carrying capacity of the beam, a rapid increase in deformation and severe cracking of the beam. The S-B-9 and S-B-13, on the other hand, did not fracture even when the beam was loaded to the yielding stage and the concrete in the top compression zone was broken due to the small loss of cross-sectional area, until the deflection at the bottom of the beam increased to about 45mm and the strand fractured. The load carrying capacity of the beam suddenly decreased and cracking occurred. Thus, the ultimate load carrying capacity of S-B-9 and S-B-13 is reduced very little and the concrete at the top breaks up severely, with significant cracking occurring at the final failure.

3.3.3 Ultimate load versus mid deflection

Figure 4.3 shows the load-deflection curve for the test beam. It can be seen from the curves that the load-deflection curves for the uncorroded test beam and other less corroded beams can be divided into three stages: loading to cracking, cracking to yielding, and yielding to ultimate load, with significant transitions between the stages due to a reduction in the flexural stiffness of the section caused by cracking of the concrete or yielding of the reinforcement.

In the case of S-B-7 and S-B-12-2, due to the high level of strand corrosion, the strand breaks before the longitudinal bars have yielded and the load deflection curve can be divided into two stages: the loading to cracking stage and the cracking and in to ultimate load stage. The yielding phase of a corroded beam has a relatively short mid-span deflection. And the higher the corrosion, the less the mid-span deflection increases in the yielding phase, which is caused by the reduction in the cross-sectional area of the strand due to corrosion, resulting in a reduction in the ultimate load.
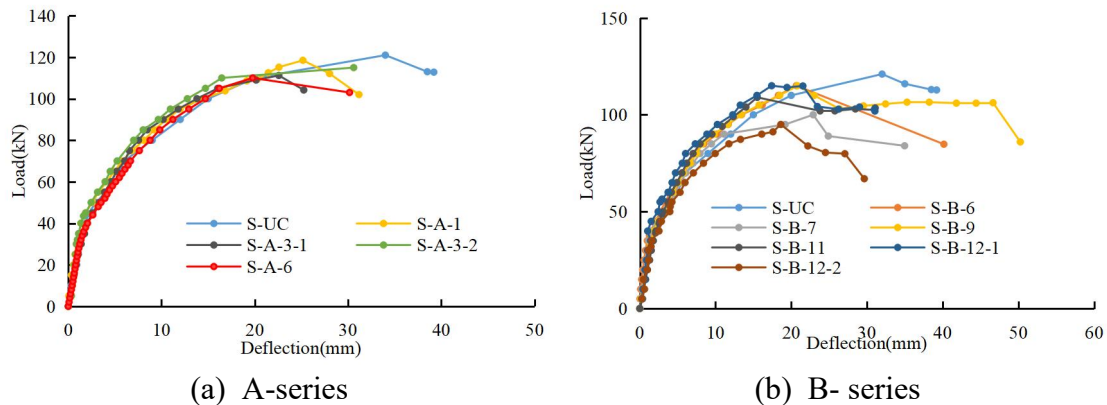

| (a) A-series   (b) B- series |
| Fig. 4.3   Load- deflection curve |

The relationship between the ultimate load carrying capacity of the beam and the maximum cross-sectional area is shown in **Fig. 4.4**. As the loss of cross-sectional area of the strand increases, the ultimate load carrying capacity of the specimen decreases continuously. The degradation of the ultimate load carrying capacity is not obvious for specimens where the strand does not break. For specimens where the strand breaks, where the S-B-9 and S-B-13 strands break after the concrete in the compression zone of the beam breaks, the effect on the ultimate load is less. In the case of S-B-7 and S-B-12-2 the reduction in ultimate load is particularly pronounced due to the strand breaking early in the second stage of loading. Comparing A-Series and B-Series, it can be seen that the ultimate load capacity of the beam is more affected by the location of the corrosion in the purely bending section when the corrosion level is the same.
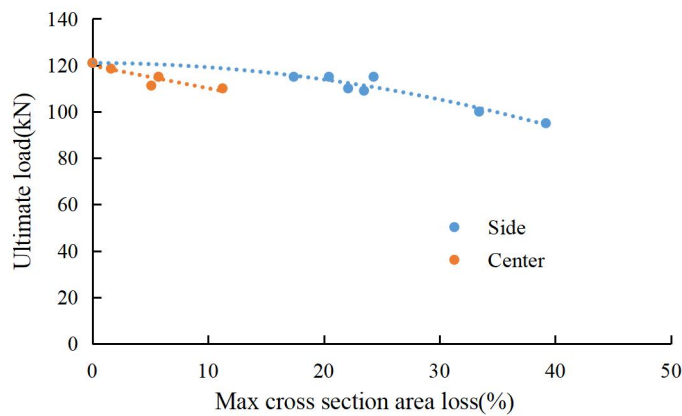
Fig.4.4   Ultimate load versus Max cross sectionarealoss

4.3.4 Change in angle during loading of the specimen

The effect of strand corrosion on the beam during loading was investigated by measuring the angle change from the loading point on the corroded side to the edge of the beam in relation to the degree of corrosion. The angle measurements are shown in **Fig. 4.5**. **Figure 4.6** shows the relationship between the angle and the degree of corrosion at the pre-cracking stage (30kN) and the pre-yielding stage (95kN). It can be observed that at the early stages of loading, the angle increases with mass loss due to the greater effect of prestress on the deflection at the bottom of the beam and that the location of corrosion has a greater effect on the increase in angle. When the beam is loaded to 95kN, the effect of deflection due to strand area loss on the angle becomes greater and the maximum cross-sectional area is chosen to indicate the degree of corrosion. As the corrosion level rises, the angle increases. Comparing the different corrosion locations, it can be found that corrosion in the bending zone has little effect on the angle change, and in the bending and shearing zone there is a significant increase in angle when the strand cross-sectional area loss reaches around 25%.
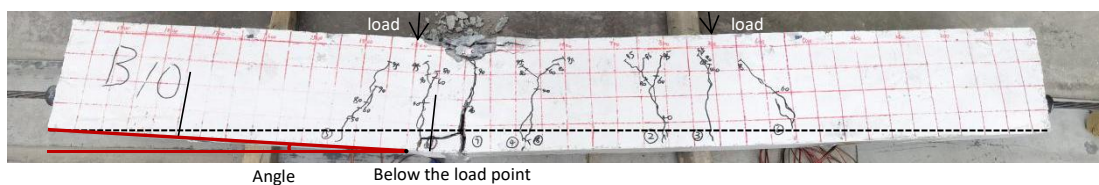

Fig.4.5 The Angle at the loading point
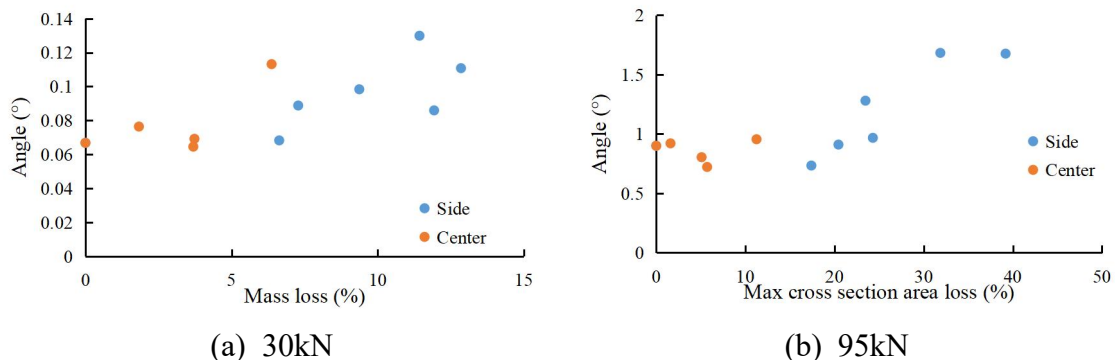

(a) 30kN

(b) 95kN

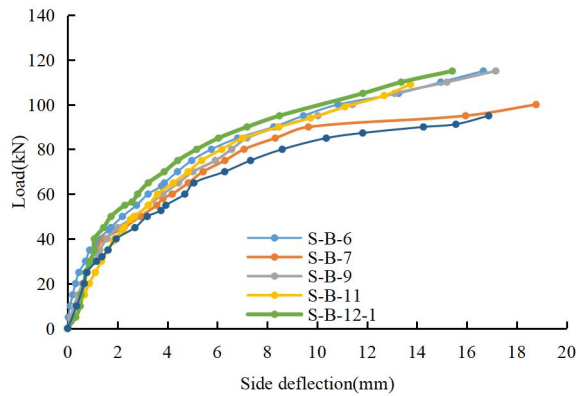Fig. 4.6   Angle versus Max cross section area loss
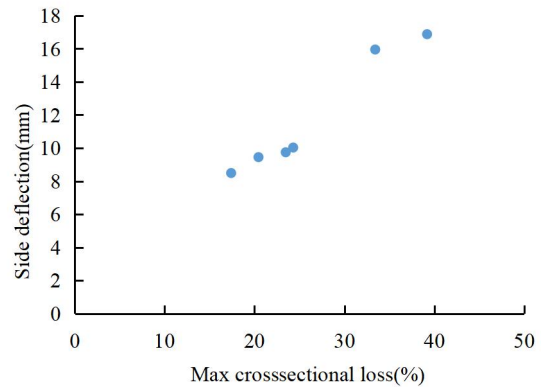
Fig. 4.7 Corrosion side load- deflection curve

Fig. 4.8 Side deflection versus max cross section area loss

To further determine the effect of edge corrosion on the beam, the load - side deflection curves is shown in **Fig.4.7.** For visual comparison, the load was taken as 95kN and the deflection of the corrosion side loading point of each specimen is shown in **Fig. 4.8**. It can be found that when the load is loaded to the second stage, as the load continues to increase, the deflection of the corrosion side of the specimen varies greatly for different degrees of corrosion. Observing **Fig. 4.8**, it can be found that under the same load, the greater the degree of corrosion, the greater the deflection at the loading point on the corrosion side, which also leads to the main cracks in the specimen being closer to the corrosion side.

4.3.5 Crack width and crack space

The variation in the width of the main crack during loading is shown in **Fig. 4.9**. With the increase in load, the main crack width of each specimen increased continuously and at an increasing rate. The volume expansion of the corrosion products leads to cracking of the concrete, a decrease in bond performance and an increase in strand slip, leading to an increase in crack width. On the other hand, the reduction in the cross-sectional area of the strand leads to a decrease in the stiffness of the specimen, resulting in greater deformation under the same load, leading to an increase in crack width. Therefore, at the same level of corrosion, the main crack width was greater for specimens with spanwise corrosion at the same load. The test measured the average crack spacing after fatigue loading test, as shown in **Fig. 4.10.** There was a tendency for the crack spacing of the specimens to increase with increasing corrosion, but there was little increase at lower levels of corrosion and at more remote locations of corrosion. This is because for heavily corroded beams, cracking causes a significant reduction in the strain energy of the concrete in tension due to the poor bond performance of the strands to the concrete. The transfer of tensile strains in concrete requires a long transfer length and the increment of tensile strains in concrete becomes slower along the transfer length. The residual tensile strain in concrete is small. Therefore, new cracks will only appear when the beam is deformed in larger increments and at larger intervals. In contrast, the corroded strands on the side of the beam have less influence on the deformation of the purely bending section and the crack spacing does not increase significantly.
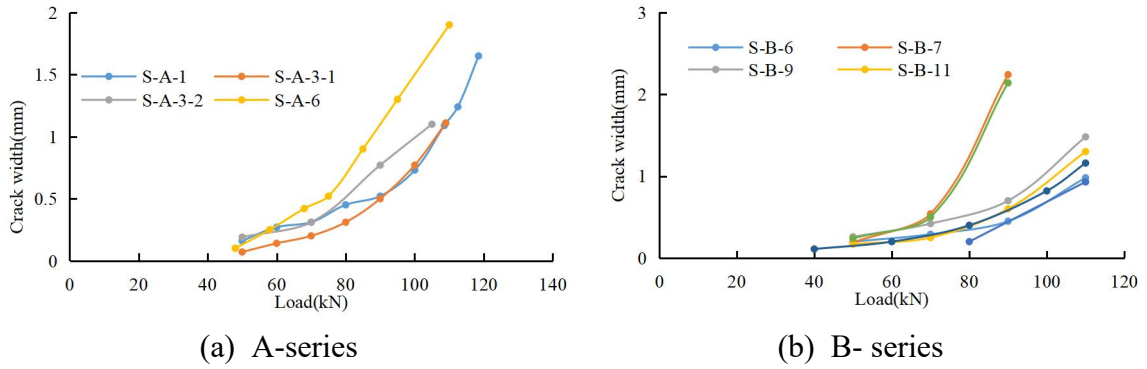
(a) A-series   (b) B- series
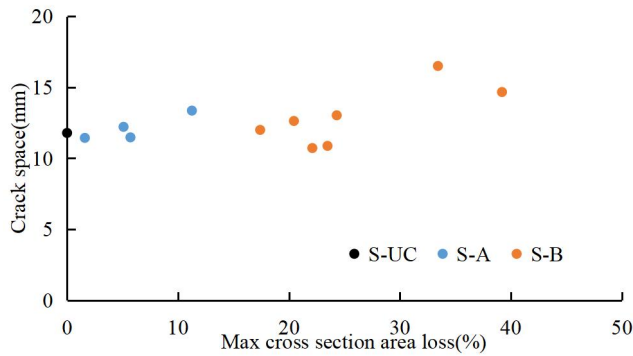
Fig.4.9   Crack width

Fig. 4.10   Crack space versus max cross section area loss(%)

(a) A- series   (b) B- series
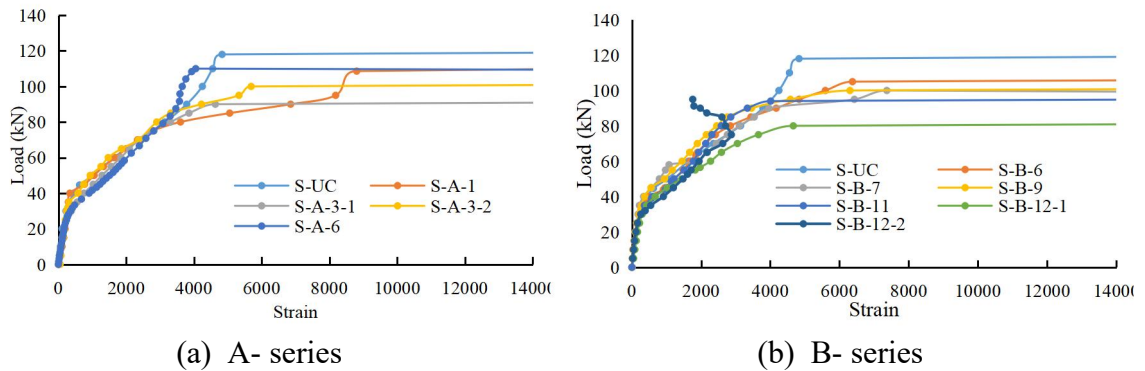
Fig. 4.11   Strain of longitudinal steel bars versus load

4.3.6 Variation of strain in longitudinal steel bars

Figure 4.11 illustrates the change in strain in the mid-span position of the longitudinal bars during loading. The reinforcement strain increases with increasing load, concrete cracking occurs near the turning point of the curve, the reinforcement strain of the specimen increases very little before cracking and the strain of the common reinforcement of the test beam increases very significantly after cracking. The more severe the corrosion of the strands, the faster the increase in reinforcement strain after concrete cracking. And this increase correlates well with mass loss, the greater the mass loss, the faster the strain increase. A further decrease in strain can be found for S-B-12-2 when loaded to 75 kN, which is due to the cracking of the concrete at the loading point, which increases the strain at the crack and decreases the strain at the mid-span position. S-B-7 shows a sudden increase in strain when loaded to 58 kN. This is because during the initial loading, the strain of the steel bar under the loading point is greater than the

strain of the steel bar in the mid-span. When the loading reaches 58kN, the crack width in the mid-span rapidly increases, and the strain of the steel bar in the mid-span suddenly increases.

4.4 Predict the steel strand rupture by displacement of beam

According to the damage of the specimen, it is found that serious corrosion of the strand will lead to a serious reduction in the bearing capacity of the specimen, and the damage of the specimen will be transformed from slow and ductile damage with forewarning to sudden brittle damage without signs, which will cause huge human and economic losses in the actual project. The root cause of this damage is the sudden fracture of the strand, so to predict the damage to the specimen, it is necessary to study the fracture of the strand after corrosion at different locations during the loading process. The fracture of the strand will occur during the loading of the specimen and also after the load capacity of the specimen has been reduced, and is directly related to the deformation of the specimen. Assume the same effect on bonding properties, Calculate the strand elongation during loading according to **Fig. 4.12**.
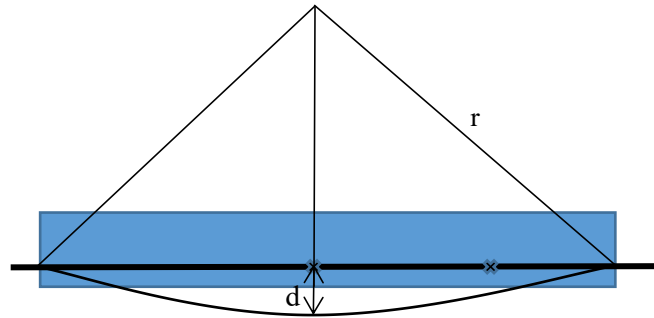
Fig. 4.12   Steel strand elongation calculation diagram

$$r = (\frac{(0.5l_0)^2}{d} + d)/2$$

$$\Delta l = (2\pi r \times \frac{2\arcsin(0.5l_0/r)}{360}) - l_0 \tag{4.1}$$

where, d is mid deflection, Δl is elongation of PC strand, l_0 is the length of span. According to the strain distribution obtained from the moment distribution diagram, it can be seen that the strand deformation Δl in the span is calculated by Eq (4.2), and then the strain in the span is calculated according to Eq (4.3), and the strain at x mm from the span is calculated according to Eq (4.4)

$$\Delta l_{mid} = \frac{\Delta l}{2} \tag{4.2}$$

$$\varepsilon_{mid} = \frac{\Delta l_{mid}}{l_F} \tag{4.3}$$

where, l_F is distance of two load point

$$\varepsilon_x = \begin{cases} \varepsilon_{mid}, x \le 0.5 l_F \\ \dfrac{(0.5 l_0 - x) \times \varepsilon_{mid}}{0.5 l_0 - 0.5 l_F}, x \ge 0.5 l_F \end{cases}$$

(4.4)

The load at the corrosion is calculated according to Eq(5)

$$F_x = \varepsilon_x E A_0 + P_c$$

(4.5)

where, F_x is the force in PC strands at the point where xmm from mid point of beam, E is elastic modulus of PC strands, A_0 is the cross section area of strands, P_c is prestress after corroded.

Eq (3.1) is used to calculate the prestress loss by the degree of corrosion，

$$P_c/P_0 = -0.23n + 1.0$$

(4.6)

where, P_c is the prestressing force of the steel strand after corrosion; n is the mass loss of the steel strand; P_0 is the prestress load at 24 hours of corrosion time.

Calculate the internal strand loads for beams at different mid-span displacements from Eq (4.1), Eq (4.2), Eq (4.3), Eq (4.4), Eq (4.5) and Eq (3.1).

The mid-span deflection at break is obtained by calculating the specimen breaking load by Eq (4.6) and Eq (4.7) mentioned in Chapter 3 and Chapter 2.

$$F_u = 273.41 - 258.67n$$

(4.7)

where, F_u is the ultimate tensile load， n is the average max cross section area loss of fractured wires.

The maximum error in the calculated load is 3 kN and the maximum error in the displacement is 1.38 mm, which is within acceptable limits due to the large differences in the tension of the wire at different locations during the loading process.

Table 4.2 shows the calculation results ：

Table 4.2　Caculation result

	S-B-7	S-B-9	S-B-12-2	S-B-13
D_m/mm	18.47	46	24.6	44.38
D_c/mm	17.68	45.1	23.4	43.0
F_x/kN	137	156.85	121	148.2
F_u/kN	136	155	118	146.92

Note: D_m is the measured value of the deflection when steel wires fracture, D_c is the calculated value of the deflection when steel wires fracture, F_x is the calculated value of prestress force when steel wires fracture, F_u is the calculated value of ultimate tensile force.

4.5 The effect of fracture characteristic on failure condition of PC beam

Table 4.3 shows the strand fracture sections condition for specimens S-B-7, S-B-9, S-B-12-2 and S-B-13. All the fracture types can be divided into three basic fracture types: cup and cone type, milling cutter type, split type, and their combination. Macroscopic photos of various fracture type are shown in **Fig. 4.13**. The necking phenomenon appeared near both the cup and cone fracture type and the milling cutter fracture type (the necking degree of the cup and cone type is relatively light), which shows ductile failure.

Cup and cone type   Milling cutter type   Split type   Milling cutter-Split type

Fig.4.13　　Fracture type of corroded steel wires[47]

Table 4.3　　Fracture condition of wires

Specimen No.	Fracture	Fracture type	Cross section area loss/%	Necking degree	Rupture timing
S-B-7-1		Split type	69.95	None	BC
S-B-7-2		Split type	60.57	None	BC
S-B-7-3		Cup and cone type	49.45	Sever	AC
S-B-7-4		Cup and cone type	43.71	Sever	AC
S-B-9-1		Milling cutter-Split type	58.48	Slight	AC
S-B-9-2		Milling cutter-Split type	38.59	Slight	AC
S-B-12-2-1		Split type	77.50	None	BC
S-B-12-2-2		Split type	66.67	None	BC
S-B-12-2-3		Milling cutter type	44.46	Sever	AC
S-B-12-2-4		Milling cutter type	38.7	Sever	AC
S-B-13-1		Milling cutter type	49.25	Sever	AC
S-B-13-2		Milling cutter type	48.55	Sever	AC

Note: BC means that the steel wire ruptured before the concrete at the top of the beam was crushed, AC means that the steel wire ruptured after the concrete at the top of the beam was crushed.

According to Table 7, it can be found that the wires that fractured before the top concrete of the beam was crushed were S-B-7-1, S-B-7-2, S-B-12-2-1 and S-B-12-2-2, and their fracture types were split type without necking phenomenon, belonging to the brittle failure. Among the wires fractured after the top concrete of the beam was crushed, S-B-9-1 and S-B-9-2 were milling cutter-split type with slight necking phenomenon, which was brittle damage, and the other wires were cup - cone type and milling cutter type with obvious necking phenomenon, belonging to ductile failure. Therefore, when the fracture type of the PC strands is split type, the ultimate load carrying capacity of the PC beam decreases significantly and occurs brittle failure. For the specimens whose PC strands fracture type is cup and cone type, milling cutter type, and milling cutter-split type, the magnitude of the decrease in ultimate load carrying capacity is

almost the same as that of the specimen whose failure characteristic is the top concrete crush. It is because for the specimens with PC strand fracture, the damage characteristics and ultimate load capacity deterioration magnitude depend on which occurs first, the wire fracture or the top of the beam concrete crush. Previous studies have indicated a wire with a split fracture type usually has a larger maximum cross-sectional area loss and is prone to stress concentration at the fracture point, which makes it more prone to rupture compared to other fracture types. In this paper, for the B-series specimens, brittle failure of the beam may occur when the maximum cross-sectional area loss of the wire reaches 60.57%. This value is affected by the distance of the corrosion point from the loading and the position of the corrosion point on the strand.

4.6 Chapter summary:

1. At the beginning of loading, before the specimen cracks, the deflection of the specimen is related to the mass loss. At the end of loading, when the specimen is approaching its ultimate load, the deflection of the specimen is related to the maximum cross-sectional area loss.

2. When the corrosion degree of PC strand is lower, ultimate load of PC beams decreases slowly with the increase of the corrosion degree, the damage characteristics of prestressed beams are top concrete crushing. When the corrosion degree is medium, the failure characteristics of PC beams are top concrete crush and PC strand rupture, and there is no change in the trend of ultimate load decrease. When the corrosion degree of steel strand is serious, the damage characteristics of PC beams are strand rupture, and the ultimate load carrying capacity of beams decreases greatly, and the damage mode changes from ductile damage to brittle damage.

3. The type of strand fracture has a significant effect on the ultimate load carrying capacity and failure mode of the PC beam. When the fracture type of PC strand is split type, the ultimate bearing capacity of the PC beams decreases significantly and the failure mode is brittle failure.

Chapter 5 Effect of corrosion of PC strands on bending behaviour of PC beams under fatigue loading

5.1 Introduction

Fatigue damage can occur in all members under repeated loading, causing changes in the mechanical properties of the material or member and having an effect on the subsequent mechanical behaviour of the member. There has been some research into the development of fatigue damage in uncorroded prestressed beams, but less research into the fatigue properties of prestressed beams after corrosion of prestressing strands.

In this chapter, the fatigue properties of prestressing beams after corrosion of prestressing strands are investigated from various aspects such as residual deflection, longitudinal strain and bending stiffness of the specimen, and the effects of different degrees of corrosion and different corrosion locations on the fatigue properties of prestressing beams are analyzed.

5.2 Test overview

The specimen design for this test has been mentioned in Chapter 3. The specimens were fatigue loaded after the corrosion test. The position of the strain gauges pasted inside the beam was the same as in Chapter 3. The fatigue test loading schematic, displacement meter measurement points and surface concrete strain gauges pasting locations are shown in **Fig. 5.1**. Four strain gauges were affixed to the mid-span section to measure the strain in the mid-span section; strain gauges were affixed to the punching surface on the corrosion side from the bottom of the beam to the loading point for measurement. Photographs of the actual loading are shown in **Fig. 5.2**.

The beams were simply supported and subjected to four-point bending. Each beam had a clear span of 1800 mm and the length of loading point is 600 mm. The test was carried out using a 200T electro-hydraulic servo fatigue tester. A total of seven beams were fatigue tested, one of which was not corroded as a comparison, three beams were corroded in the middle and three beams were corroded at the edge. As the test was mainly to study the effect of corrosion of prestressing strands on the fatigue performance of the specimen, the lower limit of fatigue load for the fatigue test was uniformly taken as 20% of the ultimate bearing capacity of the beam, and the upper limit of fatigue load was uniformly taken as 50% of the ultimate bearing capacity of the test beam.

S-A-M-H-2 was loaded in the same load range as the other specimens for the first 150,000 loadings, followed by a fatigue load range of 20%-60% for the next 150,000 loadings to measure the performance of the specimen under different loadings, with the specific test groupings shown in **Table 5.1**. Previous tests have shown that the effect of frequency on the mechanical properties of the member is negligible when the test beam in air is loaded at a frequency of less than 5Hz. The loading frequency for this test was 2Hz, and the test beam was loaded in an equal amplitude cycle using load control, with a sine wave load waveform. Due to the high loading evaluation rate ordinary displacement sensors are difficult to measure the displacement change accurately, laser displacement sensor is used to measure the deflection change in the mid-span and below the two loading points, and it was fixed with two magnetic blocks. The laser displacement sensor is shown in **Fig.5.3**. Before the fatigue test, three static load tests

were carried out, loading to the upper limit of the fatigue load in six steps and then unloading, measuring the cracking load, strain and deflection during the first loading. The fatigue test is repeated three times, and after each load cycle has been completed a certain number of times, the fatigue test is stopped and loaded from zero to the upper fatigue load limit, and strain, deformation and crack width are measured. The fatigue test was terminated when fatigue damage occurs or the number of cycles reached 30w times. In order to reduce the effects of friction during the fatigue test, two Teflon plates were placed under the steel hinge bearing and lubricant was applied between them to simulate the sliding restraint of the hinge bearing.

Table 5.1　Specimen group

Specimen	Prestress level/%	Corrosion location	Ultimate load	Fatigue load range
F-UC		-	120kN	20-50%
F-A-1		Center		20-50%
F-A-7-1	50	Center		20-50%
F-A-7-2		Center		20-50%
				20-60%
F-B-6		Side		20-50%
F-B-5		Side		20-50%
F-B-12		Side		20-50%

Note: F means fatigue test. A represent corrosion location is center; B means corrosion location is side. 'UC' means uncorrosion; the first number is mass loss.
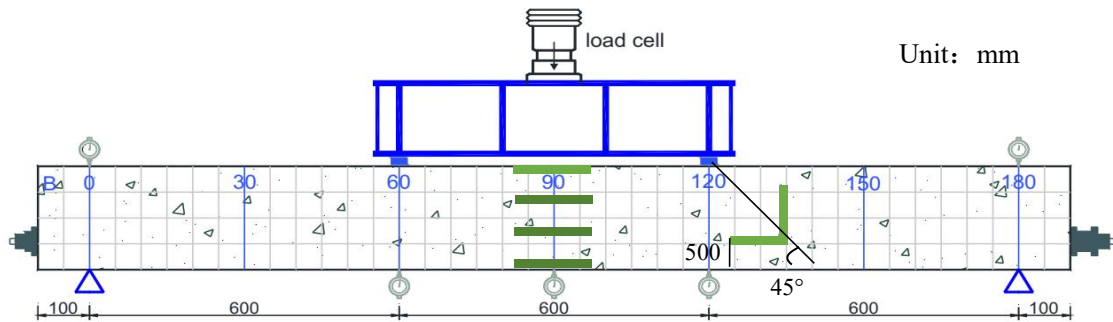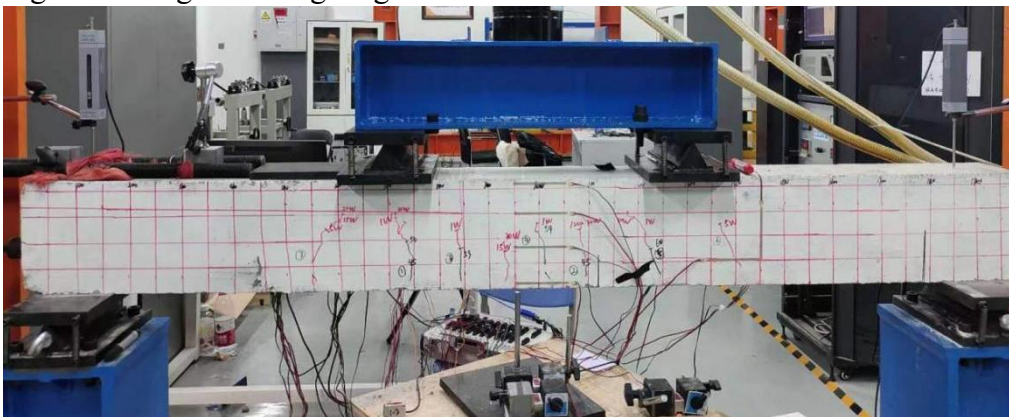

Fig 5.1　Fatigue loading diagram

Fig 5.2　Fatigue loading device

Fig 5.3   Laser displacement sensor GFL-Z200N

## 5.3 Test result and discussion
5.3.1 Test result

In order to study the fatigue performance of prestressed beams after strand corrosion, a total of seven beams were carried out fatigue tests and the test results are shown in **Table 5.2**. Only F-A-7-2 was damaged during the fatigue test due to brittle fracture of the longitudinal reinforcement and fragmentation of the concrete in the top compressive zone. Comparing F-A-7-2 with F-A-7-1, it can be seen that the corrosion locations are the same and the degree of corrosion is close, so the increase in the maximum fatigue load will significantly reduce fatigue life and increase fatigue damage. The mid-span deflection under the 300,000th maximum load was recorded. The comparison shows that when the load range, loading frequency, loading times are the same, as the degree of corrosion increases, the mid-span deflection also increases.

Table 5.2   Fatigue loading test result

| Specimen No.	Mass loss(%)	Max cross section area loss(%)	Load range(kN)	Number of cycles	Deflection/mm (30000, 60kN)
F-UC	0	0	24-60	300000	4.23
F-A-1	1.29	2.10	24-60	300000	4.28
F-A-7-1	7.25	18.64	24-60	300000	8.4
F-A-7-2	7.34	11.7	24-60	150000	Longitudinal steel bar rupture
			24-72	100000	
F-B-6	6.40	16.47	24-60	300000	5.4
F-B-5	5.17	19.42	24-60	300000	5.2
F-B-12	12.73	30.07	24-60	300000	6.4

5.3.2 Specimens after fatigue testing

Loading cracks were drawn during the first loading, the crack development load was marked, the crack development was observed during the subsequent fatigue tests and the number of loading times was marked. The damage to the specimen during fatigue is shown in **Fig. 5.4**. Throughout the fatigue process of the PC beam, a small number of vertical cracks of short lengths appeared in the purely bending section in the span during the early stages of fatigue. In the middle stage of fatigue, the vertical cracks in the pure bending section gradually became wider and longer, and the number of cracks increased; inclined cracks appeared in the bending and shearing section near the loading point. Under cyclic loading, the cracks open and close continuously and join the cracks on both sides at the bottom end of the beam. During this phase, the width, length and number of cracks continue to develop. Throughout the fatigue process, damage to
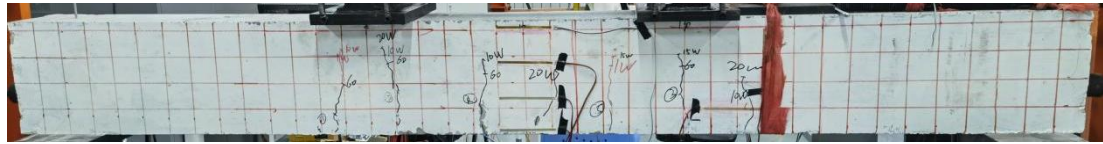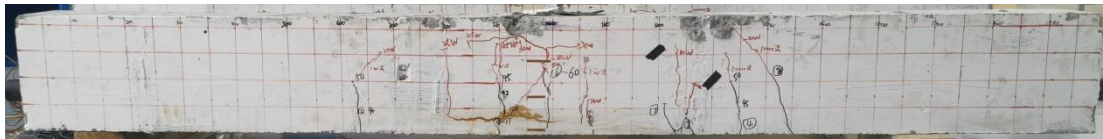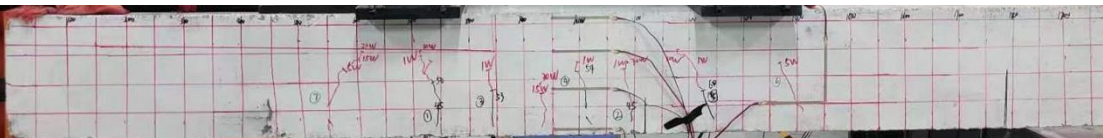
(a) F-UC

(b) F-A-1
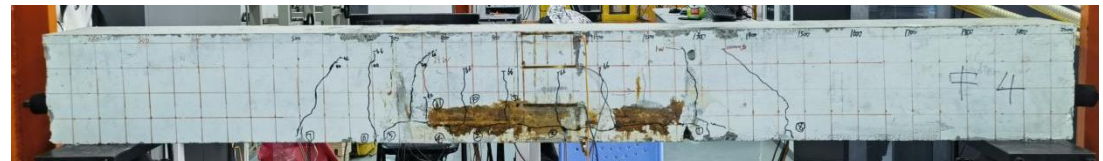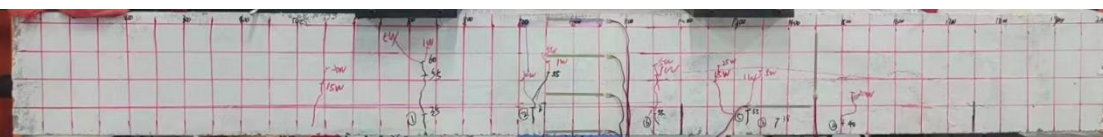

(c) F-A-7-1

(d) F-A-7-2

(e) F-B-6

(f) F-B-5

(g) F-B-12

Fig. 5.4 Fatigue damage condition

the reinforcement and prestressing strands gradually accumulates due to dynamic creep. Observation of the damage pattern in **Fig. 5.4**, F-A-7-2 reveals a distinct dendritic diagonal crack in the final stages of fatigue. When the tensile stress in the bottom reinforcement reaches the tensile critical point, the reinforcement suddenly fractures and the displacement and the width of the main crack increases sharply. At this point the test beam has reached fatigue damage and the beam still has the ability to withstand fatigue loads, but the external loads applied to the beam are significantly reduced. Overall, cracks continue to develop throughout the fatigue process, resulting in a progressive
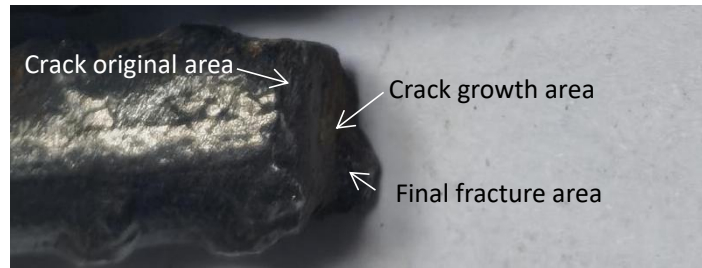
70

Fig. 5.5   Fracture cross section condition of longitudinal steel bar of F-A-7-2

breakdown of the bond co-ordination between steel and concrete. Fatigue damage to the bottom tensile reinforcement accumulates and develops, and the sudden fracture of the reinforcement eventually leads to fatigue damage of the PC beam. Comparing the damage states of the specimens, the fatigue damage stages of the different specimens can be observed more clearly. F-A-7-1 and F-B-12 have a tendency to form dendritic cracks and are in the late stage of the middle fatigue stage. A comparison of the specimens at different corrosion locations shows that the longitudinal cracks produced by corrosion in the pure bending zone are interspersed with cracks produced by fatigue and gradually deteriorate during fatigue. A typical fatigue fracture of a tensile steel bar is shown in the **Fig.5.5** (F-A-7-2 as an example). The fracture surface consists of three main zones, namely the zone of crack origin, the zone of stable crack extension and the zone of final rupture due to the weakening of the net section. The absence of necking is classified as brittle damage.
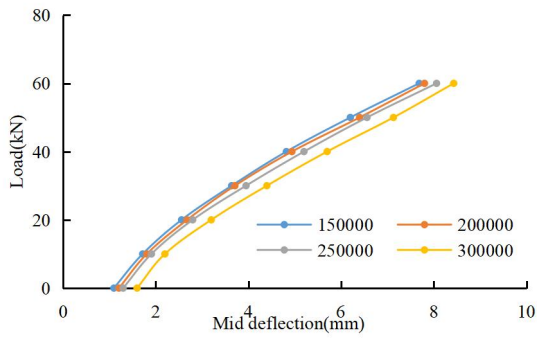
5.3.3 Load-deflection curve

The load-displacement curves of constant-amplitude fatigue test beams are shown in **Fig. 5.6**. As the number of fatigue cycles increases, the load-displacement curves continue to "move" in the direction of increasing displacement. The load-displacement curves of F-A-7-2 in the early stage and final stage of fatigue were sparsely distributed, while those in the middle stage of fatigue were relatively dense, showing the characteristics of three stages of "sparse-density-sparse" throughout the process. The other specimens only showed the discrete characteristics at the beginning of loading because they were not damaged. In addition, as the number of cycles increases, the slope of the load-displacement curve gradually decreases, indicating that the test beam tends to soften and its stiffness gradually decreases. Comparing the load-displacement curves of different specimens, it can be found that the higher the degree of corrosion the greater the dispersion in the medium term, and the lower the degree of corrosion the more dense the curve. Observation Fig.4-5(d) In the whole fatigue process of F-A-7-2, the slope of the load-displacement curve was becoming smaller, and it is necessary to quantitatively describe the slope (i.e. bending stiffness) development law of the load-displacement curve with the increase of fatigue load amplitude. It is necessary to quantitatively describe the slope (i.e. bending stiffness) development law of the load-displacement curve with the increase of fatigue load amplitude.
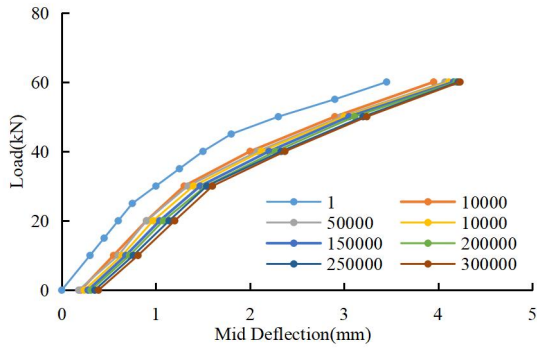
(a) F-UC
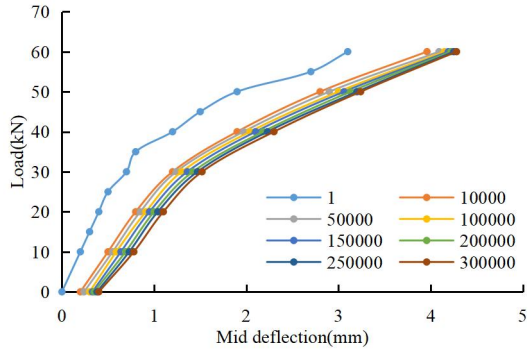
(b) F-A-1

(c) F-A-7-1
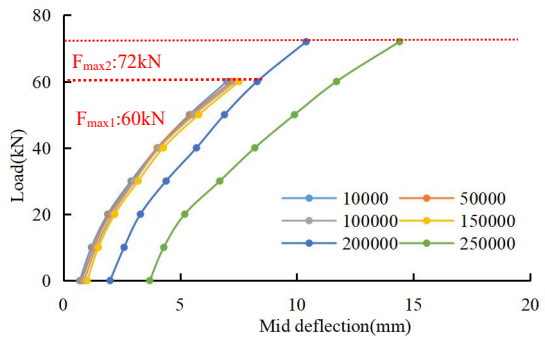
(d) F-A-7-2

(e) F-B-6

(f) F-B-5

(g) F-B-12

Fig 5.6   Load- deflection curve

The relationship between the mid-span deflection and the number of cycles is shown in **Fig. 5.7**. It can be found that the span deflection of all specimens increases with the increase of loading times. And the mid-span deflection curves of corroded and non-corroded beams have a similar rule of change. The whole fatigue test span

deflection increase can be divided into three stages; in the fatigue loading of the initial span deflection growth, which is the fi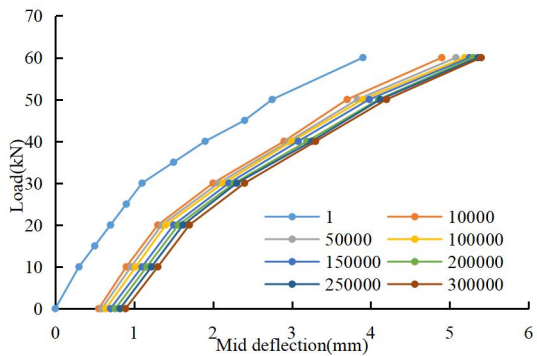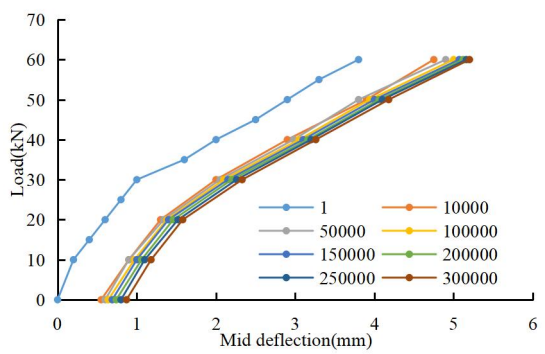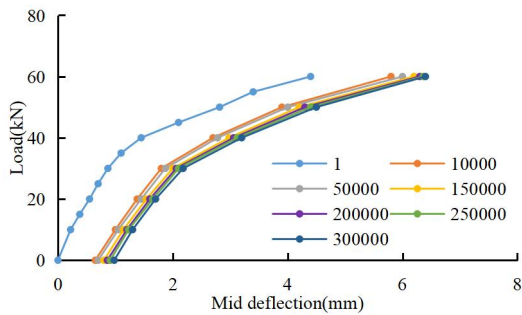rst stage of fatigue development, accounting for about 5% of the whole fatigue process, and then enter into the second stage, when the increase in span deflection has become slower, this stage is relatively long about 90% of the fatigue life of the test beam. Since this test was loaded only 30w times, the fatigue damage development of most specimens stopped at the second stage. Finally, the mid-span deflection increases faster in the third stage, and the specimen reinforcement will suddenly fracture in a very small number of cycles, and this process is relatively short, accounting for about 5% of the fatigue life. The mid-span deflection of specimen F-A-7-1 has a more obvious increase when loaded up to 30w times, with a tendency to enter the third stage. Specimen F-A-7-2, due to the increase of the upper limit of fatigue load after loading to 150,000 cycles, the specimen was damaged at 25w cycles.
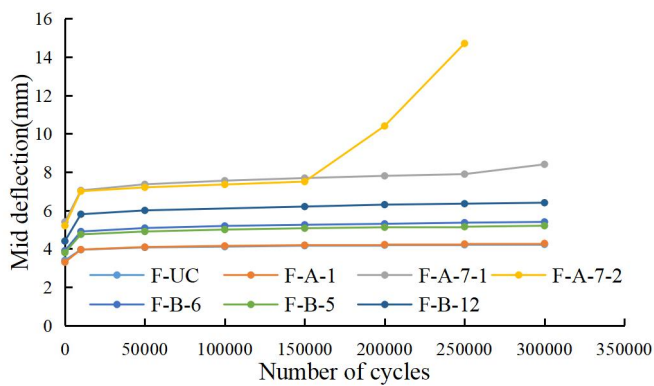

Fig. 5.7   Deflection increase ratio

5.3.4 Crack width

Figures 5.8 show the variation of the main crack in individual specimens during the fatigue test. Comparing the crack widths of different specimens, the same corrosion location and the greater the loss of cross-sectional area, the greater the fatigue crack width, and the same degree of corrosion, the greater the main crack width for specimens with corrosion across the centre. Observation of the change in the main crack width during fatigue loading reveals that the main crack width of the specimen accelerates and widens at the beginning of loading, then the increase becomes flat. the fatigue upper limit load of F-A-7-2 increases and accelerates the fatigue damage process of the specimen, the crack width increases rapidly before the damage, the development of the main crack presents a three-stage law of fallen S shape and the width of main crack is 5.1 mm when fatigue failure. Although fatigue failure did not occur in F-A-7-1, the development of the width of multiple cracks shows the same development pattern as F-A-7-2, indicating that the fatigue development of F-A-H The fatigue development of F-A-7-1 has reached the third stage of unstable growth.

Figure 5.9 shows the average crack space of the specimen after fatigue loading and the specimen after the static loading. It is found that when the corrosion degree is low, fatigue loading does not significantly increase the crack space of the specimen. When the corrosion degree is high, the fatigue effect has an obvious effect on the increase of crack space. High corrosion degree can magnify the damage of fatigue to the bonding properties of specimens, and the effect is more significant when the corrosion position is located at the main stress position.
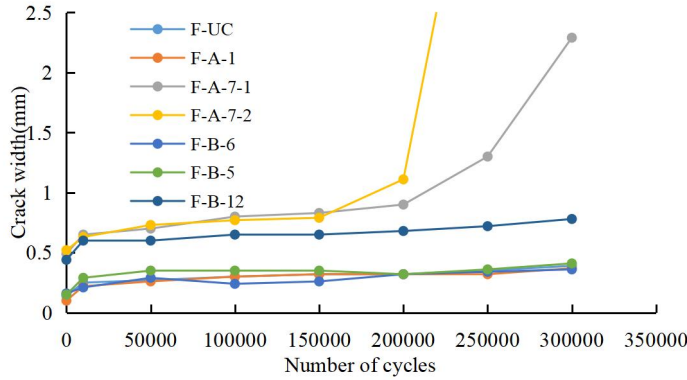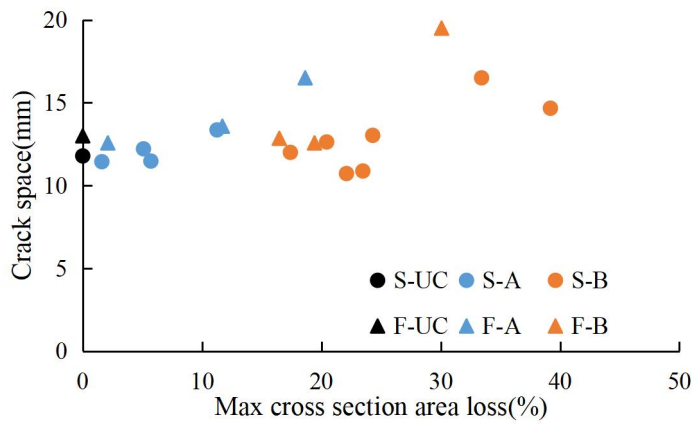
73

Fig. 5.8   Crack width

Fig. 5.9   Crack space

5.3.5 Max deflection at mid-span versus the logarithm of the number of cycles

Figure 5.10 shows the fitted plot of the maximum deflection at mid-span versus the logarithm of the number of fatigue cycles for the fatigue phase I and II of the test beams under fatigue loading. And the mass loss of the specimen, the fitted equation and R2 are summarized in Table 5.3 . From the regression curves in the graphs, it can be seen that the mid-span deflection in the first and second stages increases linearly with the logarithm of the number of cycles increase. And the mid-span deflection has a good correlation with the logarithm of the number of cycles.

$D_N=D_0+alg(N)$

Where, D_N is the max deflection of mid-span after N times load, D_0 is the max deflection of mid- span. a is variable coefficient represent the increase ratio of mid deflection.

The relationship between the growth rate of mid-span deflection a and the mass loss of each specimen is shown in Fig. 5.11 , and it can be found that under the same fatigue load, the growth rate of mid-span deflection a increases with the increase of strand decay candle rate. And the growth rate of mid-span deflection has a good linear relationship with mass loss.

74

Table 5.3   Equation of deflection

Specimen No.	Mass loss	D_0(mm)	Equation of linear regression	R^2
F-UC	0	3.4	$D_N=D_0+0.1489lg(N)$	0.9959
F-A-1	1.29	3.3	$D_N=D_0+0.1751lg(N)$	0.9937
F-A-7-1	7.25	5.4	$D_N=D_0+0.4389lg(N)$	0.9934
F-A-7-2	7.34	5.2	$D_N=D_0+0.4355g(N)$	0.9977
F-B-6	6.40	3.9	$D_N=D_0+0.2668lg(N)$	0.9933
F-B-5	5.17	3.8	$D_N=D_0+0.2489lg(N)$	0.9943
F-B-12	12.73	4.4	$D_N=D_0+0.3579lg(N)$	0.9964

(a) A series   (b) B series
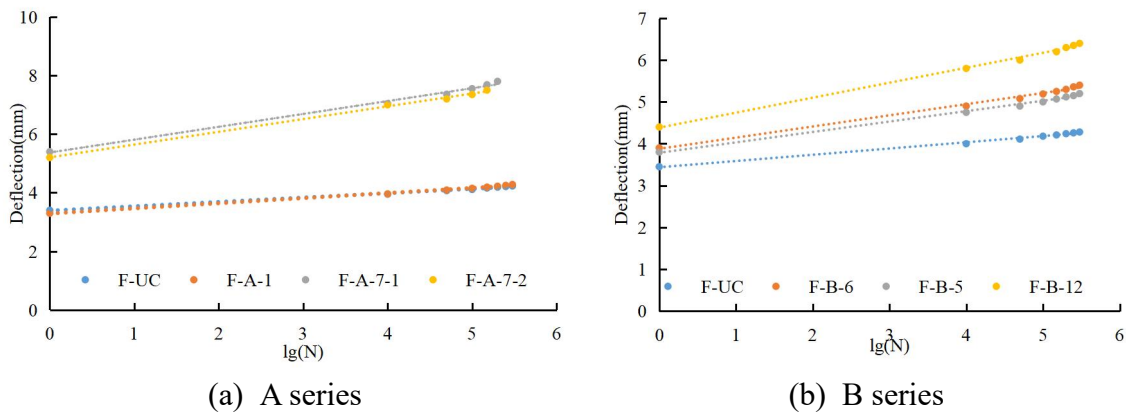
Fig. 5.10   Max deflection at mid-span versus the logarithm of the number of cycles
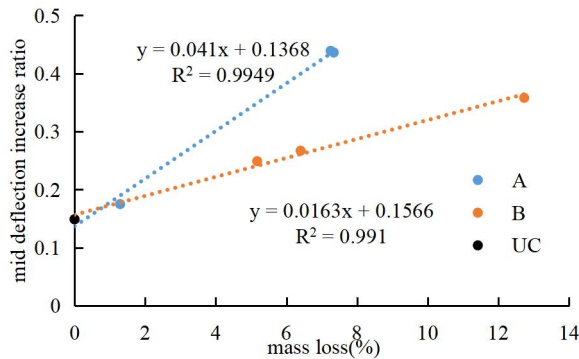
Fig. 5.11   Mid deflection increase ratio

5.3.6 Degradation of bending stiffness

According to the material mechanics, the calculation formula for the displacement of simply supported beam under external load is shown as follows [49]:

$$D = S \cdot F / B \tag{5.1}$$

where: D is mid deflection under the corresponding to the external load., S is a constant coefficient related to the beam length, the load position and the supporting condition. F is the external load.

According to Eq. (5.1), The bending stiffness of test beam after N times of fatigue cycles can be calculated by the following formula:

$$B_N = S \cdot F_N / D_N \tag{5.2}$$

where, F_N is the upper fatigue load constant, D_N is the mid-span displacement under the upper fatigue load after n loads.

The stiffness degradation during the fatigue test is calculated using Eq.(5.3)

$$B_{loss} = 1 - \frac{B_N}{B_0} \tag{5.3}$$

where, B_{loss} is the bending stiffness decrease ratio, B_0 is the stiffness at the first loading.

The degradation of flexural stiffness with the number of loading is shown in the **Fig. 5.12** It can be found that with the increase of loading, the flexural stiffness degrades continuously, and degrades faster at the beginning of loading, and then becomes smooth, F-A-7-2 enters the third stage of fatigue due to the increase of load, and the degradation of stiffness accelerates, F-A-7-1 and F-B-12 have a tendency to accelerate the degradation of stiffness, and it is judged that the third stage of fatigue is about to start - The third stage of fatigue is judged to be about to start - the instability increasing stage. Comparing different specimens, it can be found that as the degree of corrosion increases, the greater the degree of stiffness deterioration, and the faster the deterioration rate. Analysing the effect of corrosion on flexural stiffness deterioration and central deflection, it can be found that corrosion can amplify the effect of fatigue on the specimen and accelerate the fatigue damage process.
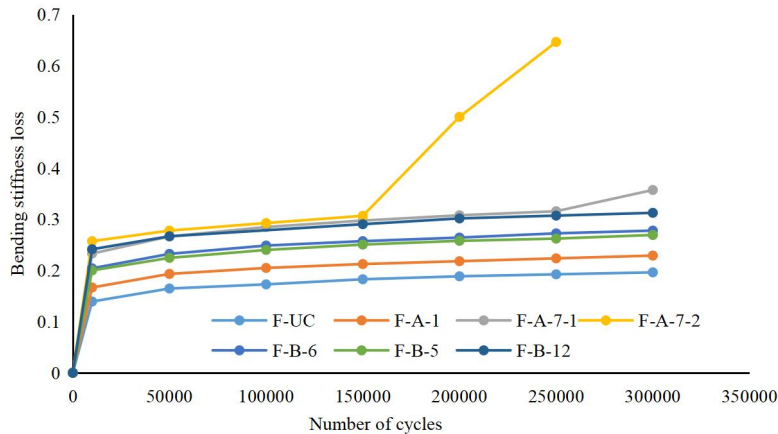
Fig. 5.12   Bending stiffness loss versus number of cycles

5.3.7 Strain of reinforcement

Figure 5.13 shows the variation of strain of the longitudinal steel bars in the mid-span of the specimens during the fatigue process. It can be found that similar to the mid-span deflection, the maximum strain development pattern of the longitudinal steel bars of the specimens also has an obvious three-stage characteristic, (1) a rapid growth stage at the beginning of the fatigue loading, which accounts for about 5% of the fatigue life, (2) a stable development stage in the middle of the fatigue loading, which maintains a certain rate of growth, and accounts for a large part of the fatigue life. (3) Unstable damage stage with sudden increase at the later stage.

Observe the development curve of the maximum strain of longitudinal reinforcement in the mid-span with the number of load cycles. The longitudinal

reinforcement stress in partially prestressed concrete beams under multiple cyclic loading increases significantly compared with the longitudinal reinforcement stress at the 1st loading. The increment of longitudinal reinforcement stress consisted of two parts: one part was caused by concrete cracking in the tension zone and the other part was generated under multiple repeated loading. The increase of the stresses in the reinforcement due to cracking of the concrete in the tension zone is caused by cracking of the tension zone, withdrawal of the concrete from the work and reduction of the resistance moment of the beam cross-section. Comparison of specimens with different degrees of corrosion under the same number of fatigue loads reveals that the strain in the longitudinal bars increases with the increase in the degree of corrosion, and that the mid-span corrosion has a greater effect on the strain in the reinforcement than the edge corrosion for the same degree of corrosion. Corrosion accelerates the damage caused by fatigue loading on the specimen, and the effect of corrosion in the main stress area is particularly obvious.
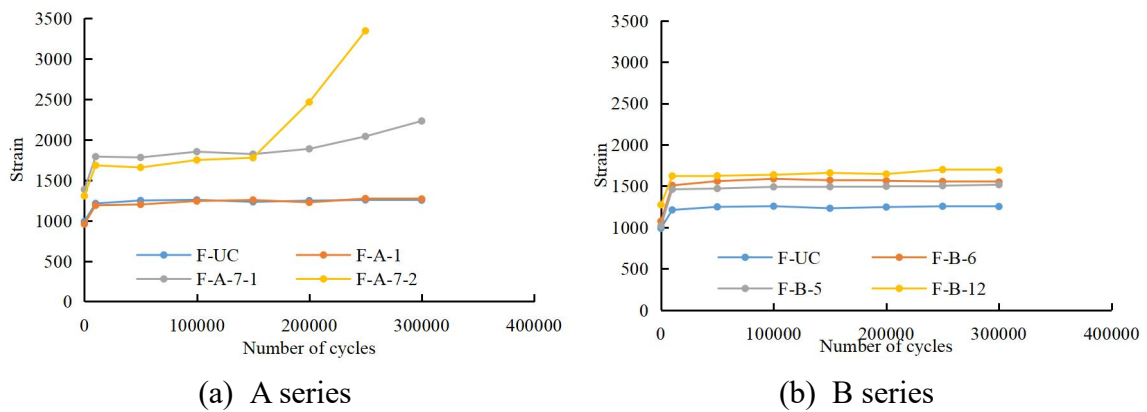

(a) A series   (b) B series

Fig. 5.13   Strain of reinforcement versus number of cycles

5.3.8 Strain of inter concrete.

Figure 5.14 illustrates the variation of internal concrete strain near the strand at mid-span. It can be found that the internal concrete strain increases with the increase in the number of loading cycles and develops in the same pattern as the longitudinal reinforcement, mid-span deflection. Comparing the strains after the same cycle of loading, it can be found that the internal concrete strain increases with the degree of corrosion, and the magnitude of the increase also increases with the degree of corrosion. The strain of uncorroded strand has a very small effect under fatigue, and the initial strain of F-A-1 is smaller than that of the uncorroded specimen F-UC, which is due to the fact that the slight corrosion and its corrosion products did not cause cracking of the concrete, but instead increased the bond between the concrete and the reinforcement, which resulted in an increase in the flexural stiffness of the specimen and a smaller beam deformation. After 10,000 loadings, the internal concrete strain of F-A-1 increased rapidly, which was due to the fatigue loading, the specimen cracked, the internal corrosion products were broken, and the bond between the concrete and steel reinforcement deteriorated seriously, so that the beam deformation increased during the loading process.B series, despite the corrosion of the higher degree of corrosion,

corrosion-induced cracking is more serious compared to F-A-1, due to the corrosion location at the edge of the beam, the impact of the fatigue loading is relatively more serious than the corrosion of the beam, and the corrosion products are not caused by the corrosion. The influence of fatigue loading is relatively small, and the deterioration of bond properties at the side also has a relatively small influence on the mid-span deformation of the beams.
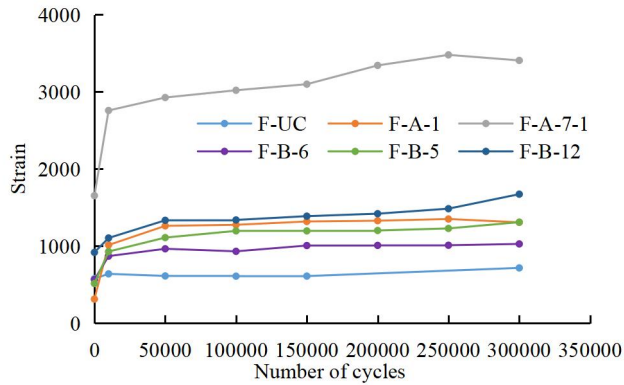

Fig. 5.14 Strain of inter concrete versus number of cycles

5.4 Chapter summary

1. Comparing the crack spacing of specimens under fatigue loading and static loading, it can be found that when the degree of corrosion is lower, the fatigue loading does not increase the crack spacing significantly. When the degree of corrosion is higher, fatigue loading can significantly increase the crack spacing, and it is especially significant for specimens with corrosion in the span. This suggests that fatigue loading can lead to significant deterioration in the bond properties of the severely corroded specimens, and the deterioration can be more severe when the corrosion location is the main stress area.
2. The mid-span deflection in the first and second stages increases linearly with the logarithm of the number of cycles increase. And the growth coefficient of mid-span deflection has a good linear relationship with mass loss.
3. The specimens with corroded strands were the same as the uncorroded specimens, and their mid-span deflections, longitudinal reinforcement strains, mid-span internal concrete strains around the PC strands and crack widths demonstrated a typical fatigue development pattern with the increase in the number of cycles. Comparing the fatigue development curves of different specimens, it can be found that the higher corrosion degree has a significant accelerating effect on the development process of fatigue damage. It means corrosion of PC strands amplifies the effects of fatigue loading on various properties of the specimens.

Chapter 6   Residual bending behaviour of PC beam with corroded PC strands after fatigue loading test

6.1 Introduction

Corrosion and fatigue test lead to the main cause of bridge damage service life reduction, in order to study the effect of fatigue damage as well as strand corrosion on the mechanical properties of beams. In this chapter, static load tests were carried out on specimens after fatigue loading. Their residual ultimate load capacity, deflection, cracks and partial reinforcement strains were measured. The static load test results are compared with those of the corroded PC beams without fatigue damage to analyse the mechanism of the effect of fatigue damage on the bending behaviour of the PC beams.

6.2 Experimental procedures

PC beams after 30w of fatigue loading were used as specimens for the static loading tests in this section, of which F-A-7-2 was damaged due to the increase of fatigue max load after the 150,000th loading, so only the remaining six beams were statically loaded. The bottom and sides of the specimens were distributed with longitudinal cracks due to strand corrosion and expansion of corroded production, and flexural and shear cracks due to fatigue loading.

The test loading apparatus is the same as the loading apparatus in Chapter 4, and the displacement meter measurement position, and strain gauge arrangement position are also the same, as shown in **Fig. 6.1** and **Fig. 6.2.** The test mainly measured the deflection at the bottom of the specimen, the longitudinal bar strain, the crack width, the ultimate bearing capacity and so on. The loading process is also divided into two stages, the first stage loading method adopts force control method until the peak load is reached. The second stage loading method adopts displacement control method for loading until the bearing capacity decreases to 80% of the peak load or the physical deterioration of the beam is obvious, then the loading test is stopped. Due to the low mechanical properties of the specimens after fatigue action, the force control method was loaded at a rate of 2kN/min and the displacement control method was loaded at a rate of 1mm/min, with 2mm per loading.As the specimens were already cracked, the initial cracks did not need to be measured, and testing of the width of the major cracks was started when the load reached 40 or 50kN. In order to make a distinction from fatigue cracks, the development of cracks at different loads was depicted with a black pen during the loading process.
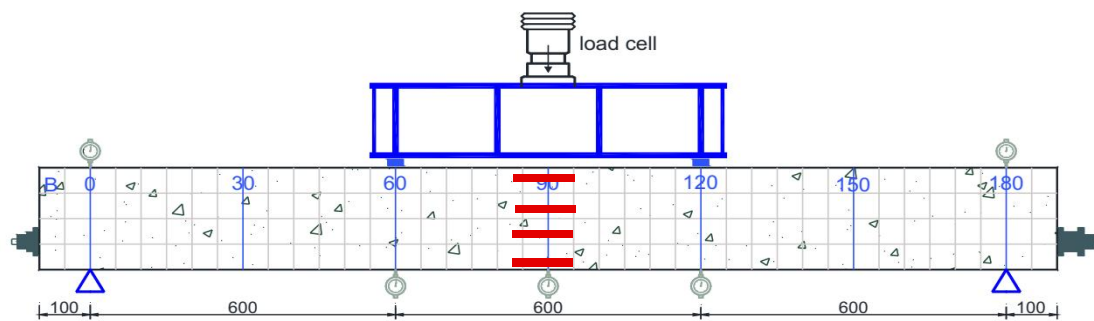

Fig. 6.1   Loading diaram

Fig. 6.2   Static loading test

6.3 Static loading test result discussion
6.3.1 Static loading test result

The 6 specimens that were not damaged after 300,000 times of fatigue loading were subjected to static loading tests to test their residual load capacity, and the test results were obtained as shown in **Table 6.1**. It can be found that the larger the loss of cross-sectional area the lower the load capacity of the specimen. When the corrosion location is the same and the corrosion degree is close to each other, there is a significant decrease in the ultimate load carrying capacity compared to the specimens that have not been subjected to fatigue damage.

Table 6.1   Static loading test result

Specimen No	Mass loss(%)	Max cross section area loss(%)	Ultimate load(kN)	Failure mode
F-UC	0	0	113	CC
F-A-1	1.29	2.10	112.3	CC
F-A-7-1	7.25	18.64	98	CC
F-B-6	6.40	16.47	110	CC
F-B-5	6.17	19.42	109.2	CC
F-B-12	12.73	30.07	102.56	WR

Note: CC means concrete crushed, WR means wires rupture.

6.3.2 Failure mode

Figure 6.3 shows the failure condition of the specimens after the static loading test, the fracture location of the PC strand and its distance from the center of the specimen are also marked in the figure. Observation of the damage photographs reveals that the distribution of damage cracks in the specimen under static loading after fatigue is significantly reduced compared with that of the specimen damaged by direct static loading in the bending-shear region, which is due to the obvious deterioration of the flexural strength of the specimen under the continuous fatigue action. at the whole loading process, few new cracks appeared in the specimen. When the load exceeded the upper fatigue load, fatigue-generated cracks continued to develop longer and wider. F-A-7-1 had a high degree of corrosion and the corrosion location was located in the middle of the span of the specimen. Before the fatigue loading, the sides and bottom of
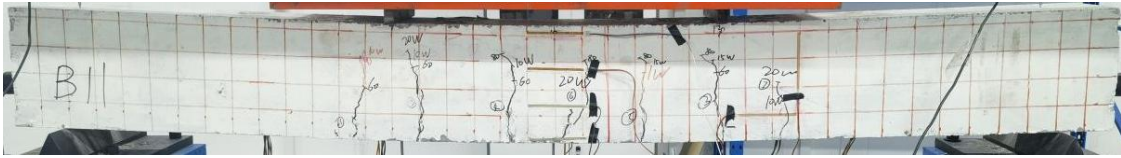
(a) F-UC
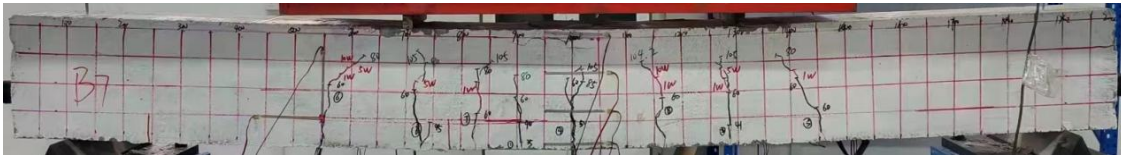

(b) F-A-1

(c) F-A-7-1

(d) F-B-6

(e) F-B-5

(f) F-B-12

Fig. 6.3   Failure condition

Fig 6.4   F-B-12 wire fracture type

the beam had longitudinal cracks caused by expansion of the corrosion products, and the longitudinal cracks were intersected with the transverse cracks during the fatigue loading, which substantially reduced the bottom bond performance. In the static load

test, with the continuous increase of the load, the intersecting cracks develop and become wider, and finally the top concrete crumbles, the bottom concrete spalls, and the specimen is damaged. F-B-12 , due to the high degree of corrosion of the specimen, the strand has high residual strain after fatigue, and the strand fractured before the concrete in the loading process. The strand fractured at the top compression zone after the beam was loaded to the yield stage, resulting in a significant reduction in the load carrying capacity of the specimen and destruction of the specimen. The other specimens were damaged due to the concrete fracture at the top compression zone. **Figure 6.4** illustrates the cross-sectional damage pattern of the F-B-12 fractured strand. It can be observed that there is a slight necking phenomenon and the fracture type is split-milling cutter which is a brittle damage.

6.3.3 Load- deflection curve

The load-displacement curves of six static loading test beams are shown in **Fig. 6.5**. The concrete has cracked after the fatigue test and the displacement-load curve does not have a more obvious inflection point at the beginning of the loading. Specimen F-A-7-1 has a more severe corrosion, the concrete at the bottom of the bending zone of the beam is severely cracked and the grout is cracked at the beginning of the loading, resulting in a significant drop in the prestress in the specimen and the slope of the load displacement curve is much smaller than the other specimens. Due to the high level of corrosion, the fatigue damage sustained during the fatigue test was greater and the accumulation of strain at the top of the concrete caused it to fragment and the specimen to break under the lower external load. The strand of F-B-12 broke suddenly when the specimen was loaded to yield and the load carrying capacity dropped instantly, without the concrete in the top compression zone being crushed. As the specimen had already reached the ultimate state of load bearing before the wire broke, the strand breakage had a small effect on the ultimate load bearing capacity.

The test results of specimens with close corrosion degree in Chapter 4 and not subjected to fatigue damage are selected and summarized with the test results in this chapter to obtain **Fig. 6.6**. Observation reveals that, due to the fatigue damage reducing the stiffness of the specimens, the specimens subjected to fatigue load have higher displacements under the same load at the early stage of loading. Since higher corrosion levels accelerate the fatigue damage process, the higher the corrosion level, the more pronounced the stiffness reduction and the higher the displacement.
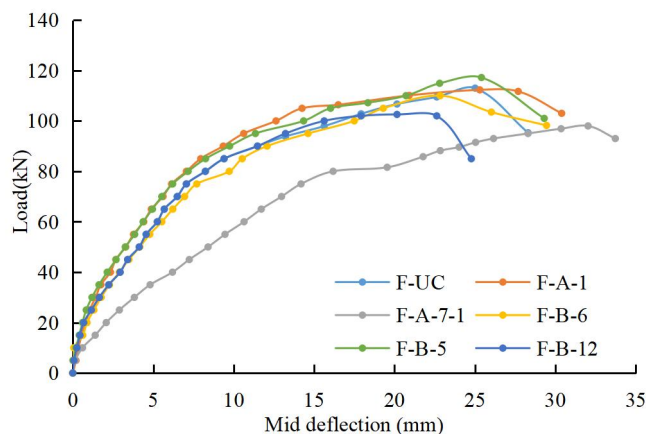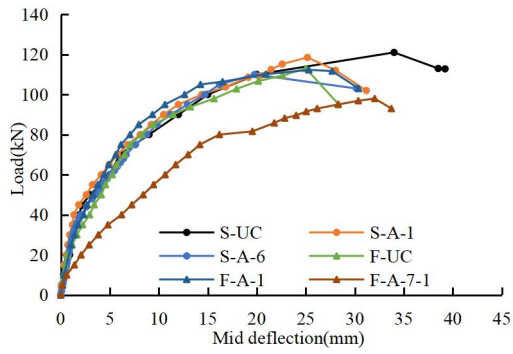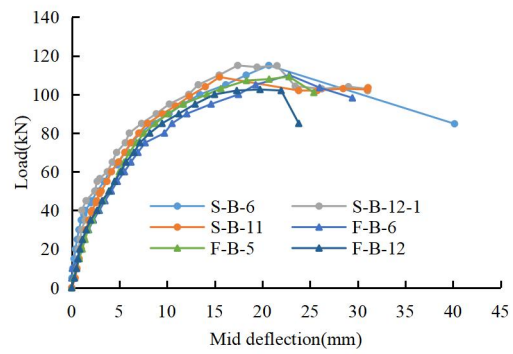

Fig. 6.5   Load-deflection curve

(c) A series   (d) B series

Fig. 6.6   Load-deflection curve

6.3.4 Ultimate load

The ultimate load carrying capacity of the specimen static loaded after the fatigue test and the specimen directly static loaded are shown in Fig. 6.7, and the comparison indicates that under the same corrosion degree the specimen subjected to fatigue damage has a significantly lower ultimate load carrying capacity. Comparing the specimens with concrete crush in the compression zone as the damage characteristic, it can be found that the ultimate load carrying capacity of the specimens is reduced to almost the same, this is because the concrete strain continues to accumulate during the fatigue test, the fatigue damage suffered by the specimens is similar, and the concrete in the compression zone crushed at the lower loading. However, when the cross-sectional area loss reaches 30%, the ultimate load carrying capacity of the specimens after fatigue testing is higher even though the corrosion degree is very close to each other, this is because the failure mode of these specimens is wires fracture. Among them, the reduction in the ultimate load capacity of two beams in S-B series was caused by wires fracture. As for one beam of the F-B series, its steel wires broke when the concrete in the compression zone of the specimen was going to crush, thus the wires fracture has a smaller effect on the ultimate load carrying capacity. The specimens with a sudden decrease in ultimate load capacity due to wires fracture, the ultimate load capacity is determined by the load when the wires fracture, thus the trend of decrease in ultimate load carrying capacity is different from that of the specimens whose failure characteristics are concrete crushing.

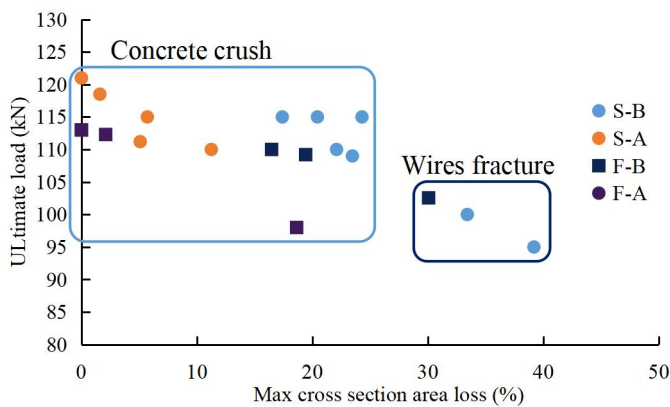

Fig. 6.7   The ultimate load versus Max cross section area loss

Figure 6.8 shows the relationship between the concrete strain at the top of the span and the ultimate load capacity of the specimen after 30w loadings, and it can be found

83

that the ultimate load capacity of the specimen decreases with the increase of the compressive strain in the span, and the two are approximately linear. For the specimen with relatively low corrosion degree, the effect of fatigue on its ultimate bearing capacity is mainly reflected in the effect of fatigue on the residual strain of concrete at the top of the specimen span.
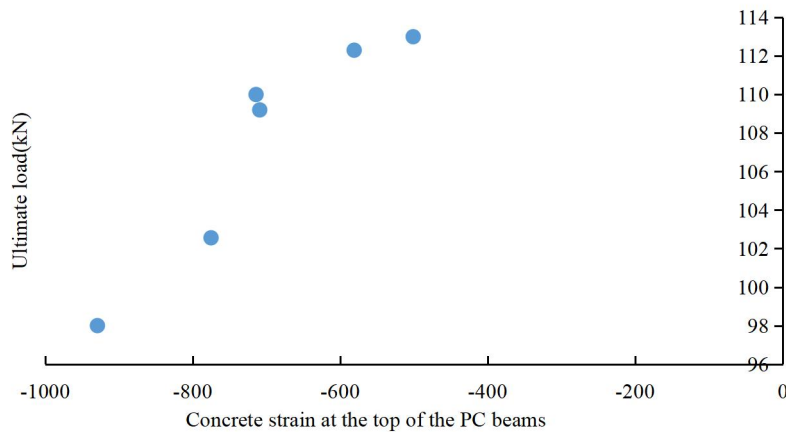

Fig 6.8   Ultimate load versus concrete strain at the top of the PC beam

6.3.5 Strain of inter concrete around strand at mid span.

Figure 6.9 shows relationship of the strain of inter concrete around strand at mid span and load. Under the same load, the higher corrosion degree the higher concrete strain. The failure characteristics of the specimen can also be judged by the development of the concrete strain around the middle span of the strand. Due to the high degree of corrosion, the flexural stiffness of F-B-12 deteriorated seriously during the fatigue loading process. In the static loading test, the strain growth of F-B-12 was faster than that of other specimens, and the deformation was larger, and finally the steel strand broke. The strain growth of the other specimens stopped when the top concrete crush.
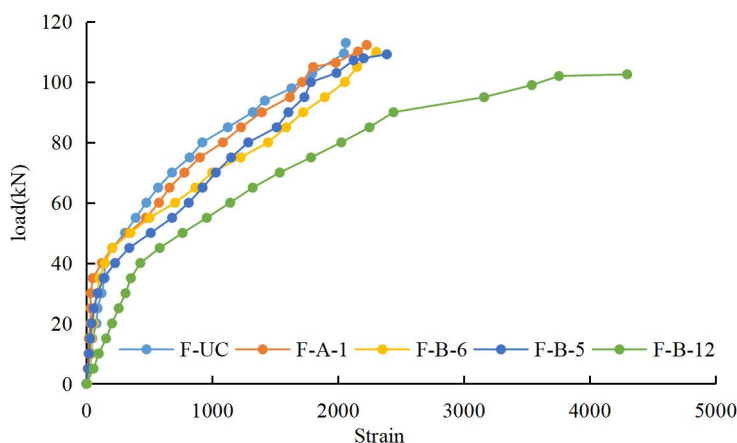

Fig. 6.9   Strain of inter concrete versus load

6.3.6 Crack width

The crack widths from the two static load tests are summarized in **Fig. 6.10**. It can

be seen that the crack widths of the fatigue-damaged specimens are greater when the corrosion is the same and the applied loads are the same. This indicates that fatigue has a more severe effect on the bonding properties and bending stiffness of the specimens.
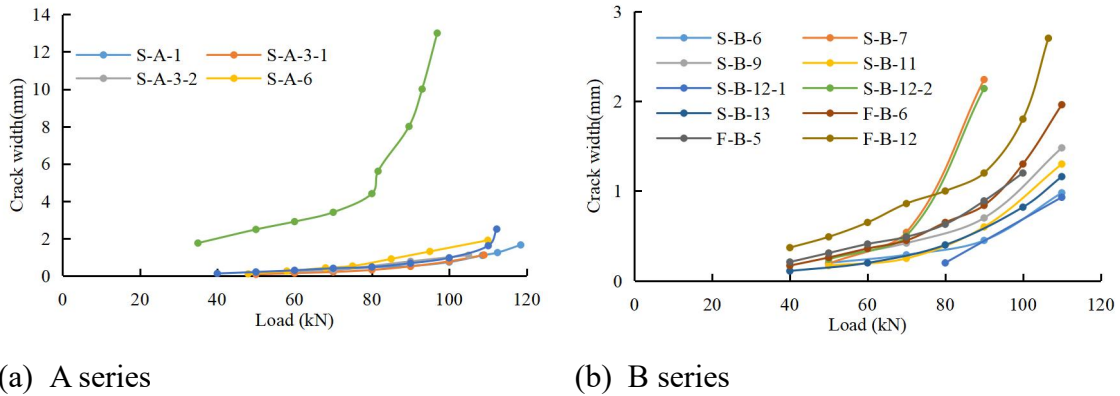

(a) A series   (b) B series

Fig. 6.10 Crack width versus load

6.3.7 Effect of fatigue on fracture of PC strand

In order to investigate the effect of fatigue on strand fracture, the forces at strand fracture for specimen F-B-12 in the static load test were calculated by using the prediction method mentioned in Chapter 4, and the ultimate capacity of strand for specimen F-B-12 without fatigue loading was calculated based on the results of the study in Chapter 2, and the results are shown in Table 6.2. It is found that the fatigue effect significantly reduces the tensile capacity of the prestressing strand.

Table 6.2 Calculation result

Specimen. No	Avergae max cross section area loss of fractured wires (%)	F_x(kN)	F_u(kN)
F-B-12	47.61	130.92	150.26

Note: F_x is the calculated value of prestress force when steel wires fracture, F_u is the calculated value of ultimate tensile force.

6.4 Chapter summary

1. After fatigue damage, the ultimate load carrying capacity of the specimen, bending stiffness are significantly reduced, and the more serious the corrosion, the more obvious the reduction. This is related to the amplification effect of corrosion on fatigue damage, so when corrosion degree is same, the ultimate load carrying capacity of the specimens corroded at mi-span is reduced more than the beam edge corrosion.

2. When the strand corrosion is lower, the specimen failure mode is crushing of the top concrete compression zone. Fatigue load increases the residual strain in the concrete compression zone at the top of the PC beams, which is the main reason why fatigue leads to a reduction in the ultimate capacity of the PC beams with lower corrosion degree. When the degree of corrosion is higher, the specimen failure mode become the steel wires fracture. Calculation result indicated that

fatigue significantly reduces the ultimate tensile capacity of the corroded strand. In this case, the reduction in the tensile properties of the strand due to fatigue damage becomes the main reason for the reduction in the ultimate load capacity of the PC beams.

Chapter 7 Conclusions

For partially prestressed concrete bridge structures in service in corrosive environments, structural cracks can occur as a result of long-term fatigue loading, and the presence of corrosive factors such as chloride ions and moisture in the environment can lead to corrosion of the strand, thus causing a change in the fatigue damage mode of the beam and having a serious impact on the fatigue performance of the beam. However, less research has been carried out on the fatigue related problems of partially prestressed reinforced concrete beams after the strand has been subjected to corrosion. In this paper, the following conclusions are drawn from the analysis of static load and fatigue mechanics tests of prestressed beams after corrosion of prestressing strands by conducting corrosion tests of prestressing strands in working condition:

1. The degradation of prestressing force of the 1×7 unbonded PC strand during corrosion test can be divided into two stages after the effect of relaxation. In the first stage the prestress decreases linearly with the mass loss of the strand due to the corrosion, and the second stage starts when the maximum cross-sectional area loss of the corroded wire in the strand reaches around 36%.

2. The deterioration of the ultimate tensile properties of the strand after corrosion can be divided into two stages, which are basically the same as the deterioration stage of prestressing. When the maximum cross-sectional area loss of fractured wire is less than around 40%, the ultimate tensile capacity decreases linearly with the increase of the maximum cross-sectional area loss, and the fracture type is milling cutter type with ductile damage. When the maximum cross-sectional area loss of the fractured wire exceeds around 40%, the wire fracture type changes to the split type or split-milling cutter type with brittle damage, and the ultimate tensile capacity of the specimen with the fracture type of split-milling cutter type is slightly higher than that of the specimen with the fracture type of split type.

3. Within prestressed beams, the effect of corrosion on prestressing deterioration remains significant, with initial cracking loads decreasing linearly with increasing strand mass loss, and beam deflection increasing with strand mass loss during the loading phase prior to concrete cracking. Comparing the deterioration of the prestressing force of bonded and unbonded PC strands during the corrosion process, it can be found that the bond property doesn't influence the prestressing force deterioration regulation of the PC strand, however, significantly reduces the prestressing force loss under the same corrosion degree.

4. Severely corroded strands significantly reduce the ultimate load carrying capacity of the beam and change the damage mode of the prestressed beam from ductile to brittle damage. The damage mode of the beam is not only related to the cross-sectional area loss of PC strands, but also, to the type of strand corrosion section. The type of strand fracture has a significant effect on the ultimate load carrying capacity of the beam.

5. The specimens with corroded strands were the same as the uncorroded specimens, and their mid-span deflections, longitudinal reinforcement strains, mid-span internal concrete strains around the PC strands and crack widths demonstrated a typical fatigue development pattern with the increase in the number of cycles. Comparing the fatigue development curves of different specimens, it can be found that the higher corrosion degree has a significant accelerating effect on the development process of fatigue damage. It means corrosion of PC strands amplifies the effects of fatigue loading on various properties of the specimens.

6. When the strand corrosion is lower, the specimen failure mode is crushing of the top concrete compression zone. Fatigue load increases the residual strain in the concrete compression zone at the top of the PC beams, which is the main reason why fatigue leads to a reduction in the ultimate capacity of the PC beams with lower corrosion degree. When the degree of corrosion is higher, the specimen failure mode become the steel wires fracture. Calculation result indicated that fatigue significantly reduces the ultimate tensile capacity of the corroded strand. In this case, the reduction in the tensile properties of the strand due to fatigue damage becomes the main reason for the reduction in the ultimate load capacity of the PC beams

The strands used in this paper are all 1×7 strands, and the corrosion test will be carried out in the future for more specifications of strands (e.g., 1*19) to observe whether the prestress deterioration law is the same. The corrosion test of prestressed beams proved that the bond between strand and concrete would inhibit the prestressing force reduction caused by corrosion, while the deterioration process of the bond and prestressing force interacting with each other as the degree of corrosion increases still needs to be further investigated in the future. Meanwhile, in order to measure the residual performance after fatigue damage in this test, the specimens were not loaded to fatigue failure. In the future, more times of fatigue loading will be performed on the corroded beams to study and predict their fatigue life.

Reference

[1] Li Xiaowen, Tong Yuesheng. Principles of concrete structure design [M]. Wuhan: Huazhong University of Science and Technology, 1-10, 2009.

[2] Ye Mishou. Principles of structural design [M]. Beijing: People's Traffic Press. 290-300, 1996.

[3] Fang Zhenzheng. Unbonded and partially prestressed structures [M]. Beijing: People's Traffic Press. 29-32, 1999.

[4] JOINT ACI-ASCE COMMITTEE. State-of-the-art report on partially prestressed concrete[R]. American Concrete Institute, 1999.

[5] Che Huimin, Shao Houkun, Li Xiaoping. Partially Prestressed Concrete - Theoretical Design Engineering Practice [M]. Sichuan: Southwest Jiaotong University Press, 120-126, 1992.

[6] Bruce S M , Mccarten P S , Freitag S A , et al. Deterioration of Prestressed Concrete Bridge Beams[J]. land transport new zealand research report, 2006.

[7] Zivanovic i., Lecinq B. and Fuzier JP., Durability specific for prestressing, Proceedings of the first fib congress: Concrete structures in the 21st century, Session 8, Osaka, Japan, 447-454, 2002.

[8] Concrete Society/Concrete Bridge Development Group. Durable post-tensioned concrete bridges[R]. Technical Report No. 47 Crowthome, UK: 2002.

[9] Vehovar L, Kuhar V, Vehovar A. Hydrogen-assisted stress-corrosion of prestressing wires in a motorway viaduct[J]. Engineering Failure Analysis, 5(1): 21-27, 1998.

[10] Proverbio, E. and Ricciardi, G. "Failure of a 40 years old post-tensioned bridge near seaside." *Proceedings of the International Conference Eurocorr,* 10-14, *2000.*

[11] Cederquist, S. C. "Motor speedway bridge collapse caused by corrosion." *Materials Performance*, 36(7), 18-19, 2000.

[12] Darmawan, M. S. and Stewart, M. G. "Effect of Pitting Corrosion on Capacity of Prestressing Wires." *Magazine of Concrete Research*, 59 (2), 131-139, 2007.

[13] Woodward, R.J., Wilson, D. L. S. "Deformation of segmental post-tensioned precast bridges as a result of corrosion of the tendons." Proc. Inst. Civ. Eng, 90, 397-419

[14] Kondo, T., et al. "Mechanical properties of cut artificially PC strand." In: Proceedings of the 25th Symposium on the Development of Prestressed Concrete, 25, 263-268, 2016. (in Japanese)

[15] Kitano, I. "Research on PC bridge remodeling technology, Part 1: Study on mechanical properties of corroded prestressed steel." *Prestressed Concrete Engineering Society*, 52-56, 2007.

[16] Tanaka, Y., et al. "Mechanical properties of corroded PC shavings Prestressed concrete residual strength." *Prestressed Concrete Engineering Society*, 21, 211-216, 2012.

[17] Wang, L., Zhang, X., Zhang, J., et al. "Effect of insufficient grouting and strand corrosion on flexural behavior of PC beams." *Construction & Building Materials*, 53, 213-224, 2014.

[18] Jeon, C., Lee, J, Lon, S., et al. "Equivalent material model of corroded prestressing steel strand." *Journal of Materials Research and Technology*, 8(2), 2450-2460, 2019.

[19] Jeon, C., Cuong, D. N., and Chang, S. S. "Assessment of Mechanical Properties of Corroded Prestressing Strands." Applied Sciences10, no. 12: 4055, 2020.

[20] Zhang, X., Wang, L., Zhang, J., et al. "Corrosion-induced flexural behavior degradation of locally ungrouted post-tensioned concrete beams." *Construction & Building Materials*, 134, 7-17, 2017a.

[21] Wang, L., Li, T., et al. "Corrosion Morphology and Mechanical Behavior of Corroded Prestressing Strands." *Journal of Advanced Concrete Technology,* 18, 545-557, 2020.

[22] Vecchi, F., Franceschini, L., et al. "Corrosion morphology of prestressing steel strands in naturally corroded PC beams." Construction and Building Materials, 296, 123720.1-123720.20, 2021

[23] Lee, J., Lee, Y., et al. "Probabilistic prediction of mechanical characteristics of corroded strands." Engineering Structures, Volume 203, 109882, 2020.

[24] Chen, Y., Qin, W., et al. "Influence of corrosion pit on the tensile mechanical properties of a multi-layered wire rope strand." Construction and Building Materials, Volume 302, 124387, 2021.

[25] Chen, Y., Qin, W., et al. "Study on the mechanical performance of a three-layered wire rope strand with a surface pit in varied corrosion direction into the wire." Engineering Failure Analysis, Volume 136, 106181, 2022.

[26] Wang, L., Yi, J., et al. "Effect of corrosion-induced crack on the bond between strand and concrete." Construction and Building Materials, Volume 153, 598-606, 2017.

[27] Li, F., Qu, Y., et al. "Bond life degradation of steel strand and concrete under combined corrosion and fatigue." Engineering Failure Analysis, Volume 80, 186-196, 2017.

[28] Li, F., Yuan, Y., et al. "Effects of corrosion on bond behavior between steel strand and concrete." Construction and Building Materials, Volume 38, 413-422, 2013.

[29] Lizhao Dai, Lei Wang, Jianren Zhang, Xuhui Zhang, A global model for corrosion-induced cracking in prestressed concrete structures,Engineering Failure Analysis, Volume 62, Pages 263-275, ISSN 1350-6307, 2016.

[30] Zeng, Hong Y . Resaerch on Bending Behavior of Corroded PC Beams[J]. Applied Mechanics and Materials, 351-352:1662-1668, 2013.

[31] Lei Wang, Xuhui Zhang, Jianren Zhang, Yafei Ma, Yibing Xiang, Yongming Liu,Effect of insufficient grouting and strand corrosion on flexural behavior of PC beams, Construction and Building Materials, Volume 53, Pages 213-224, ISSN 0950-0618, 2014

[32] Zhang, X., Wang, L., Zhang, J., et al. "Corrosion-induced flexural behavior degradation of locally ungrouted post-tensioned concrete beams." Construction & Building Materials, 134, 7-17, 2016b.

[33] Qian-Qian Yu, Xiang-Lin Gu, Yan-Hong Zeng, Wei-Ping Zhang, Flexural behavior of Corrosion-Damaged prestressed concrete beams,Engineering Structures, Volume

272, 114985, ISSN 0141-0296, 2022.

[34] Giuseppe Campione, Maria Zizzo, Influence of strands corrosion on the flexural behavior of prestressed concrete beams, Structures, Volume 45, Pages 1366-1375, ISSN 2352-0124, 2022.

[35] Zhao-Hui Lu, Qi-Hao Zhou, Hai Li, Yan-Gang Zhao, A new empirical model for residual flexural capacity of corroded post-tensioned prestressed concrete beams, Structures,Volume 34, 4308-4321, ISSN 2352-0124, 2021.

[36] Bennett E. W., Chandrasekhar C S. Supplementary tensile reinforcment in prestressed concrete beams[J]. Concrete, 6(10): 35-39, 1972.

[37] Abeles P W, Brown E I, Hu C H. Behavior of under reinforced prestressed beams subjected to different stress range [J]. ACI SP 41-12, :279-300, 1947.

[38] Abeles P W, Brown E I,Hu C H. Fatigue resistances of under-reinforced prestressed beams subjected to different stress range: Miner's Hypothesis[J]. ACI SP 141-11, :237-277, 1974.

[39] Fauchart J, Kavyrchine M, Trinh J.   [J]. Annales de l' Institute Technique du Batiment et des Travaux Publics, (326): 21-31 1975.

[40] Harajli M H, Naaman A E. Static and fatigue tests on partially prestressed beams [J]. Journal of Structural Engineering, 111(7): 1602-1619, 1985.

[41] EI Shahawi M, Batchelor B D. Fatigue of partially prestressed concrete[J]. Journal of Structural Engineering, 112(3): 524-537, 1986.

[42] Yongxiao Du, Jun Wei, Jian Yuan, Yanfeng Lai, Dinghao Sun, Experimental research on fatigue behavior of prestressed concrete beams under constant-amplitude and variable-amplitude fatigue loading, Construction and Building Materials, Volume 259, 119852, ISSN 0950-0618, 2020.

[43] Resmi, G., Amlan, K., et al. "An Assessment of the Deterioration of Flexural Capacity of a Pretensioned Concrete Girder Due to Strand Corrosion." Recent Advances in Structural Engineering, Volume 2, Lecture Notes in Civil Engineering, Volume 12, 515-525, 2016

[44] Feng, W., Dong, Z., et al. "An experimental study on the influence of applied voltage on current efficiency of rebars with a modified accelerated corrosion test." *Cement and Concrete Composites*, 122, 0958-9465, 2021

[45] Hong, S., Zheng, F., Shi, G., et al. "Determination of impressed current efficiency during accelerated corrosion of reinforcement." *Cement and Concrete Composites*, 108, 0958-9465, 2020

[46] Kim, J. K., Kim, J. S., Kwon, S. H. "Mechanical properties of a new prestressing strand with ultimate strength of 2160 MPa." KSCE J Civil Eng, 18(2), 607-15, 2014

[47] Li, J., Miki, T., Yang, Q, Mao, M. (2022). "Experimental study on prestressing force of corroded prestressed concrete steel strands." *Journal of Advanced Concrete Technology*, 20, 550-563.

[48] Li, J., Miki, T., Yang, Q, Mao, M. (2023). "Mechanism of Corrosion on Prestressing Force and Residual Tensile Capacity of Corroded Prestressed Concrete Steel Strands," *Journal of Advanced Concrete Technology*, 21(11) 957-971.

[49] F.P. Liu, J.T. Zhou, Experimental Research on Fatigue Damage of Reinforced Concrete Rectangular Beam, KSCE J. Civ. Eng. 22 (9) 3512–3523, 2018.